Project Title: Apatite and sodalite based glass-bonded waste forms for immobilization of ^{129}I and mixed halide radioactive wastes

Reporting Period: October 1, 2014 – September 30, 2017

Date of Report: December 30, 2017

Award Number: NU-14-NJ-RU-0203-02

Project Number: 14-6285

Principal Investigator: Ashutosh Goel
Rutgers, The State University of New Jersey

Collaborators: Washington State University (WSU), Pullman, WA
(Co-PI: John. S. McCloy)

Pacific Northwest National Laboratory (PNNL)
(Brian J. Riley & Josef Matyas)

Acronyms and Abbreviations

CAN	Cancrinite
DIW	deionized water
DSC	differential scanning calorimetry
DTA	differential thermal analysis
FTIR	Fourier transform infrared spectroscopy
HSM	Hot-stage microscopy
HSOD	Hydroxysodalite
IC	ion chromatography
ICP-MS	Inductively coupled plasma – mass spectroscopy
ICP-OES	Inductively coupled plasma – optical emission spectroscopy
ISOD	Iodosodalite
NE	Nuclear Energy
NMR	Nuclear Magnetic Resonance
PCT	Product Consistency Test
PNNL	Pacific Northwest National Laboratory
SEM	Scanning Electron Microscope
SPFT	Single Pass Flow Through test
TEOS	Tetraethyl orthosilicate
TGA	Thermogravimetric Analysis
U.S. DOE	United States – Department of Energy
WSU	Washington State University
XRD	X-ray diffraction
XRF	X-ray fluorescence

Report Summary

This report provides an overview of the research activities conducted during three years, i.e. October 1, 2014 to September 30, 2017. The project was divided into two parts. The first part dealt with the synthesis and characterization of glass-bonded-iodoapatite waste forms and was led by Rutgers University. The second part comprised the synthesis and characterization of glass-bonded-iodosodalite based waste forms and was led by WSU. The PNNL collaborators were mainly involved with chemical durability testing of glass-bonded-ceramic waste forms. The report includes the summary of the project objectives, approaches, results and deliverables.

Scientific Accomplishments

Part 1. Synthesis and characterization of glass-bonded-apatite waste form

- Iodide containing calcium phosphate apatite [$Ca_{10}(PO_4)_6I_2$] could not be synthesized using wet chemical precipitation or hydrothermal route. However, Iodate (IO_3^-) containing calcium phosphate apatite [$Ca_{10}(PO_4)_6(OH)_{(2-x)}(IO_3^-)_x$] was synthesized via wet chemical precipitation technique. The presence of iodine in apatite structure was confirmed by FTIR and XRF.
- Investigated the feasibility of hydrothermal synthesis of iodide containing lead vanadate apatite [$Pb_{10}(VO_4)_6I_2$].
- Synthesis of iodide containing lead vanadate apatite [$Pb_{10}(VO_4)_6I_2$] was achieved *via* wet chemical precipitation (at room temperature) route. The presence of iodine in apatite structure was confirmed by XRD, XRF, and ICP-MS. The uptake of iodine for synthesized waste form has been shown to be 94.6%.
- Studied the formation of solid solutions in apatites with general formula [$Pb_{(10-x)}Ca_x(VO_4)_{(6-y)}(PO_4)_yI_2$] via wet chemical precipitation technique. Characterization included XRD Rietveld, XRF, ICP-MS, and Raman spectroscopies.
- $Pb_{10}(VO_4)_6I_2$ was successfully synthesized using NaI and AgI as iodine precursors, respectively. The choice of precursor materials was made considering the nature of iodine waste extracted from caustic scrubbers or solid sorbents coated with silver compounds.
- Designed and characterized PbO-V_2O_5-P_2O_5 based glass binder.
- Investigated the sintering ability of glass binders using DSC, HSM, XRD and SEM along with some physical properties including linear shrinkage and density.
- Prepared glass-bonded-apatite waste forms and studied their chemical durability in accordance with ASTM C1308-14.

Part 2. Synthesis and characterization of glass-bonded-sodalite waste form

- Iodosodalite, $Na_8Al_6Si_6O_{24}I_2$, was synthesized using hydrothermal and aqueous methods.
- The effects of NaOH concentration, temperature, aging time, Al/Si ratio, dilution, and precursors on the hydrothermal synthesis were investigated using XRD-Rietveld, SEM, FTIR, and XPS.
- The effects of NaOH concentration, drying temperature, dilution, and precursors on the aqueous synthesis were investigated using XRD-Rietveld and SEM.
- The optimal synthesis conditions for both hydrothermal and aqueous synthesis were found.
- Iodosodalite was synthesized without using excess NaOH and unwashed after reaction for glass-bonded waste form study. This was done to avoid the effect of mineralizing agent

and loss of unreacted iodine and other residuals.

- Glass-bonded waste forms were synthesized with baseline iodosodalite powders from both hydrothermal and aqueous methods and two borosilicate glasses, NBS-4 and SA-800.
- The effects of sintering temperature, glass binders, and mixed glass binder amounts on the glass-bonded sodalite waste forms were investigated using XRD-Rietveld, SEM-EDS, FTIR, TGA-DSC, NAA, volumetric titration, porosity, and ASTM 1308 chemical durability test.

Ongoing and future activities

- Manuscript writing in progress on design and performance of glass binders for iododpatite waste forms.
- The identical iodosodalite powders mixed with/without glass binders used for glass-bonded waste forms were HIPped at 900 °C and 175 MPa for 3hrs, and XRD and SEM-EDS will be performed on the resulting samples.
- PCT will be performed on the same sample that was tested with ASTM 1308 to understand the difference in the chemical durability tests.
- Anion competition between I^-, Cl^-, and OH^- is investigated to understand the anion selectivity by the β-cage of the sodalite.
- Capturing capacity of iodine gas with anhydrous sodalite, $Na_6Al_6Si_6O_{24}$, will be investigated.

Publications

- C. Cao, S. Chong, L. Thirion, J.C. Mauro, J.S. McCloy, A. Goel, *Wet chemical synthesis of apatite-based waste forms - A novel room temperature method for the immobilization of radioactive iodine*, Journal of Materials Chemistry A 5 (2017) 14331-14342.
- C. Cao, A. Goel, *Apatite based ceramic waste forms for immobilization of radioactive iodine – An Overview (16155)*, Proceedings of Waste Management Conference (WM2016), March 6-10, 2016, Phoenix, AZ.
- S. Chong, J. Peterson, B. Riley, and J.S. McCloy, *Hydrothermal synthesis and analysis of iodine-containing sodalite (16153)*, Proceedings of Waste Management Conference (WM2016), March 6-10, 2016, Phoenix, AZ.
- S. Chong, J. Peterson, J. Nam, B. Riley, and J.S. McCloy, *Synthesis and characterization of iodosodalite*, Journal of the American Ceramic Society 100 (2017) 2273-2284.
- J. Nam, S. Chong, B.J. Riley, J.S. McCloy, *Iodosodalite waste forms from low-temperature aqueous process*, MRS Advances (2017) Submitted.
- S. Chong, J. Peterson, B. Riley, D. Tabada, D. Wall, J.S. McCloy, *Glass-bonded iodosodalite waste form for immobilization of I-129*, Journal of Nuclear Materials (2017) Submitted.

Presentations

- J.S. McCloy, S. Chong, B. Riley, J. Nam, *Characterization of sodalite-based waste forms for immobilization of ^{129}I*, Materials Research Society sponsored Scientific Basis for Nuclear Waste Management, Nov 1, 2017, Sydney, Australia **(Oral Presentation)**.
- C. Cao, S. Chong, L. Thirion, J.C. Mauro, J.S. McCloy, A. Goel, *Wet chemical synthesis of apatite based waste forms for immobilization of radioactive iodine*, 2016 American Nuclear Society (ANS) Winter Meeting & Expo, Nov 6 – 10, 2016, Las Vegas, NV **(Award presentation).**

- C. Cao, J.S. McCloy, A. Goel, *Wet chemical synthesis of apatite based waste forms for immobilization of radioactive iodine*, 2016 MRS Fall Meeting, Nov 27 – Dec 2, 2016, Boston, MA **(Oral Presentation)**.
- S. Chong, J. Peterson, B. Riley, J. McCloy, *Hydrothermal synthesis and analysis of iodine-containing sodalite*, Waste Management Symposium, Phoenix, AZ, March 5-9, 2016 **(Oral Presentation)**.
- C. Cao and A. Goel, *A novel approach towards synthesis of apatite based ceramic waste forms for immobilization of radioactive iodine (^{129}I)*, Waste Management Symposium, Phoenix, AZ, March 5-9, 2016 **(Oral Presentation)**.
- J.S McCloy and A. Goel, *Iodine-129 waste forms: Apatite & Sodalite*, DOE-NE Materials Recovery & Waste Form Development (MRWFD) Campaign Working Group Meeting, Pacific Northwest National Laboratory, Richland, WA, March 23, 2016 **(Oral Presentation)**.

Theses

- C. Cao, *Wet chemical synthesis of apatite based ceramic waste forms for immobilization of ^{129}I*, M.S. Thesis, 2017, Rutgers University.
- J. Nam, *Aqueous synthesis of iodide sodalite for the immobilization of I-129* M.S. Thesis, 2016, WSU.
- S. Chong, *Characterization of Sodalite Based Waste Forms for Immobilization of ^{129}I*, Ph.D. Thesis, 2017, WSU

Awards

- Innovations in Fuel Cycle Research Awards, U.S. Department of Energy – Second Prize, Category for Material Recovery and Waste Form Development, 2016.

Table of Contents

Contents

1 PROJECT BACKGROUND

The highly volatile radionuclide, I-129, has a long half-life and is difficult to immobilize. Iodine is not easily vitrified by conventional routes due to its volatility at typical glass processing temperatures. Therefore, there have been many efforts to develop an alternative waste form for iodine, but none has been uniquely accepted by the nuclear waste community due to trade-offs regarding loading capacity, chemical durability, processing efficiency, and cost. Some prominent approaches to immobilize iodine include the development of AgI containing glasses, bismuth-oxyiodide minerals, silver functionalized silica aerogels, metal-organic frameworks, Pb and/or Ag containing vanadinite apatites, and sodalite.

Apatite and sodalite are good candidates for baseline waste form for iodine immobilization due to their crystal structure, low temperature synthesis, and superior chemical durability. The project was aimed at developing glass bonded waste form with sodalite and apatite for the capture and immobilization of the radionuclides of interest. The goals and specific objectives for the research are stated below.

Project Goals and Objectives

The goal of the project was to utilize the knowledge accumulated by the team, in working with minerals for chloride wastes and biological apatites, toward the development of advanced waste forms for immobilizing ^{129}I and mixed-halide wastes. Based on our knowledge, experience, and thorough literature review, we had selected two minerals with different crystal structures and potential for high chemical durability, sodalite and CaP/PbV-apatite, to form the basis of this project. The focus of the proposed effort was towards: (i) low temperature synthesis of proposed minerals (iodine containing sodalite and apatite) leading to the development of monolithic waste forms, (ii) development of a fundamental understanding of the atomic-scale to meso-scale mechanisms of radionuclide incorporation in them, and (iii) understanding of the mechanism of their chemical corrosion, alteration mechanism, and rates. The proposed work was divided into four broad sections.

1. Synthesis of materials
2. Materials structural and thermal characterization
3. Design of glass compositions and synthesis glass-bonded minerals, and
4. Chemical durability testing of materials.

Approach

The proposed research was broken down into the following separate tasks in order to accomplish the objectives stated above:

1. Synthesis of iodine-containing minerals: Apatite and sodalite minerals were synthesized using wet chemical synthesis, hydrothermal synthesis, or/and sol-gel synthesis.
2. Structural and thermal characterization of waste forms: The elemental concentration of halides incorporated into the ceramic waste forms has been analyzed by XRF and ICP-MS while the crystalline phase evolution and thermal transformation in these waste forms has been followed with XRD, NMR and DSC-TGA
3. Design and synthesis of monolithic waste forms: The low-temperature melting (≤1000 °C) PbO-V_2O_5-P_2O_5 based glass compositions were designed to be used as binders for consolidation of iodoapatites. Iodosodalite was consolidated using borosilicate based glas binders.
4. Chemical durability of glass bonded waste forms: The chemical durability of the iodine

waste forms was studied in accordance with ASTM C1308.

2 SUMMARY OF ACTIVITIES CONDUCTED (October 1, 2014 – September 30, 2017)

2.1 Activities conducted in the Fiscal Year 2015

- The project team met the TPOC for this project (Dr. William Ebert) at 2014 MRS Fall Meeting in Boston, MA. The scientific and technical work scope of the project was discussed and finalized in this meeting.
- Work package describing all the technical details of the final work plan has been submitted to PICSNE. The work package has been approved by concerned DoE authorities.
- A sub-contract has been established between Rutgers and WSU.
- Hydroxyapatite, $Ca_{10}(PO_4)_6(OH)_2$, and lead vanadate apatite, $Pb_{10}(VO_4)_6(OH)_2$, were synthesized via wet chemical precipitation and hydrothermal methods and analyzed with FTIR and DTA-TGA.
- A series of apatite based solid solutions with general formula $Ca_{10}(PO_4)_{(6-x)}(VO_4)_x(OH)_2$ was synthesized via wet chemical precipitation route.
- Iodide sodalite, $Na_8Al_6Si_6O_{24}I_2$, was synthesized via hydrothermal method. The iodide sodalite formation is favored under high pH (13-14).
- Attempts were made to synthesize $Ca_{10}(PO_4)_6I_2$ via wet chemical precipitation and hydrothermal synthesis. FTIR and XRD of the product was compared to that of $Ca_{10}(PO_4)_6(OH)_2$, but there was no difference. Therefore, the presence of iodine in the structure was not confirmed.
- Attempts were made to synthesize $Ca_{10}(PO_4)_6(IO_3)_2$ via wet chemical precipitation method. FTIR and iodine *3d* X-ray photoelectron spectra confirmed the presence of iodine in the crystal structure.
- Lead vanadate apatite, $Pb_{10}(VO_4)_6I_2$, was synthesized by heating the reaction mixture from wet chemical precipitation method in an autoclave at 200 °C for 24 hours.
- The analysis on the effects of NaOH concentration, aging time, and precursor concentration on the hydrothermal synthesis of iodide sodalite was performed. XRD pattern of sample with 20 days of aging time at 100 ℃ resulted in almost pure iodide sodalite. Lowering precursor concentration with water resulted in formation of nepheline hydrate 1 phase.
- Preliminary experiments were performed looking at glass binders and pellet synthesis. Iodide sodalite and nepheline were the main crystalline products in all fired pellets. Further investigation was required to understand the precise phase distribution and identity of some sodium aluminosilicate phases.
- XRF was performed on synthesized Ca–P–I, Ca–P-IO_3, and Pb–V–I apatite minerals to analyze iodine waste loading. The apatite minerals samples are sent to Bryce at University of Ottawa, Canada and WSU for NMR and XRD Rietveld analysis respectively.
- Lead vanadate apatite was synthesized hydrothermally, and the resulting product shows higher crystallinity than that of wet chemical precipitation method.
- The influence of temperature and environment on the synthesis of Pb-V-I apatite was studied.
- Some preliminary experiments were performed to study the sintering behavior and iodine

volatilization from Pb-V-I apatite powders.

- The influence of NaOH concentration, temperature, precursor concentration, Al/Si ratio, and aging time on the hydrothermal synthesis of iodide sodalite was analyzed with XRD and Rietveld method.
- Preliminary syntheses of iodide sodalite using aqueous method was performed.

2.2 Activities conducted in the Fiscal Year 2016

- Successfully synthesized $Pb_{10}(VO_4)_{6-x}(PO_4)_xI_2$ solid solution series, where x varied between 0 – 1.2. Quantitative crystalline/amorphous phase analysis of $Pb_{(10-x)}Ca_x(VO_4)_6I_2$ apatite samples by XRD Rietveld refinement.
- Characterization of $Pb_{(10-x)}Ca_x(VO_4)_6I_2$ and $Pb_{10}(VO_4)_{(6-x)}(PO_4)_xI_2$ powders by FTIR, Raman, and XRF spectroscopies. The chemical analysis of remnant solution was made by ICP-MS.
- Synthesis of $Pb_{10}(VO_4)_6I_2$ apatite by wet chemical precipitation using AgI as iodine source.
- Design and synthesis of glasses in the system $(60 - x)PbO–(10+x)V_2O_5–30P_2O_5$, and $40PbO–(55-y)V_2O_5–(5+y)P_2O_5$ [x varies between 5 – 50 mol.%, and y varies between 5 – 20 mol.%] for sintering experiments.
- Thermal analysis of Pb-V-P-O glasses by DSC and HSM.
- Sintering of glass powders at 400 and 425 °C in argon environment.
- Iodosodalite, $Na_8Al_6Si_6O_{24}I_2$, was hydrothermally synthesized from different precursors including kaolinite, $Al_2Si_2O_5(OH)_4$, zeolite 4A, $Na_{12}Al_{12}Si_{12}O_{48}{\cdot}XH_2O$, and $NaAlO_2+SiO_2$ and analyzed with XRD and SEM.
- The as synthesized iodosodalite was characterized by XRD, XPS and FTIR to understand the chemistry of iodine.
- Based on the optimal conditions from the variables experiments, iodosodalite was synthesized at 150 °C for 1, 2, 4, 8, 16, 20, and 32 days and analyzed with XRD, SEM, and FTIR. The result showed the increase in iodosodalite fraction with increase in aging time. The result is in good agreement with previous result.
- In addition to other precursors, meta-kaolin, $Al_2Si_2O_7$, was synthesized and used as a precursor for iodosodalite synthesis. All the synthesized powders from different precursors were analyzed with XRD and Rietveld refinement for phase quantification and SEM for surface morphology. Zeolite 4A precursor yielded the highest iodosodalite phase, and SEM showed that iodosodalite obtained from different precursors have similar polycrystalline feature.
- Iodosodalite was synthesized with aqueous method from different precursors including kaolinite, meta-kaolin, zeolite 4A, sodium aluminate + TEOS, gibbsite + colloidal silica, and sodium aluminate + colloidal silica. Kaolinite, meta-kaolin, and sodium aluminate + colloidal silica yielded significantly higher fraction of iodosodalite compared to zeolite 4A, sodium aluminate + TEOS, and gibbsite + colloidal silica.
- For hydrothermally grown baseline powder for glass-bonded waste form study, the unwashed and washed iodosodalite powders from zeolite 4A were compared. The washed iodosodalite synthesized from zeolite 4A was not usable due to the presence of I and Na in the washed solution, and the unwashed powder was very hygroscopic from excess NaOH. We wanted to ensure that all the materials would be included in the final waste form. Among other precursors, meta-kaolin and kaolinite yielded the highest iodosodalite

fraction for hydrothermal and aqueous methods respectively when no excess NaOH was added and the reacted powders were unwashed.

- ~60 g of unwashed iodosodalite from meta-kaolin was hydrothermally synthesized for the sintering experiment, and ~40 g of unwashed iodosodalite from kaolinite was synthesized with aqueous method.
- Two glass binders, NBS-4 and SA-800, were synthesized.
- Glass-bonded sodalite waste forms were synthesized using NBS-4 and SA-800 glass binder with/without 10 or 20% fractions at 650, 750, and 850 °C sintering temperatures.
- Preliminary XRD study was done on the pellets with hydrothermal iodosodalite and different NBS-4 glass binder fraction sintered at 650 and 750 °C, and iodosodalite was the major phase in the pellet samples. Phase quantification with Rietveld was performed on all the powders synthesized by the aqueous method.

2.3 Activities conducted in the Fiscal Year 2017

- Optimize the conversion of solid AgI into aqueous NaI in order to thereby synthesize the apatite, $Pb_{10}(VO_4)_6I_2$.
- Investigate the influence of ambient air atmosphere and argon atmosphere on the conversion of solid AgI to aqueous NaI
- Characterization of glass binders by XRD after sintering their powders at 400°C and 425°C in an argon environment
- Preliminary experiments into apatite-glass consolidation
- Further explore different apatite-glass sintering conditions, including apatite-glass mass ratios and glass binder composition selections. Characterize experimental sintered samples by XRD and SEM
- Investigate alternative glass binder compositions, including binary $PbO\text{-}V_2O_5$ glass and $Bi_2O_3\text{-}P_2O_5\text{-}PbO\text{-}V_2O_5$ glass along with preliminary sintering with apatite
- Investigate into the synthesis of $Ba_{10}(VO_4)_6I_2$, including testing various synthesis parameters along with the proper characterization (XRD, XRF, SEM)
- Glass-bonded iodosodalite waste forms were characterized with XRD-Rietveld.
- Porosities of all the waste form pellets were calculated.
- Selected pellets with high iodosodalite fractions were sent out to Nuclear Science Center at Washington State University and Galbraith Laboratories Inc for iodine quantification using NAA and volumetric methods respectively.
- SEM-EDS were performed on the polished surfaces of the selected pellets.
- The identical baseline sodalite powder mixed with glass binders were HIPped at Oak Ridge National Laboratory (ORNL).
- Sodalite with mixed anions were synthesized hydrothermally to understand the anion selectivity of the β-cage.
- Anhydrous sodalite was synthesized for possible application in iodine gas capture.
- Chemical durability testing of glass-bonded-apatite and glass-bonded-sodalite waste forms in accordance with ASTM 1308.

3 SUMMARY AND CONCLUSIONS

3.1 Glass-bonded-apatite based waste forms

- A novel wet chemical synthesis method has been developed to produce $Pb_{10}(VO_4)_6I_2$ based apatite waste forms for immobilization of radioactive iodine under ambient conditions. The proposed methodology can be applied to iodide containing waste streams from caustic scrubbing and silver solid adsorbents. The $Pb_{10}(VO_4)_6I_2$ apatite waste form synthesized using the proposed method has been shown to exhibit an iodine waste loading of 9.4 wt.%, while its loading efficiency has been experimentally calculated to be 94.6%. In terms of solid solutions, it was found that calcium has a minimal tendency to form apatite solid solutions when substituted for lead in the system, $Pb_{(10-x)}Ca_x(VO_4)_6I_2$. On the other hand, phosphate ion forms a solid solution with $Pb_{10}(VO_4)_6I_2$ when partially substituted for the vanadate ion.

- The choice of glass binder to consolidate apatite based waste form was made in PbO-V_2O_5-P_2O_5 system. Glasses with compositions $(60 - x)PbO–(10+x)V_2O_5–30P_2O_5$ and $40PbO–(55-y)V_2O_5–(5+y)P_2O_5$ [x varies between 0 – 50 mol.%, and y varies between 0 – 20 mol.%] were synthesized by melt-quench technique and characterized for their sintering and crystallization behavior. After a detailed study on the abovementioned glass system, two glass compositions – 20 P_2O_5 – 40 PbO – 40 V_2O_5 and 30 P_2O_5 – 10 PbO – 60 V_2O_5 (mol.%) – were selected to consolidate the $Pb_{10}(VO_4)_6I_2$ apatite powders produced by wet chemical synthesis.
- Glass powders were mixed with apatite powders in the ratio of 20:80 and 15:85 (glass:apatite) by mass. The mixtures were pressed into pellets and sintered at 400 °C for 1 h in flowing argon environment. The as produced pellets were studied for their chemical durability as per ASTM 1308. The normalized loss (NL) of elements from the glass – bonded – apatite pellets were much higher when compared with glass – bonded – iodosodalite pellets. The NL of iodine varied between 597 g m^{-2} – 1498 g m^{-2} depending on the surface area – to – volume ratio (8 – 80 m^{-1}) and composition of glass binder. The hypothesized model of dissolution of these waste forms is that the apatite dissolves independently of the glass (represented by P), and that iodine is preferentially leached from the apatite with diffusion-controlled kinetics while the Pb-V-O structure dissolves. The initially fast iodine release slows as it is depleted from the surface and eventually becomes limited by the dissolution rate of the Pb-V-O structure.

3.2 Glass-bonded-iodosodalite based waste forms

3.2.1 Hydrothermal synthesis

- The effect of six variables (pH, aging time, temperature, Al/Si ratio, differing precursors, and precursor concentration) on the hydrothermal synthesis of iodosodalite was investigated. Higher pH and longer aging time increased the iodosodalite yield along with the overall crystalline fraction with in the tested range. The crystallization of iodosodalite was favored in the temperature range between 140°C and180°C. A lower water amount and Al/Si molar ratio of unity yielded a higher mass% of iodosodalite (up to ~50 mass%, with the remainder being X-ray amorphous). From aging time and temperature variation experiments, the phase transformation of zeolite A→sodalite→cancrinite was observed with longer aging time and higher temperature, respectively. Among the tested precursors,

the product synthesized via zeolite 4A had the highest mass% of iodosodalite. XPS and FTIR verified the presence of iodide but not iodate.

- Glass-bonded iodosodalite waste forms were synthesized by mixing iodosodalite powder with NBS-4 or SA-800 borosilicate glass binders, and firing pellets at different temperatures of 650, 750, or 850 °C. The effects of firing temperature and glass loading (i.e., 0, 10, and 20 mass%) were investigated. Heat-treatment at 750 °C resulted in the best waste form as the pellets heat-treated at 650 °C were not well sintered, and ones at 850 °C contained low fractions of iodosodalite and high amorphous content. As the temperature increased from 650 to 850 °C, higher nepheline fractions were observed. The pellets mixed with NBS-4 had higher iodosodalite phase compared SA-800 under the same heat-treatment temperature and mixed amount of glass binder after heat-treatment at 750 °C. The glass SA-800 came out to be a better binder in comparison to NBS-4 as the former was effective in closing the pores in the sintered waste form. the sintering temperatures. The iodine masses in the sintered pellets showed that ~38-44% of the as-batched iodine remained in these pellets. The chemical durability test on these samples showed that iodine release rate was lower than sodium and silicon during the first 10 days and decreased significantly to 0.23 and 1.29 $g/m^2/d$ for 80 or 8 $m^{-1\ in}$ the 10 – 24-day interval, respectively. The linear release behavior of iodine indicated congruent dissolution of iodosodalite.

3.2.2 Aqueous synthesis

- The effects of drying temperature, pH (NaOH concentration), and precursor variation (concentration and identity) on the aqueous synthesis of iodosodalite was investigated. An iodosodalite synthesis procedure was established to yield a product with an iodosodalite phase purity of up to 95% using a kaolinite-based precursor route by drying at 100°C with 15 mL of deionized water. The product had a measured density of 99.4% of the theoretical value. A sample with this high phase purity and density before sintering has never been reported before with aqueous synthesis methods.
- For the waste form study, ~55–70 mass% of the original iodine remained in the heat treated pellets. The loss of iodine is likely due to the decomposition of iodosodalite, transition of sodalite to nepheline, and volatilization of iodine from the amorphous fraction. In general, pellets made with NBS-4 resulted in higher iodosodalite fractions compared to those made with SA-800, but the addition of SA-800 resulted in pellets with lower porosities. The best synthesis conditions for iodosodalite waste forms according to this study are 10 mass% of glass binder and a heat treatment of 750°C. The chemical durability shows the congruent dissolution of sodalite phase, but there are likely other phases present that contain Na and Si, considering that their dissolution rates are higher than those for I or Al. Further investigation will be performed on iodine dissolution.
- Iodosodalite synthesis with aqueous methods may yield higher iodosodalite fractions than hydrothermal methods based on comparison to a previous study. After aqueous or hydrothermal synthesis, not all precursors are converted into iodosodalite, and there is usually an amorphous fraction in the resulting product. In the waste form study, having higher fractions of initial iodosodalite present in the product seems to affect the outcome of the resulting iodine fraction present, because the iodine in the sodalite is less likely to volatilize during heat treatment compared to iodine present in the amorphous fraction due to low iodine solubility in silicate glasses. This results in better iodine incorporation and

lower dissolution rate. To optimize the iodine retention in the waste form, more crystalline iodosodalite baseline powder or glass binder with lower sintering temperature are needed.

4 RECOMMENDATIONS FOR FUTURE WORK

4.1 Iodoapatite

- Apatites are potential materials for immobilization of radioactive iodine. Significant advancement has been made towards developing novel methods to synthesize apatite based ceramic waste forms, with particular emphasis on Pb-V-I and Ca-P-I systems. There still exist potential candidate waste forms that have not been explored, for example, $Ba_{10}(VO_4)_6I_2$. The discovery of wet chemical synthesis methodology for $Pb_{10}(VO_4)_6I_2$ based apatite waste form has opened a possibility to synthesize these unexplored apatites. Future work should be focused on optimizing the wet chemical routes to synthesize novel apatite based waste forms.
- One major challenge that needs to be addressed for successful immobilization of radioactive iodine is the conversion of $IO_3^- \rightarrow I^-$ in the waste stream. While the waste stream contains iodine primarily in the iodide (I-) form, it also contains low volumes of iodate (IO_3^-). Although waste form development with iodide precursors (especially NaI) helps in immobilizing the majority of waste stream, it does not account for the leftover iodate species in the waste stream. Therefore, a mechanism needs to be devised to convert iodate species in the waste stream to iodide before it can be immobilized into a suitable waste form.
- Chemically durable glass binders with low sintering temperatures (<400 °C) need to be designed for successful consolidation of $Pb_{10}(VO_4)_6I_2$ based apatites.

4.2 Iodosodalite

- Refine the glass-bonded-sodalite waste forms to minimize porosity and thus, improve chemical durability, such as possibly hot isostatic pressing, glass binder optimization.
- Revisit aqueous methods for sodalite synthesis as they appear to keep more iodine in the structure.
- Explore microwave synthesis of iodosodalite and potential paths to use it with the radioactive waste.
- Explore the role of other alkali (Li, K) or Ag in sodalite for holding on to iodine.

Apatite Based Ceramic Waste Forms for Immobilization of Radioactive Iodine, An Overview - 16155

Charles Cao*, Ashutosh Goel*
* Department of Materials Science and Engineering, Rutgers University, Piscataway, NJ, USA

ABSTRACT

Apatite based ceramic waste forms are the most promising candidates for immobilization of radioactive iodine (I-129). While lead-vanadium based apatites have been studied for a long time, significant progress has been made in recent years in the domain of calcium-phosphate based apatites for iodine immobilization. This article is an attempt to present an overview of the progress that has been made in terms of developing novel synthesis and processing routes to contain iodine in apatite based ceramic waste forms. The challenges associated with current state-of-the art waste form synthesis techniques along with novel routes to synthesize these waste forms at low temperatures have also been discussed.

INTRODUCTION

One of the key components to a feasible and sustainable nuclear fuel cycle is a viable set of waste forms for the radionuclides and fission products. Of particular concern are the highly volatile radionuclides, e.g., H-3, Tc-99, I-129, Cs-137. In particular, the long half-life of I-129 ($\sim 1.6\times10^7$ years) combined with its high solubility in water (in anionic state) and its technical challenges associated with its capture in conventional radioactive waste forms (glasses or cements) pose serious concerns for its geological disposal.[1] The current proposed technology for the removal of iodine from reprocessing plant off-gas is to pass it through Ag-exchanged zeolite (AgZ) to form chemisorbed AgI.[2] Since silver is an RCRA metal, iodine is typically extracted from AgZ and further processed for immobilization into a durable waste form. Iodine is not amenable to conventional borosilicate vitrification routes because of its low solubility in some glass chemistries, but more importantly due to its high volatility at typical glass processing temperatures (1000–1100°C).[3] Therefore, considerable effort is being made to develop alternative waste forms for iodine. However, most proposed waste forms to date have not achieved sufficient maturity and satisfactory properties (specifically: ease of processing, high waste loading, and high chemical durability) to be considered as promising technologies. This article presents an overview of the current state of research pertaining to the development of apatite based ceramic waste forms for the immobilization of radioactive iodine.

JUSTIFICATION FOR THE USE OF APATITES

Apatites have been long been considered as a potential waste form for the immobilization of iodine isotopes. Due to their unique channel structure, it is easily

amenable to the incorporation of a wide range of fission products, including halides, into its crystal structure.[4] In addition, it has also been suggested that apatites have acceptable durability against radiation.[5, 6] The challenge, however, lies in the large ionic radius of the iodide ion. Considering the large ionic radius of iodide (I^-, 196 pm), it is difficult to find any naturally existing iodine containing apatites, thus leading to a scarce amount of knowledge and basic understanding about iodo-apatites.[4] Due to these reasons, most of the iodine containing apatites produced so far have had several shortcomings that have not allowed them to be adopted for iodine immobilization. The shortcomings may be issues, such as low waste (iodine) loading, poor chemical durability, or inability to scale up production. Progress is being made in the development of apatites for iodine immobilization, but in order to find the solution to the problem, one must thoroughly investigate the problem and understand the work that has led to the current state of apatite research within the scientific community.

Early Iodo-Apatites

Early on, iodine-containing apatites were synthesized by various researchers for various purposes. None of those, however, aimed at developing a waste form for immobilization of radioactive iodine. It began as early as 1959 when Merker and Wondratschek were studying lead apatites.[7] It was not, until about four decades later, however, when the topic of iodine immobilization in apatites was brought to light by Audubert et al.[8] Within that timeframe, there were only a few other investigations into iodo-apatites. Sudarsanan et al. synthesized cadmium vanadate iodide apatite from the melt of cadmium vanadate and cadmium iodide. [9, 10] It was concluded that due to a short c-dimension, there were deficiencies in the halide content and, as a result, modifications in the typical apatite structure occurred. This led to the formation of vacancies in the Cd(2) position (which formulates the apatite channel) in order to maintain charge balance. Apart from that, the only other iodo-apatite studies that were reported in this timeframe involved the use of pyramidal perrhenates (ReO_5).[11, 12] This is a step away from the standard structural and chemical moieties, which comprise of a tetrahedral MO_4 structure. For example, Baud et al. made an attempt to synthesize barium perrhenate iodide ($Ba_{10}(ReO_5)_6I_2$) *via* solid state route.[11] However, the as synthesized apatite mineral had the composition $Ba_{10}(ReO_5)_6I_{0.77}(OH)_{1.23}$, depicting uptake of moisture during synthesis. It was concluded that due to the electrostatic repulsion of the oxygen atoms of the pyramidal perrhenates on the IBa_6 octahedra that hydroxyl ions began to substitute for the halogen within the channel. In another study, Schriewer and Jeitschko, made an attempt to synthesize strontium perrhenate iodide apatite ($Sr_{10}(ReO_5)_6I_2$) *via* solid state route.[12] Although we could not find any information about the experimental chemical composition of the apatite formed in this study, it is interesting to note that the as synthesized iodo-apatite had an orthorhombic crystal structure, whereas the majority of iodo-apatites have hexagonal crystal structure.

Calcium-Phosphate Iodo-Apatites

One of the most commonly-known apatites within the scientific community is hydroxyapatite, which has a chemical formula, $Ca_{10}(PO_4)_6(OH)_2$. Owing to the ability of hydroxyapatite to accommodate halide ions (F^-, Cl^-, Br^-) in its crystal structure, attempts have also been made to incorporate iodide (I^-) for the hydroxyl (OH^-) ion within the apatite channel. However, success in this direction is still eluding the scientists. The only study that has reported on successful substitution of $I^- \leftrightarrow OH^-$ in $Ca_{10}(PO_4)_6(OH)_2$ using wet chemical synthesis has been published by Phebe and Narasaraju.[13] However, their assertions were highly preliminary in nature and it has been difficult to reproduce those results by any other researcher worldwide.[14] The successful attempts to incorporate iodine into calcium phosphate apatites utilized iodate (IO_3^-) instead of iodide (I^-) as the precursor for iodine, resulting in a solid solution with the general formula, $Ca_{10}(PO_4)_6(OH)_{2-x}(IO_3)_x$. The first successful attempt was made by Henning et al. where they synthesized a superstructure of an apatite material with the chemical formula, $Ca_{15}(PO_4)_9IO_3$ using a flux method.[15] However, considering that the material was synthesized at high temperature (850 °C) and under highly controlled conditions, it was difficult to consider this technique for waste form development. Recently, Campayo et al. synthesized a calcium phosphate iodate apatite with experimental composition $Ca_{10}(PO_4)_6(OH)_{1.6}(IO_3)_{0.4}$ using low temperature wet chemical synthesis aimed at immobilizing iodine.[16] Although halide containing apatites (for example, fluorapatite) are known for their high chemical durability in neutral and basic environments, the structural analysis of iodate-containing hydroxyapatite revealed the lack of local order around the iodate ions as these ions do not cluster around the apatite channels, something that is not typically observed in apatites.[17] This raises concerns about the long term chemical durability of this waste form. Increasing iodine waste loading in these apatites is another crucial aspect that needs to be addressed in the near future.

Lead-Vanadate Iodo-Apatites

Lead-vanadate apatite [$Pb_{10}(VO_4)_6I_2$] has been extensively studied as a potential waste form for iodine immobilization. Due to the fact that lead and vanadium have larger ionic radii than calcium and phosphorous, lead-vanadate apatites are capable of incorporating iodine into its structure. Due to this, many variations on the synthesis of lead-vanadate iodide apatite have been explored over the years. Lead vanadate iodide was first synthesized by Merker and Wondratscheck by melting lead vanadate and lead iodide in a vacuum sealed vessel in the temperature range of 500-800°C, while the crystallographic data on these minerals was obtained by Audubert et al.[7, 18] Further, Audubert et al. synthesized lead vanadate iodide, $Pb_{10}(VO_4)_6I_2$ within a matrix *via* solid state sintering by compacting a lead iodide core within the center of an outer layer of lead vanadate and consolidating the green body at 700 °C and 25 MPa.[8] Other high temperature synthesis methods include (i) mixing stoichiometric amounts of the precursors (PbO, PbI_2, V_2O_5) corresponding to $Pb_{10}(VO_4)_6I_2$, and heating them in a sealed quartz ampoule at 700 °C for 5 h under 35 MPa pressure, or (ii) hot isostatic pressing at 700°C for 2 h under the pressure of 200 MPa.[19, 20]

Although various solid state synthesis routes have yielded the desired Pb-V-I apatite, the major drawback with these synthesis routes is the need for a higher processing temperature. Iodine typically volatilizes at a temperature >500 °C and, as a result, the majority of the synthesis techniques investigated so far have been confined to sealed vessels and highly controlled environments. This problem is further aggravated by the poor chemical durability of stoichiometric $Pb_{10}(VO_4)_6I_2$ which demonstrates a leach rate (in pure boiling water) that is two orders of magnitude higher than for silver iodide-embedded glass waste forms.[19] This has resulted in a significant research effort focused on developing low temperature synthesis routes and improving the chemical durability of Pb-V-I based apatites. In this pursuit, it was observed that partial substitution of $(VO_4)^{3-}$ by $(PO_4)^{3-}$ in the apatite structure, resulting in a mineral with chemical composition $Pb_{10}(VO_4)_{4.8}(PO_4)_{1.2}I_2$, not only lowered the densification temperature of the ceramic body from 700 °C to 540°C (25 MPa), but also had a significant increase in the densification of the powder compact, thus increasing its chemical durability (due to a decrease in surface area).[21] This development resulted in a flurry of studies involving synthesis of Pb-V-P-I based apatites using various other techniques including spark plasma sintering,[22, 23] microwave dielectric heating,[24] and high energy ball milling.[25] The research in this direction currently still continues to be explored.

Future research on iodine containing apatites

As discussed above, most of the research on iodine immobilization in apatites has focused either on Pb-V-I or Ca-P-I system. However, there are several other systems that have demonstrated their ability to incorporate iodine in their crystal structure. For instance, cadmium vanadate iodide ($Cd_{10}(VO_4)_6I_2$), barium rhenium perrhenate iodide ($Ba_{10}(ReO_5)_6I_2$) and strontium rhenium perrhenate iodide ($Sr_{10}(ReO_5)_6I_2$), are potential candidate waste forms for iodine immobilization.[9, 11, 12] According to a recent computational study on the structure of iodine containing apatites with general formula $A_5(XO_4)_3I$, the A-site cation is capable of holding either Ag^+, K^+, Sr^{2+}, Pb^{2+}, Ba^{2+} and Cs^+, whereas the X-site cation can hold Mn^{5+}, As^{5+}, Cr^{5+}, V^{5+}, Mo^{5+}, Si^{4+}, Ge^{4+} and Re^{7+} depending on the overall chemistry of the system.[26] Therefore, there is enough scope to design chemically durable apatite based waste forms for immobilization of radioactive iodine.

Another area that needs significant research effort in this field is to develop low temperature synthesis methods where these minerals can be produced under ambient conditions. This will not only lower the overall cost of waste form development, but will also allow the integration of a production scale-up. One such example is aqueous processing (for example, co-precipitation technique or hydrothermal synthesis) which has not been reported for Pb-V-I based apatites so far.

CONCLUSION

The development of a viable apatite based waste form for the immobilization of I-129 would be a significant contribution to the nuclear waste management

community. In comparison to current proposed technology, apatite waste forms possess a significant advantage by providing substantial financial savings along the nuclear waste processing stream. By replacing current waste form technologies utilizing precious metals, such as Ag-exchanged zeolite, with lower cost metals, such as lead and calcium, the cost-efficiency of immobilizing iodine waste becomes much improved and much more viable. In the U.K., for instance, radioactive I-129 is currently being discharged into the sea. Considering possible future changes to regulatory practices, it is necessary to review strategies for developing durable waste forms for the immobilization of I-129 and apatites are a very viable candidate.

The development of apatite based waste forms could also prove beneficial for the immobilization of other existing radioactive isotopes. Because of the ability of apatite to incorporate various halides within its crystal structure, the future potential for immobilizing mixed halide waste is very feasible. By streamlining and consolidating the steps involved with collecting reprocessing plant off-gas, the potential for financial savings would again be improved substantially. Chloride-containing apatites, for instance, have already been proposed as a potential waste form for radioactive chloride waste. Considering that I-129 holds one of the longest half-life durations among the various HLW, a success in the immobilization of iodine would translate well to the immobilization of other radioactive waste.

Lastly, the ability of apatites to be synthesized by various methods would prove to be beneficial in the immobilization of large quantities of radioactive waste. By utilizing techniques, such as wet chemical synthesis, large quantities of apatite could be produced to meet the demands of the nuclear waste management community.

As can be seen, the investigation into the immobilization of iodine waste utilizing apatite waste forms is an ongoing process within the research community. Significant advancement has been made towards developing novel methods to synthesize apatite based ceramic waste forms, with particular emphasis on Pb-V-I and Ca-P-I systems. There still exist potential candidate waste forms that have not been explored, while novel low temperature synthesis methods need to be developed in order to produce chemically durable waste forms using a simplified process. Progress, however, certainly has been made and will continue to advance in the ongoing future.

REFERENCES

1. H. Kato, O. Kato, and H. Tanabe, "Review of immobilization techniques of radioactive iodine for geological disposal," pp. 697-702.
2. T. M. Nenoff, M. A. Rodriguez, N. R. Soelberg, and K. W. Chapman, "Silver-mordenite for radiologic gas capture from complex streams: Dual catalytic CH3I decomposition and I confinement," *Microporous and Mesoporous Materials,* vol. 200, pp. 297-303, 12// 2014.
3. M. H. Langowski, J. G. Darab, and P. A. Smith, "Volatility literature of chlorine, iodine, cesium, strontium, technetium, and rhenium; technetium and rhenium volatility testing," Pacific Northwest National Laboratory, Richland, WA1996.

4. T. White, C. Ferraris, J. Kim, and S. Madhavi, *Apatite - An adaptive framework structure* vol. 57, 2005.
5. S. Utsunomiya, S. Yudintsev, L. M. Wang, and R. C. Ewing, "Ion-beam and electron-beam irradiation of synthetic britholite," *Journal of Nuclear Materials,* vol. 322, pp. 180-188, 11/1/ 2003.
6. R. C. Ewing and L. Wang, *Phosphates as nuclear waste forms* vol. 48, 2002.
7. L. Merker and H. Wondratschek, "Bleiverbindungen mit Apatitstruktur, insbesondere Blei-Jod- und Blei-Brom-Apatite," *Zeitschrift für Anorganische und Allgemeine Chemie,* vol. 300, p. 41, 05// 1959.
8. F. Audubert, J. Carpena, J. L. Lacout, and F. Tetard, "Elaboration of an iodine-bearing apatite Iodine diffusion into a Pb3(VO4)2 matrix," *Solid State Ionics,* vol. 95, pp. 113-119, 2/2/ 1997.
9. K. Sudarsanan, R. A. Young, and A. J. C. Wilson, "The structures of some cadmiumapatites' Cd5 (MO4) 3X. I. Determination of the structures of Cd5 (VO4) 3I, Cd5 (PO4) 3Br, Cd3 (AsO4) 3Br and Cd5 (VO4) 3Br," *Acta Crystallographica Section B: Structural Crystallography and Crystal Chemistry,* vol. 33, pp. 3136-3142, 1977.
10. A. J. C. Wilson, K. Sudarsanan, and R. A. Young, "The structures of some cadmiumapatites' Cd5 (MO4) 3X. II. The distributions of the halogen atoms in Cd5 (VO4) 3I, Cd5 (PO4) 3Br, Cd5 (AsO4) 3Br, Cd5 (VO4) 3Br and Cd5 (PO4) 3Cl," *Acta Crystallographica Section B: Structural Crystallography and Crystal Chemistry,* vol. 33, pp. 3142-3154, 1977.
11. G. Baud, J. P. Besse, G. Sueur, and R. Chevalier, "Structure de nouvelles apatites au rhenium contenant des anions volumineux: Ba10(ReO5)6X2 (X = Br, I)," *Materials Research Bulletin,* vol. 14, pp. 675-682, 01 / 01 / 1979.
12. M. S. Schriewer and W. Jeitschko, "Preparation and Crystal Structure of the Isotypic Orthorhombic Strontium Perrhenate Halides Sr5(ReO5)3X (X = Cl, Br, I) and Structure Refinement of the Related Hexagonal Apatite-like Compound Ba5(ReO5)3Cl," *Journal of Solid State Chemistry,* vol. 107, pp. 1-11, 11// 1993.
13. D. E. Phebe and T. S. B. Narasaraju, "Preparation and characterization of hydroxyl and iodide apatites of calcium and their solid solutions," *Journal of Materials Science Letters,* vol. 14, pp. 229-231, 1995/01/01 1995.
14. N. J. Flora, K. W. Hamilton, R. W. Schaeffer, and C. H. Yoder, "A Comparative Study of the Synthesis of Calcium, Strontium, Barium, Cadmium, and Lead Apatites in Aqueous Solution," *Synthesis & Reactivity in Inorganic & Metal-Organic Chemistry,* vol. 34, pp. 503-521, 2004.
15. P. A. Henning, S. Lidin, and V. Petricek, "Iodo-oxyapatite, the first example from a new class of modulated apatites," *Acta Crystallographica,* vol. 55, pp. 165-169, 1999.
16. L. Campayo, A. Grandjean, A. Coulon, R. Delorme, D. Vantelon, and D. Laurencin, "Incorporation of iodates into hydroxyapatites: a new approach for the confinement of radioactive iodine," *Journal of Materials Chemistry,* vol. 21, pp. 17609-17611, 2011 2011.
17. D. Laurencin, D. Vantelon, V. Briois, C. Gervais, A. Coulon, L. Campayo*, et al.*, "Investigation of the local environment of iodate in hydroxyapatite by combination of X-

ray absorption spectroscopy and DFT modeling," *RSC Advances,* vol. 4, pp. 14700-14707, 01 / 01 / 2014.
18. F. Audubert, J. M. Savariault, and J. L. Lacout, "Pentalead tris(vanadate) iodide, a defect vanadinite-type compound," *Acta Crystallographica Section C: Crystal Structure Communications,* vol. 55, pp. 271-273, 03 / 15 / 1999.
19. M. Uno, M. Shinohara, K. Kurosaki, and S. Yamanaka, "Some properties of a lead vanado-iodoapatite $Pb_{10}(VO_4)_6I_2$," *J. Nucl. Mater.,* vol. 294, pp. 119-122, // 2001.
20. M. Zhang, E. R. Maddrell, P. K. Abraitis, and E. K. H. Salje, "Impact of leach on lead vanado-iodoapatite [Pb5(VO4)3I]: An infrared and Raman spectroscopic study," *Materials Science and Engineering: B,* vol. 137, pp. 149-155, 2/25/ 2007.
21. C. Guy, F. Audubert, J.-E. Lartigue, C. Latrille, T. Advocat, and C. Fillet, "New conditionings for separated long-lived radionuclides," *Comptes Rendus Physique,* vol. 3, pp. 827-837, 9// 2002.
22. L. Campayo, S. Le Gallet, Y. Grin, E. Courtois, F. Bernard, and F. Bart, "Spark plasma sintering of lead phosphovanadate $Pb_3(VO_4)_{1.6}(PO_4)_{0.4}$," *Journal of the European Ceramic Society,* vol. 29, pp. 1477-1484, 5// 2009.
23. T. Yao, F. Lu, H. Sun, J. Wang, R. C. Ewing, and J. Lian, "Bulk Iodoapatite Ceramic Densified by Spark Plasma Sintering with Exceptional Thermal Stability," *Journal of the American Ceramic Society,* vol. 97, pp. 2409-2412, 2014.
24. M. C. Stennett, I. J. Pinnock, and N. C. Hyatt, "Rapid synthesis of Pb5(VO4)3I, for the immobilisation of iodine radioisotopes, by microwave dielectric heating," *J. Nucl. Mater.,* vol. 414, pp. 352-359, // 2011.
25. F. Lu, T. Yao, J. Xu, J. Wang, S. Scott, Z. Dong*, et al.*, "Facile low temperature solid state synthesis of iodoapatite by high-energy ball milling," *RSC Advances,* vol. 4, pp. 38718-38725, 2014.
26. J. Wang, "Incorporation of iodine into apatite structure: a crystal chemistry approach using Artificial Neural Network," *Frontiers in Earth Science,* vol. 3, 2015.

ACKNOWLEDGEMENTS

This work is supported by US Department of Energy – Nuclear Energy University Program (NEUP) under the award # DE-NE0008257.

Journal of Materials Chemistry A

PAPER

View Article Online
View Journal | View Issue

Cite this: J. Mater. Chem. A, 2017, 5, 14331

Wet chemical synthesis of apatite-based waste forms – A novel room temperature method for the immobilization of radioactive iodine†

Charles Cao,[a] Saehwa Chong,[b] Lynn Thirion,[c] John C. Mauro,[c] John S. McCloy[b] and Ashutosh Goel*[a]

Received 8th January 2017
Accepted 13th June 2017

DOI: 10.1039/c7ta00230k

rsc.li/materials-a

Iodine isotopes make up ~0.69% of the fission products of ^{235}U slow neutron fission, *i.e.* ~360 g iodine per metric ton of ^{235}U. The currently proposed technology for the removal of iodine from reprocessing plant off-gas is to pass it through a caustic scrubber (using ~1–2 M NaOH) to form NaI, $NaIO_3$ and possibly NaOI, or to pass it through Ag-containing solid sorbents to form chemisorbed AgI. Since iodine is not amenable to conventional vitrification routes because of its poor incorporation into borosilicate glass chemistry and high volatilization at temperatures >500 °C, considerable effort is being made to develop alternative waste forms for the immobilization of iodine at low temperatures (<100 °C). In this paper, a novel wet chemical synthesis method has been described for immobilizing radioactive iodine obtained from caustic scrubber solutions and silver solid sorbents into the apatite, $Pb_{10}(VO_4)_6I_2$, at room temperature. The uptake of iodine for the synthesized waste form has been shown to be 94.6%. In addition, investigation into the formation of solid solutions in the systems, $Pb_{(10-x)}Ca_x(VO_4)_6I_2$ and $Pb_{10}(VO_4)_{(6-y)}(PO_4)_yI_2$, by the proposed method has been discussed. The study provides an easy pathway to design novel waste forms for the immobilization of large volumes of radioactive iodine at room temperature and a methodology to potentially synthesize new compositions of iodide-containing apatites.

1. Introduction

The radioactive fission product ^{129}I has many aspects which make it problematic for immobilization and storage in an engineered nuclear waste form, and much research has been devoted to obtaining satisfactory solutions to these challenges, as has been recently reviewed.[1] The long half-life of ^{129}I (1.6×10^7 years) combined with its high solubility in water (in the anionic state) and the technical challenges associated with its capture in conventional radioactive waste forms pose serious concerns for its long-term geological disposal. In the UK and France where nuclear fuel reprocessing is practiced, the iodine fission products (both stable ^{127}I and radioactive ^{129}I) are currently discharged to the sea, relying on isotope dilution to reduce exposure risk.[2] However, considering anticipated future regulatory changes in the international community, it will become necessary to review this strategy and develop durable waste forms for the immobilization of ^{129}I.[3] In addition, meeting the current U.S. regulations (Code of Federal Regulations, CFRs, relating to the Environmental Protection Agency, EPA, and Nuclear Regulatory Commission, NRC) that are imposed on any nuclear fuel reprocessing facility requires the capture of several volatile radionuclides, namely ^{3}H, ^{14}C, ^{85}Kr, and ^{129}I, which are projected to partition to the off-gas streams in current designs for reprocessing plants. The current requirement for iodine, based on considerations of the total quantity of radioactive materials entering the general public (EPA 40 CFR 190.10) and dose limits to individual members of the public (NRC 10 CFR 20), requires an overall plant decontamination factor of ~2000 for ^{129}I, necessitating a coherent iodine management strategy for plant operations.[1,4] (For discussion of the metric of the decontamination factor, readers are referred to ref. 1). Therefore, it is imperative that solutions be developed where radioiodine can be captured, treated, and immobilized for safe disposal, where controlled release can be maintained on a geological time scale.

At present, iodine capture methods in radioactive waste reprocessing facilities mainly fall under two categories: (i) wet scrubbing, and (ii) solid sorbents.[1] In the case of wet scrubbing, the most commonly implemented technique is known as caustic scrubbing. With the use of ~1–2 M NaOH, iodine off-gas is converted to various NaI, $NaIO_3$, and possibly NaOI species in solution, based on the disproportionation shown in reaction (1).[1]

[a]Department of Materials Science and Engineering, Rutgers, The State University of New Jersey, Piscataway, NJ, USA. E-mail: ag1179@soe.rutgers.edu; Tel: +1-848-445-4512

[b]School of Mechanical and Materials Engineering and Materials Science & Engineering Program, Washington State University, Pullman, WA, USA

[c]Science and Technology Division, Corning Incorporated, Corning, NY, USA

† Electronic supplementary information (ESI) available. See DOI: 10.1039/c7ta00230k

$$3I_2(g) + 6OH^-(aq) \rightarrow 5I^-(aq) + IO_3^-(aq) + 3H_2O(l) \quad (1)$$

Often in conjunction with wet scrubbing, solid sorbents are utilized to maximize the collection of iodine off-gas. Owing to its affinity for iodine, Ag is often selected as the primary metal when determining the composition of the capture media, whether that be $AgNO_3$-loaded alumina,[5] $AgNO_3$-loaded silica,[6,7] Ag-loaded zeolites,[8] or Ag-functionalized silica aerogels.[9] Upon reaction with iodine off-gas, Ag-solid sorbents are postulated to form AgI, examples of which are shown in reactions ((2)–(5)).[1]

$$3I_2(g) + 6\,AgNO_3(s) \rightarrow 4AgI(s) + 2AgIO_3(s) + 6NO_2(g) \quad (2)$$

$$CH_3I(g) + AgNO_3(s) \rightarrow CH_3NO_3(g) + AgI(s) \quad (3)$$

$$I_2(g) + 2Ag(s) \rightarrow 2AgI(s) \quad (4)$$

$$2CH_3I(g) + 2H_2O(g) + AgI(s) \rightarrow 2AgI(s) + 2CH_3OH(g) + H_2(g) \quad (5)$$

One major challenge in developing waste forms for the immobilization of radioactive iodine is that it is not amenable to conventional borosilicate vitrification routes, the standard waste form for most nuclear waste management, because of its poor incorporation into silicate glass chemistries.[10] More importantly, iodine, when included as a component in oxide glasses at typical glass processing temperatures (1000–1100 °C), exhibits high volatility and leaves the glass melt as a gas above 500 °C.[1] Therefore, considerable effort is being made to develop waste form alternatives to glass, processed at low temperatures, for iodine immobilization.[11–16] Most proposed waste forms to date, however, have not achieved sufficient maturity and satisfactory properties (specifically: ease of processing, high waste loading, and high chemical durability) to be considered as baseline technologies.[1,17]

Apatites (general formula, $A_{10}(BO_4)_6X_2$; A and B are cations, X is an anion) have been long considered as one of the most promising candidate waste forms for the immobilization of radioactive iodine.[12,18–20] This is primarily due to their unique channel structure that allows the halide ions to be incorporated into their crystal structure,[21] their good chemical durability,[17] and their high radiation stability.[22,23] Experimentally, most investigated apatites can accommodate either F^-, Cl^-, Br^-, O^{2-}, OH^- and/or CO_3^{2-} in their X-anion site. The choice of apatite minerals where the X-anion site in the structural channel is occupied by I^- or IO_3^-, however, is highly limited due to the large size of iodide/iodate ions. Due to this reason, most of the recent research in this area has focused on only two apatite based minerals – $Ca_{10}(PO_4)_6(IO_3)_{2-x}(OH)_x$ (ref. 12 and 14) and $Pb_{10}(VO_4)_6I_2$.[18,23–26] While $Ca_{10}(PO_4)_6(IO_3)_{2-x}(OH)_x$ is an interesting candidate, it is plagued by complex synthesis routes (N_2 atmosphere and controlled pH by wet-chemical precipitation[12] or formation of low iodide loading (~6.5 wt%) calcium phosphate cements[14]) in comparison to >8 wt% for $Pb_{10}(VO_4)_6I_2$.[24] Due to these reasons, $Pb_{10}(VO_4)_6I_2$ has been the most favorable choice of candidate waste forms for iodine immobilization.[21]

While $Pb_{10}(VO_4)_6I_2$ possesses two of the most desirable features required for any waste form, *i.e.* high iodine loading (>8 wt%),[24] and acceptable chemical durability (3.98×10^{-5} g cm^{-2} d^{-1} as per MCC-5, 7-day Soxhlet leaching test[17]), there are two big challenges associated with this waste form – (i) poor densification behavior affecting the chemical durability of the waste form, and (ii) difficulty of synthesis and processing. The solution to the first problem was found by Guy *et al.*[25] wherein they reported that partial substitution of $(VO_4)^{3-}$ with $(PO_4)^{3-}$ results in a theoretical apatite composition $Pb_{10}(VO_4)_{4.8}(PO_4)_{1.2}I_2$, which not only lowers the (reactive) sintering temperature of the mineral from 700 °C to 540 °C, but also improves the densification of the apatite powder, thus reducing its total surface area and enhancing its chemical durability. However, the solution to the second problem is still to be found as most of the routes employed for the synthesis of these apatite minerals involve high temperatures (550–800 °C), and pressures.[17,23,26–29] Since iodine tends to volatilize from relevant compounds at temperatures >500 °C, all these methods have to be performed in highly controlled and sealed environments which further adds to the complexity of the synthesis. Therefore, it is highly desired to find a route for the synthesis and consolidation of these minerals at temperatures lower than 500 °C using simplified processes which can be employed in industrial settings. In this pursuit, a low temperature (~200 °C) solid state synthesis of $Pb_{10}(VO_4)_6I_2$ using high energy ball milling has been proposed by Lu *et al.*[30] The method employs high energy ball milling of a mixture of PbI_2, PbO, and V_2O_5 at ~50 °C followed by thermal annealing of ball milled powder at 200 °C to form the desired apatite phase. Although promising, it still involves a two-step synthesis process, *i.e.* (i) ball milling and (ii) annealing, thus, adding complexity to its implementation in a practical scenario. Furthermore, the choice of the iodine precursor (PbI_2) may not be the most appropriate from the viewpoint of existing or proposed technologies to be used for iodine capture in nuclear waste facilities.[1]

In this paper, we have presented a novel approach to synthesize $Pb_{10}(VO_4)_6I_2$ based apatite waste forms at temperatures <40 °C using wet chemistry. The choice of precursors used in this study makes the proposed synthesis route an attractive candidate for the immobilization of iodine waste extracted from caustic scrubbers or silver-loaded solid sorbents, generally used in most of the nuclear waste reprocessing facilities around the world.[1] In addition, the possibility of the formation of $Pb_{(10-x)}Ca_x(VO_4)_6I_2$ and $Pb_{10}(VO_4)_{(6-y)}(PO_4)_yI_2$ solid solutions has been discussed. The reason for choosing $Pb^{2+} \leftrightarrow Ca^{2+}$ substitution in these apatites is based on the fact that $Pb_{(10-x)}Ca_x(VO_4)_6X_2$ and $Pb_{(10-x)}Ca_x(PO_4)_6X_2$ have been reported where X = OH, F, Cl, or Br[31–34] but $Pb_{(10-x)}Ca_x(VO_4)_6I_2$ compounds have not been reported to the best of our knowledge. With respect to the partial substitution of $(VO_4) \leftrightarrow (PO_4)$, as has been discussed earlier, phosphate substitution in these apatites facilitates their sintering at lower temperatures.[25] Our aim is to synthesize these minerals at ambient temperature using a simple and industrially scalable method.

2. Experimental

The chemistry of precursors plays a crucial role in this synthesis method as all the precursors should exhibit high solubility in water. Accordingly, $Pb(NO_3)_2$ (99.0% min, Alfa Aesar) and Na_3VO_4 (99.9% metals basis, Alfa Aesar) were used as precursors for lead and vanadium ions, respectively. The choice of PbI_2 and NH_4VO_3 as precursors of lead and vanadium will not lead to the formation of the desired product. NaI (99.9% metals basis, Alfa Aesar) and AgI (99%, Acros Organics) have been used as iodine precursors in compliance with the sources of radioactive iodine extracted from caustic scrubbers or Ag-loaded solid sorbents, respectively.

The chemical precursors used for calcium and phosphate in the synthesis of solid solutions were $Ca(NO_3)_2\cdot 4H_2O$ (99%, Alfa Aesar) and K_3PO_4 (≥98%, Sigma Aldrich), respectively. K_3PO_4 was chosen as the phosphate precursor over Na_3PO_4 after our preliminary experimental analysis suggested that powders obtained using the former had higher crystallinity than those synthesized using the latter.

Two different synthesis routes were applied to produce apatite waste forms depending on the iodine precursor (NaI *vs.* AgI). The step-by-step synthesis of $Pb_{10}(VO_4)_6I_2$ has been described below.

2.1 NaI as iodine precursor

Step 1. The required amounts of $Pb(NO_3)_2$, Na_3VO_4 and NaI in accordance with reaction (6) are weighed and dissolved in deionized water on an individual basis.

$$10Pb(NO_3)_2 + 6Na_3VO_4 + 2NaI \rightarrow Pb_{10}(VO_4)_6I_2 + 20NaNO_3 \quad (6)$$

In our study, 9.936 g $Pb(NO_3)_2$, 3.31092 g Na_3VO_4, and 0.89934 g NaI were dissolved in 300 ml deionized water separately in three different beakers, corresponding to a 0.1 M solution of $Pb(NO_3)_2$, a 0.06 M solution of Na_3VO_4, and a 0.02 M solution of NaI. All the solutions were magnetically stirred for 1 h. The concentration of precursor solutions was kept low to ensure that all the precursors react completely.

Step 2. Mix 0.02 M NaI solution with 0.06 M Na_3VO_4 solution and stir for 1 h.

Step 3. Add 0.1 M $Pb(NO_3)_2$ solution to 0.02 M NaI + 0.06 M Na_3VO_4 solution obtained from Step 2 in a drop-by-drop manner.

Step 4. Allow the solution from Step 3 to stir for an additional 3 h ensuring the thorough formation of precipitates. The obtained precipitates are washed with deionized water and dried overnight at 70–80 °C.

The synthesis (including mixing of precursor solutions) was performed at ambient temperature (~30 °C). It was observed that temperatures higher than 45 °C (in particular for the aqueous solution of NaI and Na_3VO_4 prior to the formation of precipitates in Step 3) favored the formation of $Pb_{10}(VO_4)_6(OH)_2$ along with $Pb_{10}(VO_4)_6I_2$ considering that OH^- has a higher affinity (than I^-) to be incorporated into an X-anion site of $A_{10}(BO_4)_6X_2$ apatite due to its smaller ionic size.[21] Furthermore, no acid or base was added to control the pH of the final solution or to precipitate the apatite mineral, unlike the methodology used in the synthesis of halide-containing calcium phosphate apatites.[12,35] The addition of HNO_3 or NaOH (even in small concentrations) to the reaction medium will result in the formation of powders with undesired crystalline phases including, for example, chervetite, $Pb_2V_2O_7$, iodolaurionite, Pb(OH)I, (when HNO_3 is added) or hydroxyvanadinite, $Pb_{10}(VO_4)_6(OH)_2$ (when NaOH is added).

2.2 AgI as iodine precursor

The synthesis of apatites using AgI as the starting material poses a challenge considering its low solubility in water (3×10^{-7} g at 20 °C). Therefore, iodine was stripped off from silver and converted to water soluble NaI using reaction (7).

$$2AgI(s) + Na_2S(aq) \rightarrow 2NaI(aq) + Ag_2S(s) \quad (7)$$

In order to convert AgI to NaI, 0.72054 g $Na_2S\cdot 9H_2O$ (98.0% min, ACS Certified, Alfa Aesar) was dissolved in 300 ml deionized water and allowed to stir for 1 h at room temperature (25–30 °C). Finally, 1.40862 g AgI was added to the $Na_2S\cdot 9H_2O$ solution to produce 300 ml of 0.02 M NaI solution, in accordance with reaction (7). The experiments were performed in two different sets: (i) in an ambient environment and (ii) under a continuous flow of argon in a 3-neck flask. The hypothesis for performing this experiment in the presence of argon was to check if the exposure of aqueous sodium sulfide to air, as noted in reaction (8), has any significant effect on the conversion of AgI to NaI, given that the thiosulfate ion is not expected to substitute for iodide as the sulfide ion would.[36]

$$2Na_2S(s) + 2O_2(g) + H_2O(l) \rightarrow Na_2S_2O_3(aq) + 2NaOH(aq) \quad (8)$$

The successful execution of reaction (7) results in a NaI aqueous solution, while black-colored Ag_2S precipitates at the bottom of the flask. After removal of Ag_2S (*i.e.* filtration or centrifugation), the remaining 0.02 M NaI aqueous solution can further be used to synthesize iodoapatite powder as described in Section 2.1. It is noteworthy that conversion of AgI to NaI can also be performed using anhydrous Na_2S. However, due to the highly hygroscopic nature of Na_2S, the formation of a hydrate analogue is very likely in a humid ambient environment.

2.3 Synthesis of solid solutions

In order to synthesize $Pb_{(10-x)}Ca_x(VO_4)_6I_2$ and $Pb_{10}(VO_4)_{(6-y)}(PO_4)_yI_2$ solid solutions, the methodology is defined by the chemistry of apatites. In general, the structure of apatites with the general formula $A_{10}(BO_4)_6X_2$ consists of two cations, *i.e.* A and B, where A-cations individually occupy two functionally different sites within the crystal structure, while B-cations are found as tetrahedral units with oxygen in their specific site.[37] Theoretically, both Pb^{2+} and Ca^{2+} can be substituted at the A-cation sites, while V^{5+} and P^{5+} can be substituted at the B-cation site.[32] Accordingly, during synthesis of $Pb_{(10-x)}Ca_x(VO_4)_6I_2$ apatites, aqueous solutions of $Pb(NO_3)_2$ and $Ca(NO_3)_2\cdot 4H_2O$ (A-cation

solutions) have to be mixed completely before adding the resultant solution (drop-by-drop) to the aqueous solution of 0.02 M NaI + 0.06 M Na_3VO_4 in Step 3 of the synthesis route described in Section 2.1.

Similarly, during synthesis of $Pb_{10}(VO_4)_{(6-y)}(PO_4)_yI_2$ apatites, aqueous solutions of Na_3VO_4 and K_3PO_4 (B-cation solutions) of desired molarities need to be mixed completely with 0.02 M NaI, prior to the addition of $Pb(NO_3)_2$ in Step 3 of the synthesis route described above. If the precursors are mixed in an incorrect sequence, the solution will prematurely precipitate an undesired mineral and apatite synthesis will no longer be possible.

The qualitative and quantitative crystalline phase analyses of dried powders were performed by X-ray diffraction (XRD; PANalytical X'Pert Pro MPD; Cu-K_α source at 45 keV and 40 mA; 2θ = 10–90° with a 0.002° 2θ step size and a dwell time of 5.7 s). 5 or 10 wt% ZnO (NIST SRM-674b) was used as an internal standard. The quantitative phase analysis was performed by the Rietveld – Reference Intensity Ratio (RIR) method using PANalytical HighScore software. The structural analysis of powder samples was performed by Raman spectroscopy (Renishaw inVia Raman microscope; 633 nm wavelength laser, operating at 10% power; acquisition dwell time = 40 s from the range of 100–1700 cm^{-1} with a 50× objective). X-ray fluorescence (XRF; Epsilon 1, PANalytical B.V.; Ag anode) was used to quantify the elemental composition in powder samples. To improve quantification, oxygen was attributed to any potential B-site cations present due to their inability to be detected individually. The iodine concentration in the remnant solution was analyzed by inductively coupled plasma – mass spectroscopy (ICP-MS; PerkinElmer). The microstructural observations were done on gold sputtered powdered samples using a scanning electron microscope (SEM; ZEISS Sigma FE-SEM).

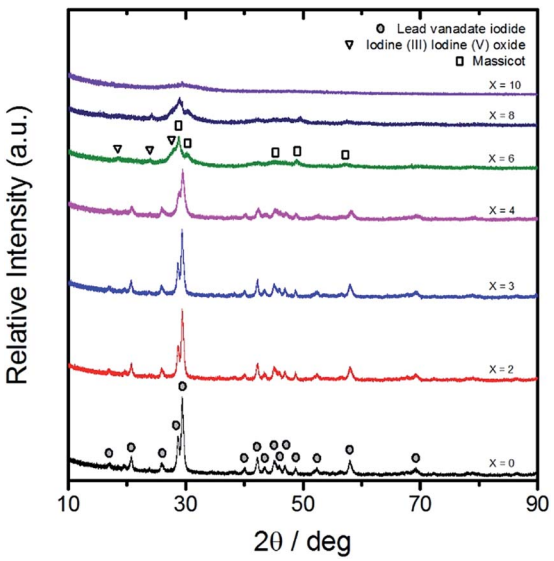

Fig. 1 XRD patterns of the $Pb_{(10-x)}Ca_x(VO_4)_6I_2$ apatite series (x = 0–10).

3. Results

3.1 Synthesis of the $Pb_{10-x}Ca_x(VO_4)_6I_2$ series (using NaI)

Fig. 1 presents the XRD data of powder samples from the series, $Pb_{(10-x)}Ca_x(VO_4)_6I_2$, where x varies between 0 and 10. For sample x = 0, the XRD data show intense phase reflections corresponding to the $Pb_{9.85}(VO_4)_6I_{1.7}$ (PDF#97-028-0065) phase, thus confirming the synthesis of the lead vanadate iodide (apatite) mineral. The deviation from the ideal stoichiometric formula of $Pb_{10}(VO_4)_6I_2$ is attributed to the presence of stoichiometric deficiencies in the structure as has been explained by Audubert *et al.*[38] The quantitative crystalline phase analysis of this sample (Table 1) reveals the presence of ~53 wt% crystallinity in the sample. The SEM analysis (Fig. 2a and b) of the as synthesized mineral reveals strongly spheroidal, agglomerated, nanoscale (<200 nm) crystals that are consistent with previous studies of lead phospho-vanadate based apatites.[29,39]

The gradual substitution of Ca^{2+} for Pb^{2+} in the theoretical apatite composition of $Pb_{(10-x)}Ca_x(VO_4)_6I_2$ resulted in broadening of XRD peaks. The quantitative crystalline phase analysis of these samples reveals an increase in amorphous content in samples with increasing Ca^{2+}/Pb^{2+} ratio (in particular for x = 6–10) with sample x = 10 being completely amorphous (Fig. 1). From the viewpoint of the formation of solid solutions, lead vanadate iodide, $Pb_{9.85}(VO_4)_6I_{1.7}$, was the only phase for the sample with x = 2. For x = 3, minor amounts (~5 wt%) of the hydroxyvanadinite phase ($Pb_{9.262}(VO_4)_6(OH)_{1.4}$; PDF#97-015-5416) were observed with $Pb_{9.85}(VO_4)_6I_{1.7}$ still being the dominant phase. Further increase in the Ca^{2+}/Pb^{2+} ratio (at x = 4) resulted in crystallization of ~2.4 wt% litharge (PbO; PDF#97-006-2842; tetragonal) along with lead vanadate iodide and

Table 1 Rietveld refinement of the $Pb_{(10-x)}Ca_x(VO_4)_6I_2$ apatite series (x = 0–10)

		Phase wt%					
x	Sample formula	Amorphous	Lead vanadate iodide $Pb_{9.85}(VO_4)_6I_{1.7}$	Hydroxyvanadinite $Pb_{9.262}(VO_4)_6(OH)_{1.4}$	Litharge PbO	Massicot PbO	Iodine(III) iodine(V) oxide I_2O_4
0	$Pb_{10}(VO_4)_6I_2$	46.8	53.2				
2	$Pb_8Ca_2(VO_4)_6I_2$	50.4	49.5				
3	$Pb_7Ca_3(VO_4)_6I_2$	44.1	50.9	5.0			
4	$Pb_6Ca_4(VO_4)_6I_2$	46.4	41.4	9.8	2.4		
6	$Pb_4Ca_6(VO_4)_6I_2$	78.1	13.9			5.2	2.9
8	$Pb_2Ca_8(VO_4)_6I_2$	83.6	8.9			6.6	0.9
10	$Ca_{10}(VO_4)_6I_2$	100.0					

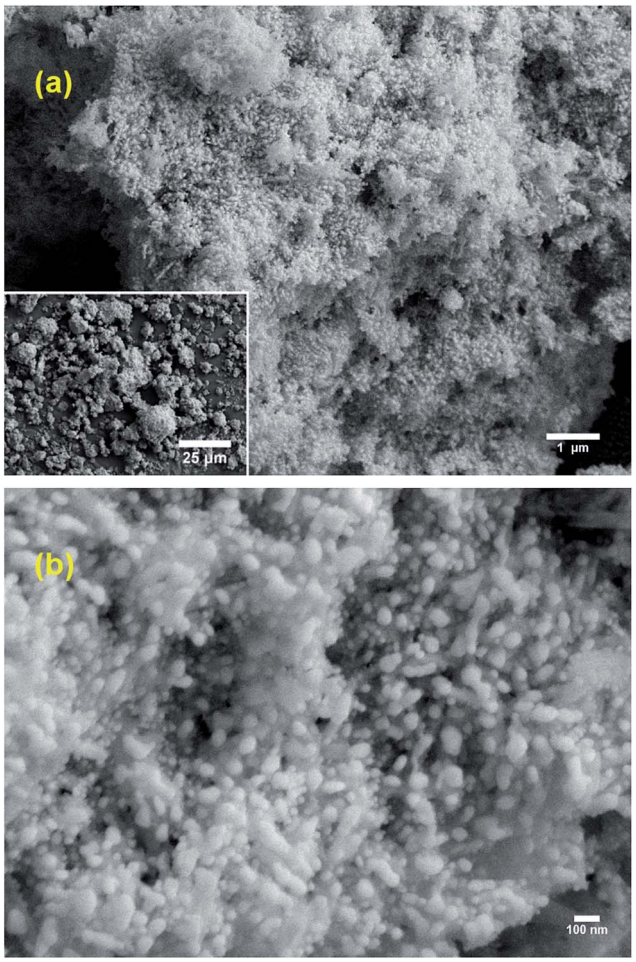

Fig. 2 SEM image of $Pb_{10}(VO_4)_6I_2$ apatite powder at magnification (a) 10k×, and (b) 50k×. The inset on the bottom left of (a) shows a low magnification (1k×) image of agglomerates.

hydroxyvanadinite, with $Pb_{9.85}(VO_4)_6I_{1.7}$ still being the primary crystalline phase (~41 wt%). For samples $x = 6$ and 8, the amorphous content in the samples significantly increased from 46.4 wt% (at $x = 4$) to 78 wt% (at $x = 6$) and 83.6 wt% (at $x = 8$). While lead vanadate iodide was still the primary crystalline phase in both the samples, massicot (PbO; PDF#97-065-3900; orthorhombic) and I_2O_4 (PDF#97-007-8386) were found in their crystalline phase assemblages at minor concentrations.

XRD data suggest the formation of apatite structure solid solutions in $Pb_{(10-x)}Ca_x(VO_4)_6I_2$ for $x = 0$–3. However, the chemical compositions of the synthesized mineral powders and their respective remnant reactant solutions, which were analyzed by XRF (Table 2) and ICP-MS (Table 3), respectively, suggest otherwise. The results obtained from chemical analysis of powder samples and reactant solutions are summarized below.

(i) The synthesized $Pb_{10}(VO_4)_6I_2$ apatite exhibited an iodine loading of ~9.4 wt% as deduced by XRF spectroscopy. This is close to the theoretical value of 8.4 wt% as calculated for stoichiometric $Pb_{10}(VO_4)_6I_2$. The concentration of iodine decreased from 2600 ppm (mg l^{-1}) in the precursor solution (0.02 M NaI) to 140 ppm in the remnant reactant solution after synthesis of $Pb_{10}(VO_4)_6I_2$ apatite (as shown in Table 3), thus, demonstrating an uptake of 94.62%.

(ii) XRF data reveal that a negligible amount of calcium was incorporated into the apatite crystal structure, thus suggesting that the A-cation sites in the structure were dominantly occupied by Pb^{2+} ions. The as synthesized $Pb_{10}(VO_4)_6I_2$ ($x = 0$) apatite contained ~990 ppm calcium (Table 2) which may be attributed to impurities present in the precursor materials. For minerals with ideal composition $Pb_{(10-x)}Ca_x(VO_4)_6I_2$ with x varying between 2 (2.99 wt%) and 4 (6.83 wt%), the concentration of calcium in the experimental analogues was found to be constant at ~0.32 wt%. Further increase in calcium content ($x =$ 6–10) in the ideal apatite composition induced high concentrations of amorphous character in their experimental analogues which allowed accommodation of significantly higher amounts of calcium as shown in Table 2. These results were corroborated by ICP-MS analysis of the remnant reactant solution where the concentration of Ca^{2+} was found to increase from 0.824 ppm (for $x = 0$) to 780 ppm (for $x = 10$) implying that most calcium stayed back in the solution as opposed to being incorporated into the crystal structure.

Since substitution of Ca^{2+} for Pb^{2+} in the $Pb_{(10-x)}Ca_x(VO_4)_6I_2$ series induced a highly amorphous character in the synthesized minerals, Raman spectroscopy was used to study their structural transformations. Fig. 3 presents the Raman spectra of all the as synthesized minerals ($x = 0$–10). The Raman spectrum of $Pb_{10}(VO_4)_6I_2$ ($x = 0$) apatite exhibits a sharp band at 824 cm^{-1} corresponding to ν_1 symmetric stretching, followed by a shoulder at 777 cm^{-1} and a small band at ~698 cm^{-1} depicting the ν_3 antisymmetric stretching of V–O bonds.[40,41] The

Table 2 XRF analysis of select apatites. Th. And Exp. are theoretical and experimental weight percent, respectively

	Normalized weight%									
Intended sample	Th. Pb%	Exp. Pb%	Th. Ca%	Exp. Ca%	Th. VO_4%	Exp. VO_4%	Th. PO_4%	Exp. PO_4%	Th. I%	Exp. I%
$Pb_{10}(VO_4)_6I_2$	68.71	70.3606	0	991 ppm	22.87	19.6800	0	0.5210	8.42	9.4384
$Pb_8Ca_2(VO_4)_6I_2$	61.82	70.0900	2.99	0.3183	25.72	19.7768	0	1.0371	9.47	8.7777
$Pb_6Ca_4(VO_4)_6I_2$	52.97	70.5788	6.83	0.3219	29.38	21.3383	0	1.0244	10.81	6.7366
$Pb_4Ca_6(VO_4)_6I_2$	41.18	64.8398	11.95	3.9584	34.26	29.8946	0	1.0115	12.61	0.2957
$Pb_2Ca_8(VO_4)_6I_2$	24.69	50.6042	19.10	11.7761	41.09	36.9168	0	0.7029	15.12	882 ppm
$Ca_{10}(VO_4)_6I_2$	0	67 ppm	29.81	35.1371	51.30	64.3260	0	0.5369	18.88	808 ppm
$Pb_{10}(VO_4)_5(PO_4)I_2$	69.17	71.7276	0	0.3332	19.22	15.6740	3.17	3.8088	8.47	8.4564

Table 3 ICP-MS analysis of select apatite synthesis remnant solutions

		Concentrations in mg L^{-1} (ppm)						
Sample	pH	Pb	Ca	V	P	I	Na	K
$Pb_{10}(VO_4)_6I_2$	3.53	~2400	0.824	<0.010	<0.050	140	~970	1.41
$Pb_8Ca_2(VO_4)_6I_2$	3.96	~800	~200	<0.010	<0.050	140	~790	1.41
$Pb_6Ca_4(VO_4)_6I_2$	4.80	6.6	~440	<0.010	<0.050	300	~870	1.61
$Pb_4Ca_6(VO_4)_6I_2$	9.10	0.016	~500	13.8	<0.050	530	~800	1.49
$Pb_2Ca_8(VO_4)_6I_2$	9.89	<0.010	~570	~90	<0.050	540	~880	1.63
$Ca_{10}(VO_4)_6I_2$	10.36	<0.010	~780	~120	0.168	670	~1200	2.08
$Pb_{10}(VO_4)_5(PO_4)I_2$	4.01	~1600	0.32	0.015	<0.050	170	~660	286
NaI reference	6.20	0.013	0.16	<0.010	<0.050	2600	~480	0.605

multiple bands in the low wavenumber region of 300–400 cm^{-1} mainly correspond to the ν_3 bending vibrations of O–V–O bonds.[41] The band at 161 cm^{-1} is presumably attributed to the libration of VO_4 parallel to the *c*-axis.[40] Similar spectra were observed for minerals with $x = 0$–4, thus, confirming minimal structural changes due to calcium incorporation. A weak band (shoulder) can be observed at 877 cm^{-1} for mineral $x = 0$ which gradually disappears with increasing calcium concentration from $x = 0$–4. This band was not observed by Zhang *et al.*[41] in their Raman spectra of $Pb_{10}(VO_4)_6I_2$ apatite. The band has been attributed to the symmetric stretching of VO_3 units in $(HVO_4)^{2-}$ and $(V_2O_7)^{4-}$ species in aqueous vanadate solutions, as observed by Griffith and Wickins,[42] and is hypothesized to be a product of the variances in solution pH among the different compositions.

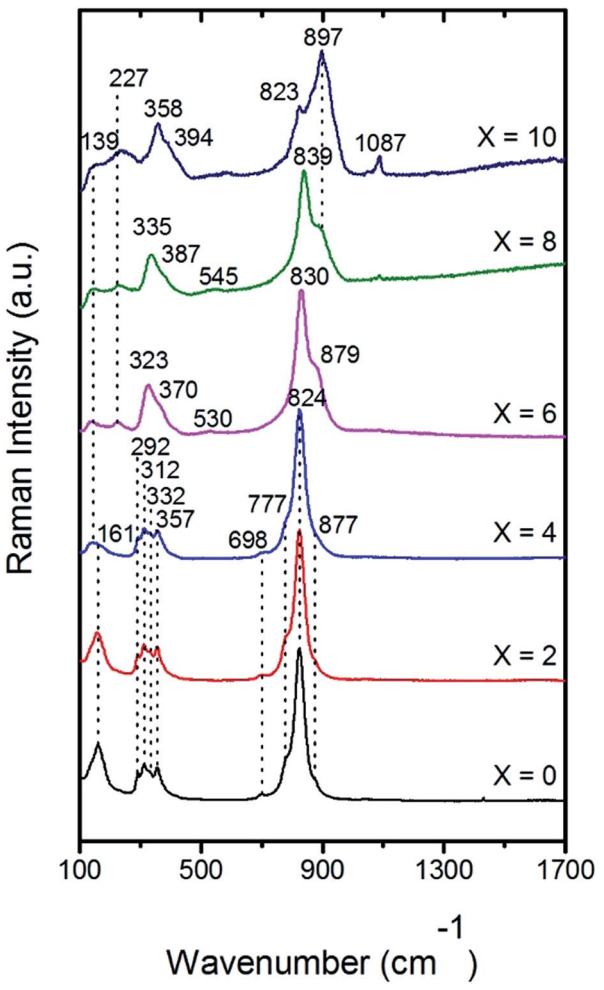

Fig. 3 Raman spectra of the $Pb_{(10-x)}Ca_x(VO_4)_6I_2$ apatite series ($x = 0$–10).

For $x = 6$–10, noticeable structural transformations occur in the synthesized minerals as is evident from their Raman spectra. The first evident observation was the broadening of Raman bands, which is typical for highly amorphous materials. The bands at 830 cm^{-1} and 839 cm^{-1} corresponding to the ν_1 symmetric stretching of V–O bonds in the apatite structure were still the most intense structural features in minerals with $x = 6$ and 8, respectively, thus corroborating the quantitative XRD results. The band at 877 cm^{-1}, corresponding to the symmetric stretching of VO_3 units, became highly prominent in the spectra of the sample with $x = 6$, while this band shifted to 897 cm^{-1} for samples $x = 8$ and 10.[42] Interestingly, the band at 897 cm^{-1} became the most intense band for the sample $x = 10$, while the band corresponding to the ν_1 symmetric stretching of V–O bonds in apatite structures appeared as a minor feature centered at ~823 cm^{-1}. This implies a dominance of amorphous $(V_2O_7)^{4-}$ structural species in the sample $x = 10$. This assertion gains support due to the presence of a broad band at ~227 cm^{-1} and an intense band in the region 300–400 cm^{-1} in samples with $x = 6$–10 confirming the presence of $(V_2O_7)^{4-}$ units.[42] The presence of amorphous $(V_2O_7)^{4-}$ units in these minerals ($x = 6$–10) is also supported by the fact that the addition of any acid during synthesis has been shown to produce chervetite ($Pb_2V_2O_7$) instead of apatite (as reported in the Experimental section of the paper). Therefore, it is highly likely that amorphous $Ca_2V_2O_7$ may have been formed in these minerals due to the deviation from ideal crystalline synthesis conditions and the analogous nature between the two cations, Pb^{2+} and Ca^{2+}.

3.2 Synthesis of the $Pb_{10}(VO_4)_{(6-y)}(PO_4)_yI_2$ series (using NaI)

Fig. 4 presents the X-ray diffractograms, while Table 4 presents the quantitative phase analysis of powder samples from the series, $Pb_{10}(VO_4)_{(6-y)}(PO_4)_yI_2$, where y varies between 0 and 2.

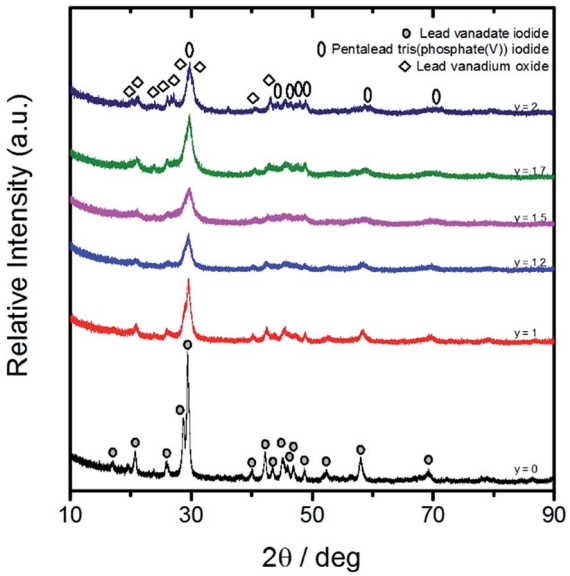

Fig. 4 XRD patterns of the $Pb_{10}(VO_4)_{(6-y)}(PO_4)_yI_2$ apatite series ($y = 0$–2).

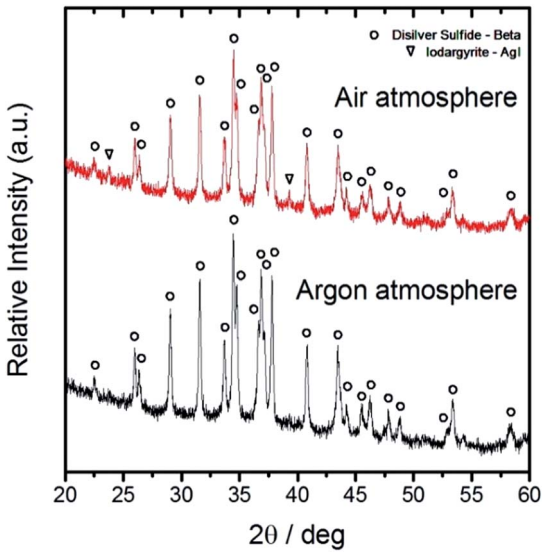

Fig. 5 XRD patterns of Ag_2S powders obtained from conversion of AgI (air environment *vs.* argon environment).

The XRD phase analysis of minerals with $y > 2$ has not been presented, as the $Pb_{10}(VO_4)_{(6-y)}(PO_4)_yI_2$ solid solution did not exist for $y \geq 2$ (as evidenced by the absence of vanadate-containing apatite phases).

For $y = 1$, a large percentage (40.8%) of the lead vanadate iodide apatite phase is present along with traces (3.4 wt%) of the OH-analogue, $Pb_{10}(VO_4)_6(OH)_2$, and a non-apatite phase, litharge (4.6 wt%), PbO. Furthermore, as the phosphate content increases, the XRD peaks become much broader. The presence of non-apatite phases along with broadening of XRD phase reflections suggests the structural disorder induced in the apatite structure due to substitution of smaller phosphate ions for larger vanadate ions. An attempt was made to understand the phosphate speciation in the structure of the as synthesized minerals using Raman spectroscopy.

However, due to an overlap between the Raman bands of vanadate and phosphate units at 290–580 and 770–950 cm^{-1}, no conclusions could be drawn (Fig. S1, ESI†).[40] However, the XRF (of powders) and ICP-MS (of liquid aliquots) data support the formation of solid solutions for the partial substitution of $(VO_4) \leftrightarrow (PO_4)$ as summarized below.

(i) When $y = 1$, the experimental weight percent of phosphate within the synthesized apatite mineral was 3.8 wt%, as seen in the XRF data in Table 2. This is in good agreement with the theoretical concentration (3.17 wt%) of phosphate ions present in the mineral.

(ii) The compositional analysis of the remnant reactant solution supports the hypothesis of solid solution formation as seen in the ICP-MS data present in Table 3. When $y = 1$, the concentration of phosphate ions remains at a low level when compared to the base apatite, $Pb_{10}(VO_4)_6I_2$, which does not undergo cation substitution. This is opposite to the observations made in the $Pb_{(10-x)}Ca_x(VO_4)_6I_2$ series where the calcium concentration in remnant solutions was found to increase with increasing the value of x. This further suggests that the phosphate ions are incorporated into the apatite crystal structure.

As is evident from XRD data (Table 4), a solid solution does not exist at $y = 2$. A combination of amorphous content and several crystalline phases, such as lead vanadium oxide ($Pb_{2.667}V_{1.333}O_{5.96}$), pentalead tris(phosphate) iodide ($Pb_{10}(PO_4)_6I_2$), and decalead hexakis(phosphate(v))dihydroxide ($Pb_{10}(PO_4)_6(OH)_2$), was observed. Therefore, several apatite syntheses were performed with values of y varying between 1 and 2 to find the limit of substitution of phosphate for vanadate ions in the apatite structure. The threshold limit of $(PO_4) \leftrightarrow (VO_4)$ substitution in $Pb_{10}(VO_4)_{(6-y)}(PO_4)_yI_2$ was found to be $y = 1.5$ (8.33 mol% or 4.77 wt%). Non-apatite phases were observed in the sample with $y = 1.7$.

Table 4 Rietveld refinement of the $Pb_{10}(VO_4)_{(6-y)}(PO_4)_yI_2$ apatite series ($y = 1$, 2)

		Phase wt%						
y	Sample formula	Amorphous	Lead vanadate iodide $Pb_{9.85}(VO_4)_6I_{1.7}$	Hydroxyvanadinite $Pb_{9.262}(VO_4)_6(OH)_{1.4}$	Litharge PbO	Lead vanadium oxide $Pb_{2.667}V_{1.333}O_{5.96}$	Pentalead tris (phosphate) iodide $Pb_{10}(PO_4)_6I_2$	Decalead hexakis(phosphate(v))-dihydroxide $Pb_{10}(PO_4)_6(OH)_2$
1	$Pb_{10}(VO_4)_5(PO_4)I_2$	40.8	51.2	3.4	4.6			
2	$Pb_{10}(VO_4)_4(PO_4)_2I_2$	30.8				39.5	16.5	13.3

3.3 Apatite synthesis using AgI

Fig. 5 presents the XRD patterns of the black precipitates, disilver sulfide, obtained in reaction (7), both in an ambient environment and under the continuous flow of argon. The XRD data reveal the formation of Ag_2S (PDF#97-018-2916, monoclinic) as the only phase when the experiment is performed in the presence of argon. However, minute phase reflections corresponding to iodargyrite (AgI; PDF#97-020-0104, hexagonal) can be observed when the same reaction is performed in an ambient environment. This proves that the environment has an impact on the conversion of AgI to NaI as Na_2S tends to react with H_2O in the presence of O_2 (ambient air) to form minor amounts of sodium thiosulfate, $Na_2S_2O_3$, in accordance with reaction (8). Fig. 6 presents the XRD patterns of apatite powders synthesized using the solutions obtained after conversion of AgI to NaI using the methodology described in Section 2.2. The powders synthesized from both air and argon-exposed solutions still primarily reveal the presence of $Pb_{9.85}(VO_4)_6I_{1.7}$ as the only crystalline phase in the samples. This is consistent with the aforementioned reactions (7) and (8) as any unreacted solid AgI will be collected along with the solid Ag_2S and will only result in a slightly under-stoichiometric NaI solution, and consequently, slightly under-stoichiometric apatite composition.

In order to determine the conversion efficiency of AgI to Ag_2S (*via* reaction (7)) in air *vs.* argon, the iodine concentration in the black Ag_2S precipitates was measured using XRF spectroscopy. As presented in Table 5, the Ag_2S precipitates obtained from the reaction in an argon environment comprised 3.14 wt% iodine in comparison to 4.47 wt% iodine detected in their ambient environment analogues. In addition, the mass ratio of Ag/S in Ag_2S precipitates obtained in the argon environment was comparatively higher than those obtained in an air environment. This is in agreement with the reaction mechanism proposed in reaction (8). The exposure of the reaction to air facilitates the formation of $Na_2S_2O_3$ from Na_2S. Since $S_2O_3^{2-}$ is unable to substitute for iodine in AgI, most of the sulfur content remains in solution as opposed to forming Ag_2S. As a result, the mass ratio of Ag/S is much lower in the ambient environment than in the argon environment.

The methodology to convert AgI(s) → NaI(aq) is highly relevant from two viewpoints: (i) it allows the production of NaI(aq) which can be further used as an iodine precursor for the development of ceramic waste forms, for example, cements, apatites, sodalite, and other zeolitic frameworks, (ii) it helps in recovering silver which comes in the list of the Resource Conservation and Recovery Act (RCRA).

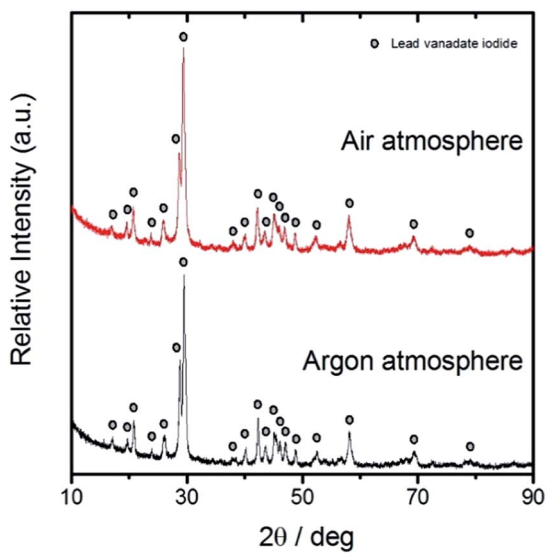

Fig. 6 XRD patterns of $Pb_{10}(VO_4)_6I_2$ synthesized from NaI, converted from AgI in an air environment *vs.* an argon environment.

4. Discussion

In preface to the discussion of the results and their implications on the waste form development for the immobilization of ^{129}I, it is helpful to appreciate the fact that while research in this domain has been active for more than two decades, no baseline technology has been defined for this purpose so far. Therefore, several candidate waste forms have been proposed for the immobilization of radioactive iodine including cements,[14,43] metal–organic frameworks,[44,45] aerogels,[9,46] sodalite and other zeolitic framework minerals,[3,47,48] glasses,[10,49] calcium phosphate apatites,[12] and lead vanadium apatites.[18,30] Despite considerable effort in this field, there still exists room for the development of novel waste forms as most of the proposed candidate waste forms pose challenges either from the viewpoint of their synthesis or their long-term performance.[1] Therefore, the discussion section has been divided into two subsections, where the first part highlights the implications of the proposed synthesis route on the design of potentially novel apatite compositions, while the second

Table 5 XRF analysis of a select Ag_2S precipitate after conversion from AgI. Th. and Exp. are the theoretical and experimental weight percent, respectively

	Normalized weight%					
Intended sample	Th. Ag%	Exp. Ag%	Th. S%	Exp. S%	Th. I%	Exp. I%
(Air) Ag_2S	87.06	86.7264	12.94	8.8059	0	4.4677
(Argon) Ag_2S	87.06	88.5719	12.94	8.2879	0	3.1403

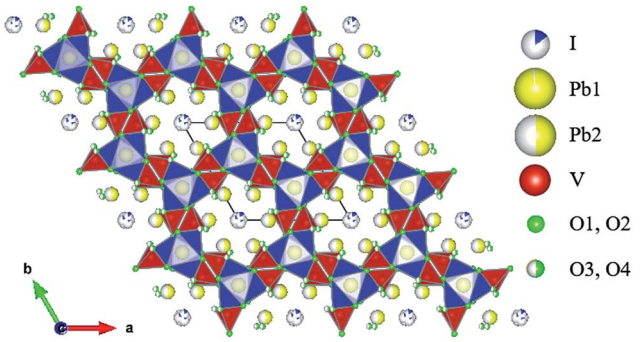

Fig. 7 Structural schematic of $Pb_{9.85}(VO_4)_6I_{1.7}$.

part discusses potential technical challenges that need to be addressed in order to develop a viable industrial-level processing route leading to a mature waste form technology.

4.1 Implications of the proposed synthesis route on the design of novel apatite compositions

The crystal structure of an apatite ($A_{10}(BO_4)_6X_2$) with $P6_3/m$ symmetry comprises A- and B-cation sites occupied by Pb and V, respectively, in $Pb_{10}(VO_4)_6I_2$, while the iodide ion occupies the X-anion site, as shown in Fig. 7‡. The A-cation is further divided into two different configurations: A(1) and A(2). The column configuration of A(1) cations along with their interaction with tetrahedral units composed of B-cations forms the walls of the characteristic apatite channel which extends along the crystallographic *c*-direction. The A(2) cations line the inside of the apatite channel and play a major role in the interaction of the intended X-anion with the apatite.

For the iodide to be incorporated into the structural channel, the channel size must be compatible with the size of the ion. Therefore, the ionic and crystal radii of cations (A and B, respectively), based on the proper charge and coordination number (CN), play a critical role in deciding the fate of anion incorporation into the apatite structure. It is noteworthy that the interaction between the channel anion and the A(2) cation is largely ionic, while the interaction between the B cation and oxygen forming the tetrahedral unit is strongly covalent, and hence the use of both ionic and crystal radii is imperative.[21] The $Pb_{10}(VO_4)_6I_2$ apatite has a relatively large Pb^{2+} ion (ionic radius: 1.19 Å, CN = 6)[50] in the A(1)/A(2) sites and VO_4 in the tetrahedron site, leading to a large channel size.[24] For this reason, it is possible to synthesize $Pb_{10}(VO_4)_6I_2$ apatite. However, substitution of a smaller ion, *i.e.* Ca^{2+} (ionic radius: 1.00 Å, CN = 6),[50] for Pb^{2+} reduces the channel size, thus not allowing the large iodide ion to be incorporated into the apatite structure. Similar reasoning can be provided for the substitution of the phosphorus ion (P^{5+}; crystal radius: 0.31 Å, CN = 4)[50] for the vanadium ion (V^{5+}; crystal radius: 0.495 Å, CN = 4)[50] at the B-cation site, which eventually results in narrowing of the channel size. Therefore, only partial substitutions of Ca^{2+} for Pb^{2+}, and P^{5+} for V^{5+} are possible in the $Pb_{10}(VO_4)_6I_2$ apatite systems. Due to these reasons, it is not possible to synthesize $Ca_{10}(PO_4)_6I_2$ based apatites.§.

In our study, the investigation of calcium substitution helps to establish a baseline of compatible cations capable of forming iodine-containing solid solutions by wet chemical synthesis. When paired with molecular modeling, a comprehensive understanding of the structural consequences of substitution can be properly grasped. In a recent study by Wang,[21] for example, an artificial neural network (ANN) approach was utilized to predict candidate cations for the synthesis of appropriate apatite compositions that are capable of incorporating iodine. The results reported in our work show a very good correlation with the computational study of Wang.[21]

By utilizing the experimental XRF data and defining the limit of calcium (wt%) that can be accommodated in $Pb_{(10-x)}Ca_x(VO_4)_6I_2$ to form a solid solution as 0.32% (as evidenced by $x = 2$, 4; Table 2) and considering the summation of A-site cations (Pb + Ca) to be equal to 10, the composition of the solid solution can be calculated to be $Pb_{9.76}Ca_{0.24}(VO_4)_6I_2$. Using a weighted average of the ionic radii of Pb (1.19 Å, 2+, CN = 6) and Ca (1.00 Å, 2+, CN = 6) calculated according to the estimated formula, the average radius of A-cations (Pb, Ca) is 1.185 Å. When correlated with the crystal radius of vanadium (0.495 Å, 5+, CN = 4), the resultant estimated channel size agrees very closely with the threshold of iodine accommodation as proposed by Wang.[21]

By applying the same methodology through reverse calculations, an ideal chemical formula for a complete iodine-containing apatite solid solution can be determined as well. In the synthesis of lead vanadate-phosphate solid solutions, by utilizing the ionic radius of lead (1.19 Å) in conjunction with the modelled apatite channel size threshold, the average crystal radius of the B-cation can be estimated to be approximately 0.475 Å. By using a weighted average for the B-cations and considering the summation of B-site cations (V + P) to be equal to 6, the predicted chemical formula for the iodine-containing solid solution is $Pb_{10}(VO_4)_{5.35}(PO_4)_{0.65}I_2$. Comparing the acquired experimental phosphate wt% of 3.8 (when $y = 1$) with the ideal calculated phosphate wt% of 2.056 of this formula with evidence from the XRD phase analysis, the model proves its utilization as a possible tool for apatite composition determination.

Most of the radioactive waste forms have been traditionally designed empirically using trial-and-error experimentation owing to the compositional complexity of radioactive waste. Historically, this approach has been successful as borosilicate and aluminophosphate glass chemistries have been defined as baseline waste forms for most of the high level radioactive

‡ For detailed information about the crystal structure of $Pb_{9.85}(VO_4)_6I_{1.7}$ apatite, readers are suggested to refer to ref. 38 (F. Audubert, J. M. Savariault, and J. L. Lacout, Pentalead tris(vanadate) iodide, a defect vanadinite-type compound, *Acta Crystallographica Section C: Crystal Structure Communications*, 1999, **55**(3), p. 271–273).

§ Calcium phosphate iodide apatite, $Ca_{10}(PO_4)_6I_2$, was claimed to have been synthesized by Phebe and Narasaraju,[66] but it has not been able to be replicated. This is concluded both by the studies of Flora, *et al.*[67] and by our own studies.

wastes around the world.[51,52] However, this approach may not work for the immobilization of secondary wastes, like ^{99}Tc and ^{129}I, which despite their low radioactivity pose technical challenges in their processing and immobilization. Therefore, a new level of conceptual understanding is required to design novel materials through the combination of experimental and computational approaches, wherein predictive modelling is used to design waste forms with desired properties, while rigorous experimental data are required to validate these models. The wet chemical synthesis route proposed in this paper for the synthesis of $Pb_{10}(VO_4)_6I_2$ based ceramics in conjunction with the computational design of apatite based materials based on ANN,[21] density functional theory (DFT),[53] and molecular dynamic simulations[54] opens a new avenue for the development of novel apatite based waste forms at room temperature as the A-site cation in the apatite ($A_{10}(BO_4)_6I_2$) structure can accommodate Ag^+, K^+, Sr^{2+}, Pb^{2+}, Ba^{2+} and Cs^+, whereas the B-site cation can hold Mn^{5+}, As^{5+}, Cr^{5+}, V^{5+}, Mo^{5+}, Si^{4+}, Ge^{4+} and Re^{7+} depending on the overall chemistry of the system.[21]

4.2 Open and relevant problem for industrial scale up of waste form technology for immobilization of ^{129}I

While there are several synthesis and processing routes proposed for the development of various waste forms for the immobilization of radioactive iodine, it is difficult to translate any of these directly into practical application due to technical challenges that need to be addressed to develop a viable waste form technology. Often these challenges are overlooked to control the scope of an investigation (*i.e.*, initial precursor selection). One major challenge that needs to be addressed is the conversion of $IO_3^- \rightarrow I^-$ in the waste stream.

As has been discussed in the introduction of the article, the two commonly utilized groups of iodine capture technologies that are either being used, or planned to be deployed in nuclear waste reprocessing plants, are caustic scrubbing (USA, France, UK, Russia, and Japan) and silver solid sorbents (USA, France, UK, Russia, Japan, Italy, and Germany).[1] As has been shown in reactions (1) and (2)–(5), while the waste stream contains iodine primarily in the iodide (I^-) form, it also contains low volumes of iodate (IO_3^-). On the other hand, most of the waste form development in this arena has focused on using iodide[19,24–26,30,55–57] or iodine[44,58] as the main precursors for iodine waste streams. Although waste form development with iodide precursors (especially NaI) helps in immobilizing the majority of the waste stream, it does not account for the leftover iodate species in the waste stream. Campayo *et al.*[12] proposed incorporating iodates into (Ca–P) hydroxyapatite based minerals, but these minerals are not able to accommodate iodide species in their structure, as discussed above. Therefore, a mechanism needs to be devised to convert iodate species in the waste stream to iodide before it can be immobilized into a waste form. One possible mechanism for converting $IO_3^- \rightarrow I^-$ can be *via* the Dushman reaction as shown in reaction (9) and the subsequent reaction (10), which results in iodide ions and an excess amount of tetrathionate ions, $S_4O_6^{2-}$.[59–61]

$$IO_3^- + 5I^- + 6H^+ \rightarrow 3I_2 + 3H_2O \quad (9)$$

$$I_2 + 2S_2O_3^{2-} \rightarrow S_4O_6^{2-} + 2I^- \quad (10)$$

However, the influence of excess tetrathionate ions on the overall immobilization process is unclear. Perhaps the $S_4O_6^{2-}$ ions can be compensated, for instance, with excess cations in solution, *i.e.* Pb^{2+}, to produce stoichiometric lead tetrathionate, PbS_4O_6, alongside the stoichiometric apatite. This hypothesis needs to be validated and the process needs to be optimized in accordance with the composition of the waste stream. Additional concerns for practical application include the possible presence of NaOI species in the caustic solution and the interactions of Na_2S on the various silver solid sorbents. The certainties of these problems, however, are unknown and will form the basis of our future studies.

Finally, considerations must be made for consolidation or incorporation of any fine-powder waste form containing iodine in order to minimize the surface area for interaction with water over a long time. Many possible methods have been proposed in general, including hot-isostatic pressing, binding with low melting point glass, and incorporation into cementitious materials, as has been reviewed elsewhere.[1] Each solution has its pros and cons. For example, direct incorporation of iodine containing materials, such as AgI, (Ba, Ca, Sr, and Hg)IO_3, and AgZ zeolite, has been demonstrated in Portland cement.[62] However, one of the challenges with cement waste forms in the U.S. satisfies the Resource Conservation and Recovery Act (RCRA) that controls the release of toxic materials including As, Ba, Cd, Cr, Pb, Hg, Se, and Ag.[63] In previous studies, no unmodified cement waste form for AgZ satisfied RCRA, so CaI_2 was added for isotopic dilution of iodine and to precipitate AgI and improve silver retention.[64] Given the additional constraint in the Pb apatite waste form for potential leaching of Pb, careful consideration must be made in developing consolidation techniques for Pb–V–I apatite-based powders.[65] Our strategy, going forward, is to use specially designed low-temperature sintering glasses to reduce the surface area and further bind the heavy metals and iodine. These waste forms will be ultimately evaluated for their aqueous chemical durability in comparison with alternative mineral and waste form combinations.

5. Conclusions

A novel wet chemical synthesis method has been proposed to produce apatite-based ceramic waste forms for the immobilization of radioactive iodine under ambient conditions. The proposed methodology can be applied to iodide containing waste streams from caustic scrubbing and silver solid sorbents. The $Pb_{10}(VO_4)_6I_2$ apatite waste form synthesized using the proposed method has been shown to exhibit an iodine waste loading of 9.4 wt%, while its loading efficiency has been experimentally calculated to be 94.62%. In terms of solid solutions, it was found that calcium has a minimal tendency to form apatite solid solutions when substituted for lead in the system, $Pb_{(10-x)}Ca_x(VO_4)_6I_2$. On the other hand, the phosphate ion

forms a solid solution with $Pb_{10}(VO_4)_6I_2$ when partially substituted for the vanadate ion. The threshold incorporation limit of (PO_4) has been found to be 4.77 wt%. The implications of the proposed route to synthesize computationally designed apatite based novel waste forms and its industrial scale-up have been discussed. Future work will assess the aqueous chemical durability of these materials in the presence of water alone or as composite waste forms consolidated with a glass binder of novel chemistry.

Acknowledgements

This research is being performed using funding received from the U.S. Department of Energy – Office of Nuclear Energy through the Nuclear Energy University Program under the award # DE-NE0008257.

Notes and references

1 B. J. Riley, J. D. Vienna, D. M. Strachan, J. S. McCloy and J. L. Jerden Jr, *J. Nucl. Mater.*, 2016, **470**, 307–326.
2 R. Michel, A. Daraoui, M. Gorny, D. Jakob, R. Sachse, L. Tosch, H. Nies, I. Goroncy, J. Herrmann, H.-A. Synal, M. Stocker and V. Alfimov, *Sci. Total Environ.*, 2012, **419**, 151–169.
3 E. R. Maddrell, E. R. Vance and D. J. Gregg, *J. Nucl. Mater.*, 2015, **467**, 271–279.
4 R. T. Jubin, N. R. Soelberg, D. M. Strachan and G. Ilas, *Fuel age impacts on gaseous fission product capture during separations, Report No. FCRD-SWF-2012-000089*, 2012.
5 H. Tanabe, T. Sakuragi, K. Yamaguchi, T. Sato and H. Owada, *Adv. Sci. Tech.*, 2010, **73**, 158–170.
6 H. Mineo, M. Gotoh, M. Iizuka, S. Fujisaki and G. Uchiyama, *J. Nucl. Sci. Technol.*, 2002, **39**, 241–247.
7 H. Mineo, M. Gotoh, M. Iizuka, S. Fujisaki, H. Hagiya and G. Uchiyama, *Sep. Sci. Technol.*, 2003, **38**, 1981–2001.
8 R. T. Jubin, *Organic iodine removal from simulated dissolver off-gas systems utilizing silver-exchanged mordenite, Annual AIChE Meeting*, 1981.
9 J. Matyas, G. E. Fryxell, B. J. Busche, K. Wallace and L. S. Fifield, *Ceram. Eng. Sci. Proc.*, 2011, **32**, 23–32.
10 B. J. Riley, M. J. Schweiger, D.-S. Kim, W. W. Lukens Jr, B. D. Williams, C. Iovin, C. P. Rodriguez, N. R. Overman, M. E. Bowden, D. R. Dixon, J. V. Crum, J. S. McCloy and A. A. Kruger, *J. Nucl. Mater.*, 2014, **452**, 178–188.
11 R. F. de Luis, A. Martinez-Amesti, E. S. Larrea, L. Lezama, A. T. Aguayoe and M. I. Arriortua, *J. Mater. Chem. A*, 2015, **3**, 19996–20012.
12 L. Campayo, A. Grandjean, A. Coulon, R. Delorme, D. Vantelon and D. Laurencin, *J. Mater. Chem.*, 2011, **21**, 17609–17611.
13 D. Laurencin, D. Vantelon, V. Briois, C. Gervais, A. Coulon, A. Grandjean and L. Campayo, *RSC Adv.*, 2014, **4**, 14700–14707.
14 A. Coulon, D. Laurencin, A. Grandjean, C. C. D. Coumes, S. Rossignol and L. Campayo, *J. Mater. Chem. A*, 2014, **2**, 20923–20932.
15 C. Pei, T. Ben, S. Xu and S. Qiu, *J. Mater. Chem. A*, 2014, **2**, 7179–7187.
16 T. C. T. Pham, S. Docao, I. C. Hwang, M. K. Song, D. Y. Choi, D. Moon, P. Oleynikov and K. B. Yoon, *Energy Environ. Sci.*, 2016, **9**, 1050–1062.
17 H. Kato, O. Kato and H. Tanabe, *Review of immobilization techniques of radioactive iodine for geological disposal, Proceed. Intern. Symp, NUCEF*, 2001, pp. 697–702.
18 F. Audubert and J.-E. Lartigue, *Iodine Immobilization in Apatites, in Atalante Conference*, 2000, vol. 4.
19 C. Cao and A. Goel, *Apatite Based Ceramic Waste Forms for Immobilization of Radioactive Iodine, An Overview, Proceed. of WM2016 Conference*, 2016.
20 M. J. Rigali, P. V. Brady and R. C. Moore, *Am. Mineral.*, 2016, **101**, 2611–2619.
21 J. Wang, *Front. Earth Sci.*, 2015, **3**, 20.
22 S. Utsunomiya, S. Yudintsev, L. M. Wang and R. C. Ewing, *J. Nucl. Mater.*, 2003, **322**, 180–188.
23 F. Lu, T. Yao, Y. Danon, J. Zhou, R. C. Ewing and J. Lian, *J. Am. Ceram. Soc.*, 2015, **98**, 3361–3366.
24 F. Audubert, J. Carpena, J. L. Lacout and F. Tetard, *Solid State Ionics*, 1997, **95**, 113–119.
25 C. Guy, F. Audubert, J.-E. Lartigue, C. Latrille, T. Advocat and C. Fillet, *C. R. Phys.*, 2002, **3**, 827–837.
26 T. Yao, F. Lu, H. Sun, J. Wang, R. C. Ewing and J. Lian, *J. Am. Ceram. Soc.*, 2014, **97**, 2409–2412.
27 L. Campayo, S. Le Gallet, Y. Grin, E. Courtois, F. Bernard and F. Bart, *J. Eur. Ceram. Soc.*, 2009, **29**, 1477–1484.
28 L. Campayo, S. Le Gallet, D. Perret, E. Courtois, C. C. D. Coumes, Y. Grin and F. Bernard, *J. Nucl. Mater.*, 2015, **457**, 63–71.
29 S. Le Gallet, L. Campayo, E. Courtois, S. Hoffman, Y. Grin, F. Bernard and F. Bart, *J. Nucl. Mater.*, 2010, **400**, 251–256.
30 F. Lu, T. Yao, J. Xu, J. Wang, S. Scott, Z. Dong, R. C. Ewing and J. Lian, *RSC Adv.*, 2014, **4**, 38718–38725.
31 Z. Dong, T. J. White, B. Wei and K. Laursen, *J. Am. Ceram. Soc.*, 2002, **85**, 2515–2522.
32 T. White, C. Ferraris, J. Kim and S. Madhavi, *Rev. Mineral. Geochem.*, 2005, **57**, 307–401.
33 J. Y. Kim, R. R. Fenton, B. A. Hunter and B. J. Kennedy, *Aust. J. Chem.*, 2000, **53**, 679–686.
34 H. Pizzala, S. Caldarelli, J.-G. Eon, A. M. Rossi, D. Laurencin and M. E. Smith, *J. Am. Chem. Soc.*, 2009, **131**, 5145–5152.
35 S. Kannan, A. F. Lemos and J. M. F. Ferreira, *Chem. Mater.*, 2006, **18**, 2181–2186.
36 S. Budavari, M. J. O'Neil, A. Smith and P. E. Heckelman, *The Merck Index*, Merck & Co. Inc., Rahway, NJ, 11th edn, 1989.
37 J. M. Hughes and J. F. Rakovan, *Elements*, 2015, **11**, 165–170.
38 F. Audubert, J.-M. Savariault and J.-L. Lacout, *Acta Crystallogr., Sect. C: Cryst. Struct. Commun.*, 1999, **55**, 271–273.
39 Y. Suetsugu, *J. Nucl. Mater.*, 2014, **454**, 223–229.
40 G. Bartholomäi and W. E. Klee, *Spectrochim. Acta, Part A*, 1978, **34**, 831–843.
41 M. Zhang, E. R. Maddrell, P. K. Abraitis and E. K. H. Salje, *Mater. Sci. Eng., B*, 2007, **137**, 149–155.

42 W. P. Griffith and T. D. Wickins, *J. Chem. Soc. A*, 1966, 1087–1090.
43 C.-W. Chung, J. Chun, W. Um, S. K. Sundaram and J. H. Westsik, *Cem. Concr. Res.*, 2013, **46**, 14–22.
44 D. F. Sava, T. J. Garino and T. M. Nenoff, *Ind. Eng. Chem. Res.*, 2012, **51**, 612–618.
45 J. L. Krumhansl, T. M. Nenoff, D. Sava, T. Garino, D. Rademacher, K. W. Chapman and P. J. Chupas, *Iodine capture in silver-loaded zeolites and metal organic frameworks and storage in novel low temperature GCM waste forms*, American Nuclear Society, 2011, p. 1103.
46 K. S. Subrahmanyam, S. Sarma, C. D. Malliakas, K. Polychronopoulou, B. J. Riley, D. A. Pierce, J. Chun and M. G. Kanatzidis, *Chem. Mater.*, 2015, **27**, 2619–2626.
47 G. P. Sheppard, J. A. Hriljac, E. R. Maddrell and N. C. Hyatt, Silver Zeolites: Iodide Occlusion and conversion to Sodalite – a Potential 129 I Waste Form, *Mater. Res. Soc. Symp. Proc.*, 2006, **932**, 36.
48 T. Nakazawa, H. Kato, K. Okada, S. Ueta and M. Mihara, Iodine immobilization by sodalite waste form, *Mater. Res. Soc. Symp. Proc.*, 2001, **663**, 51–57.
49 T. Lemesle, F. O. Méar, L. Campayo, O. Pinet, B. Revel and L. Montagne, *J. Hazard. Mater.*, 2014, **264**, 117–126.
50 R. D. Shannon, *Acta Crystallogr., Sect. A: Cryst. Phys., Diffr., Theor. Gen. Crystallogr.*, 1976, **32**, 751–767.
51 I. W. Donald, *Glass Technol.: Eur. J. Glass Sci. Technol., Part A*, 2007, **48**, 155–163.
52 I. W. Donald, B. L. Metcalfe and R. N. J. Taylor, *J. Mater. Sci.*, 1997, **32**, 5851–5887.
53 T. Tamm and M. Peld, *J. Solid State Chem.*, 2006, **179**, 1581–1587.
54 J. A. L. Rabone and N. H. De Leeuw, *J. Comput. Chem.*, 2006, **27**, 253–266.
55 S. A. T. Redfern, S. E. Smith and E. R. Maddrell, *Mineral. Mag.*, 2012, **76**, 997–1003.
56 Y. Watanabe, T. Ikoma, H. Yamada, Y. Suetsugu, Y. Komatsu, G. W. Stevens, Y. Moriyoshi and J. Tanaka, *ACS Appl. Mater. Interfaces*, 2009, **1**, 1579–1584.
57 W. C. Lepry, B. J. Riley, J. V. Crum, C. P. Rodriguez and D. A. Pierce, *J. Nucl. Mater.*, 2013, **442**, 350–359.
58 E. M. Mahdi, A. K. Chaudhuri and J. C. Tan, *Mol. Syst. Des. Eng.*, 2016, **1**, 122–131.
59 S. Dushman, *J. Phys. Chem.*, 1904, **8**, 453–482.
60 I. M. Kolthoff, E. B. Sandell, E. J. Meehan and S. Bruckenstein, *Quantitative Chemical Analysis*, Macmillan, London, 1969, p. 826.
61 W. M. Scheper and D. W. Margerum, *Inorg. Chem.*, 1992, **31**, 5466–5473.
62 L. L. Burger, R. D. Scheele and K. D. Wiemers, *Selection of a Form for Fixation of Iodine-129, Rep. PNL-4045*, 1981.
63 40 CFR 261, *Identification and Listing of Hazardous Waste. Environmental Protection Agency*, Washington, D. C., 2012.
64 R. D. Scheele and C. F. Wende, *Ann. Nucl. Energy*, 2015, **78**, 40–48.
65 M. Uno, M. Shinohara, K. Kurosaki and S. Yamanaka, *J. Nucl. Mater.*, 2001, **294**, 119–122.
66 D. E. Phebe and T. S. B. Narasaraju, *J. Mater. Sci. Lett.*, 1995, **14**, 229–231.
67 N. J. Flora, K. W. Hamilton, R. W. Schaeffer and C. H. Yoder, *Synth. React. Inorg. Met.-Org. Chem.*, 2004, **34**, 503–521.

Hydrothermal Synthesis and Analysis of Iodine-Containing Sodalite - 16153

Saehwa Chong,[1] Jacob Peterson,[2,3] Brian Riley,[1, 3] John McCloy[1, 4]

[1]Materials Science and Engineering Program, Washington State University, Pullman, WA 99164
[2]School of Chemical Engineering and Bioengineering, Washington State University, Pullman, WA 99164
[3]Pacific Northwest National Laboratory, Richland, WA 99352
[4]School of Mechanical and Materials Engineering, Washington State University, Pullman, WA 99164

ABSTRACT

Five process variables affecting hydrothermal synthesis of iodide sodalite, $Na_8Al_6Si_6O_{24}I_2$, were investigated, including NaOH concentration, aging time, temperature, Al/Si ratio, and precursor concentration. X-ray powder diffraction was performed to characterize synthesized samples, and Rietveld refinement method was used to quantify the mass fractions of phases. Iodide sodalite yield increased, in general, as NaOH concentration, aging time, and temperature increased. Lowering the Al/Si ratio from 1 to 0.5 increased the formation of cancrinite. Diluting the precursor concentration in the mixed solution with water revealed that nepheline hydrate-1, a zeolite, formed rather than sodalite. This observation, along with the preferential formation of zeolite A in samples where no NaOH was added, suggests that mechanisms for transport of the ions and formation of the aluminosilicate frameworks vary with hydrothermal conditions. The model for the best synthesis conditions based on the four significant variables is presented.

INTRODUCTION

The highly volatile radionuclide, I-129, has a long half-life and is difficult to immobilize. Iodine is not easily vitrified by conventional routes due to its volatility at typical glass processing temperatures. Therefore, there have been many efforts to develop an alternative waste form for iodine, but none has been uniquely accepted by the nuclear waste community due to trade-offs regarding loading capacity, chemical durability, processing efficiency, and cost [1-3]. Some prominent approaches to immobilize iodine include the development of AgI containing glasses [4], bismuth-oxyiodide minerals [5], silver functionalized silica aerogels [6], metal-organic frameworks [7], Pb and/or Ag containing vanadinite apatites [8, 9], and sodalite [10-12]. Sodalite, written as $M_8Al_6Si_6O_{24}X_2$ where M and X typically represent an alkali cation and monovalent anion respectively, has been studied extensively for immobilization of chlorine, and was proposed as the baseline mineral for the spent electrochemical salt waste [13, 14]. However, relatively few studies have been made on sodalite for immobilization of iodine [15-19].

Iodide sodalite is a promising candidate for immobilization of radioactive iodine due to its ability to capture iodine in the β-cage of the sodalite crystal structure. Sodalite, as portrayed in Fig. 1, is composed of aluminosilicate framework forming β-cages with an anion at the center surrounded by cations and has cubic lattice system with $P\bar{4}3n$ [20] or $I\bar{4}3m$ symmetry [21]. However, there are challenges associated with synthesizing iodine-containing sodalite, particularly for a waste form. Typical solid state processing routes require high temperatures, which might be undesirable due to the high volatility of iodine. One potential solution to this processing challenge is low temperature growth using various simple aqueous-based or hydrothermal (aqueous at higher pressure) synthesis routes.

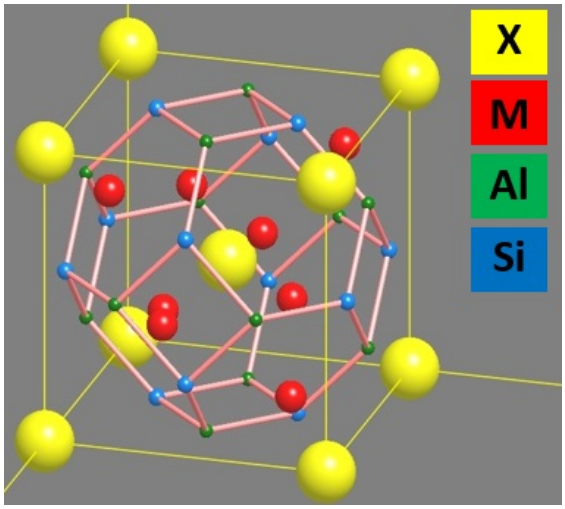

Fig. 1. Sodalite structure where X and M represent an anion and a cation, respectively.

Our current work is focused on the hydrothermal synthesis of iodide-containing sodalite. Hydrothermal synthesis is a one-step growth method at relatively low temperature (< 200°C) in a sealed vessel with water, resulting in above atmospheric pressure inside the vessel. One potential challenge with hydrothermal synthesis of iodide sodalite is competition of the hydroxide anion for iodide in the β-cage, since syntheses are typically performed at high pH using alkali hydroxide, for instance. Additionally, most studies on the hydrothermal synthesis of sodalite use excess halide reagent to avoid OH^- in the β-cage, but this is probably not realistic for a radioactive waste form process where a highly alkaline scrubber solution might be the waste stream.

In this article, we briefly report the synthesis and characterization of iodide sodalite produced without using excessive halide reagents, thus representing a more realistic waste-processing scenario. Our study shows the effects of various process variables (NaOH concentration, aging time, temperature, Al/Si ratio, and precursor concentration) and precursors (zeolite 4A, kaolinite, and sodium aluminate, colloidal silica) on the phase development and phase fraction of crystalline species. In all cases, the iodine was provided by NaI salt. This simple low-temperature synthesis approach has promising practical applications for immobilizing I-129. Our synthesized minerals were characterized by X-ray powder diffraction (XRD) for their atomic structure estimate of iodine waste loading.

EXPERIMENTAL METHODS

Sodium iodide (NaI certified grade, Fisher), sodium aluminate ($NaAlO_2$ 99.9%-Al, Stream Chemicals), colloidal silica (SiO_2, Sigma Aldrich), and sodium hydroxide (NaOH certified ACS grade, Fisher) were used as-received for variable-effect experiments, such as temperature, aging time, and water content. The stoichiometric ratio of $NaI:NaAlO_2:SiO_2$ was 1:3:3, by mole, for iodide sodalite synthesis. In general, approximately 0.500 g of NaI, 0.823 g of $NaAlO_2$, and 0.601 g of SiO_2 were mixed in 11.25 mL of deionized water (DIW).

One-variable-at-a-time experiments were conducted to investigate each effect as summarized in Table I. For the NaOH concentration variation study, a different amount of NaOH was mixed with addition of 3.75 mL of DIW to the initial 11.25 mL solution. In other words, 4 M, 8 M, and 11 M in Table I mean adding 3.75 mL of those NaOH concentrations, and the mixed solutions have NaOH concentration of 1 M, 2 M, and 2.75 M respectively. Roughly 15 mL of the mixed solution was put in an autoclave (Parr 200 mL acid digestion vessel) and placed in an oven at 180°C for 2 d. For the aging time variation study, samples were in an oven at 100°C for 1–20 d. Two sets of samples with either 0 or 11 M NaOH concentration were synthesized. For the temperature variation study, three samples were synthesized at 100°C, 140°C, or 180°C, covering the typical hydrothermal process temperature range for sodalite minerals [22-25]. For the Al/Si ratio study, an excess amount $NaAlO_2$ or SiO_2 was added to the initial stoichiometric solution to make the Al/Si ratio equal to 1.5 or 0.5. Therefore, for Al/Si ratio equal to 1.5, it is not just excess Al but also Na. For the precursor concentration study, a dilution was performed by adding 15 mL or 30 mL of extra DIW to the previously mixed solutions. The diluted solution was heated at 180°C for 2 d. After processing, all the synthesized samples were washed 3 times for 5 min each using a centrifuge at 9000 rpm then subsequently dried at 90°C overnight.

XRD and Rietveld analysis were performed on synthesized samples. XRD spectra were obtained using a PANalytical X'Pert Pro MPD (The Netherlands). Scans were performed with a Cu-Kα X-ray source at 45 keV and 40 mA in the range of 10-90° 2θ with 0.002° 2θ step and 11-s dwell. For Rietveld analysis, samples were doped with 10 mass% NIST SRM-674b (ZnO) as an internal standard to quantify phases and crystalline fraction, and subsequently analyzed using Highscore software (PANalytical).

TABLE I. One-variable-at-a-time synthesis conditions

Variable Experiment	Precursor ratio	Added NaOH concentration (M)*	Aging time (d)	Temperature (°C)	Al/Si ratio	Extra water added (mL)
NaOH conc. variation	stoichiometric	0, 4, 8, 11	2	180	1	0
Aging time variation	stoichiometric	11	1, 5, 10, 20	100	1	0
Aging time variation	stoichiometric	0	1, 5, 10, 20	100	1	0

Temperature variation	stoichiometric	11	2	100, 140, 180	1	0
Adjusting Al/Si ratio	not stoichiometric	11	2	180	0.5, 1, 1.5	0
Precursor concentration	stoichiometric	11	2	180	1	0,15,30

* 3.75 mL of X M NaOH is added where X=4, 8, or 11.

RESULTS

NaOH Concentration Variation Study

The effect of NaOH concentration on product yield was investigated by adding 3.75 mL of different NaOH concentration solution to 11.25 mL of stoichiometric solution. XRD patterns and phase mass percentages are shown in Fig. 2. As NaOH concentration increased, more iodide sodalite was formed, and overall crystalline fraction increased. Also, it can be seen that major peaks of analcime 1C phase ($NaAlSi_2O_6 \cdot H_2O$) at 25.9°(2θ) and hydrosodalite phase [$Na_8(AlSiO_4)_6 2(H_2O)(OH)_2$] at 14°(2θ) decreased as the NaOH concentration increased. It should be noted that iodide sodalite and hydrosodalite have several similar peak positions such as near 14° and 24°, which were taken into account during refinement. However, it can be seen that higher NaOH concentration favored iodide sodalite formation as a decrease in the intensity of the peak at 14°(2θ) mainly reflects the decrease in hydrosodalite yield.

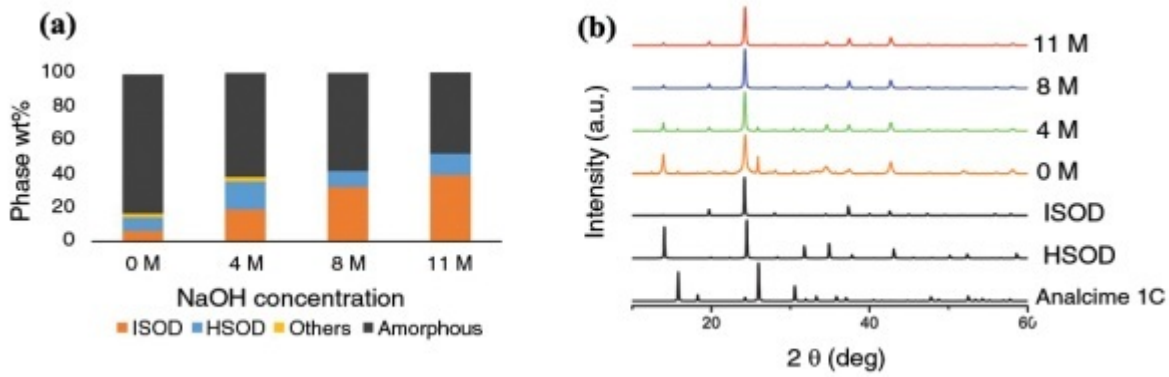

Fig. 2. (a) Phase wt% distribution for different NaOH concentration. ISOD and HSOD denote iodide sodalite and hydrosodalite respectively. **(b)** Normalized XRD patterns of synthesized minerals and reference phases (ISOD ICSD# 41193, HSOD ICSD# 413496, and analcime 1C ICSD#15811)

Aging Time Variation

The study of the effect of aging time involved 2 sets of samples, one with and one without added NaOH. The mixed solutions were aged at 100°C for 1, 5, 10, or 20 d. Longer aging time resulted in higher iodide sodalite yield as shown in Fig. 3. For 20 d of aging with 11 M NaOH, the synthesized mineral was almost pure iodide sodalite, but about half of the sample was amorphous based on Rietveld analysis. Synthesized minerals without NaOH were mainly zeolite A and zeolite P1, and almost no sodalite phase was present regardless of aging times. Zeolite A formation at 90°C was observed in other studies when NaOH concentration was low [22], thus

it is not surprising that zeolite A was observed at 100°C in experiments without added NaOH. The transformation of zeolite to sodalite can be seen between the 1-d and 5-d samples, and this zeolite-sodalite phase transformation was observed in other studies [22]. It should be noted that the colloidal SiO_2 precursor does contain some NaOH in the liquid containing the colloidal particles, and the pH of this solution was 9.0.

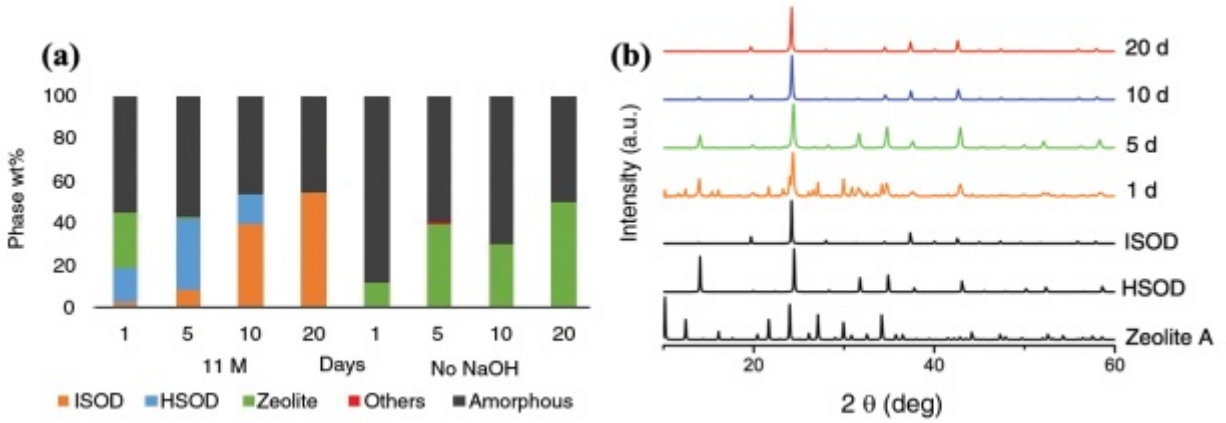

Fig. 3. (a) Phase wt% for aging time variation on 11 M and no NaOH samples. **(b)** Normalized XRD patterns of 11 M NaOH samples and reference phases (zeolite A ICSD# 183702).

Temperature Variation

The temperature variation study consisted of samples produced at 100°C, 140°C, and 180°C with 11 M NaOH and 2 d aging time. Higher temperature generally resulted in higher iodide sodalite yield (Fig. 4). The 140°C sample showed the highest yield, but it was very similar to that of 180°C. Lower processing temperatures favored formation of hydrosodalite. Crystalline fractions were similar for all 3 temperatures.

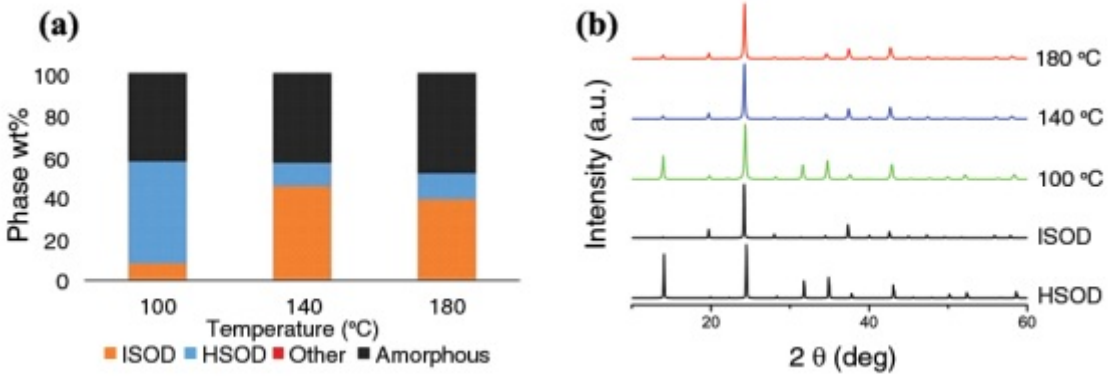

Figure. 4. (a) Phase wt% for temperature variation. **(b)** Normalized XRD patterns of synthesized mineral and reference phases.

Adjusting Al/Si Ratio

The effect of the Al/Si ratio on the product was investigated by adding excess $NaAlO_2$ or SiO_2 to initial stoichiometric solution to make the Al/Si ratio equal to 1.5

or 0.5. Excess Na and Al favored the formation of hydrosodalite, whereas the excess Si favored the formation of the cancrinite, $Na_{7.34}(AlSiO_4)_6(OH)_{1.68}(H_2O)_{7.56}$, as shown in Fig. 5. Crystalline fractions changed minimally among the different Al/Si ratios.

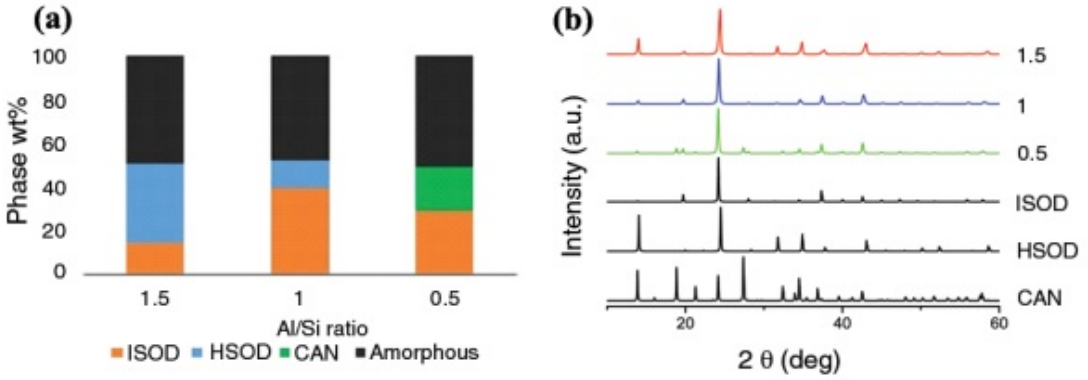

Figure. 5. (a) Phase wt% for different Al/Si ratio. **(b)** Normalized XRD patterns of synthesized samples and reference phases; CAN denotes cancrinite (CAN ICSD# 411486).

Precursor Concentration

The effect of precursor concentration variation was investigated by adding extra DIW to the initial stoichiometric solution. Three samples were synthesized at 180°C with the total amounts of DIW equal to ~15 mL, 30 mL, or 45 mL. Lowering precursor concentration favored the formation of hydrosodalite and nepheline hydrate 1, $Na_3(Al_3Si_3O_{12})(H_2O)$, a "JBW" framework zeolite [26, 27]. This result is consistent with other studies where lowering NaOH concentration favored nepheline hydrate 1 formation over sodalite at 200°C [27]. Although the current work involved lowering all precursor concentrations including NaOH, the effect should be relevant when lowering NaOH concentration alone. Also, it should be noted that with similar conditions but at a lower temperature around 100°C, lowering precursor or NaOH concentration favored the formation of zeolite A.

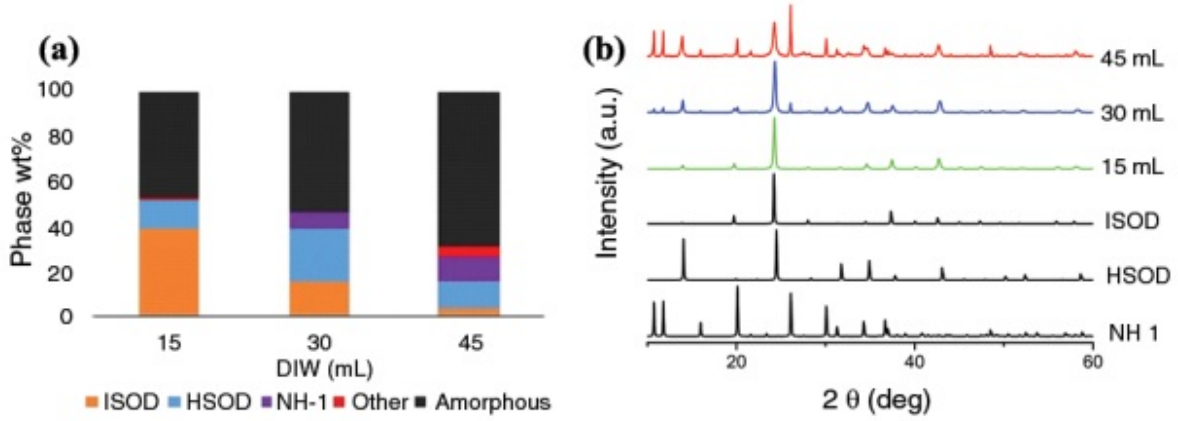

Fig. 6. (a) Phase wt% for precursor concentration variation. NH 1 denotes nepheline hydrate 1. **(b)** Normalized XRD patterns of synthesized samples and reference phases (NH 1 ICSD# 17069)

Model for Optimal Synthesis Condition

Using all the data of one-variable-at-a-time variation experiments with JMP software (version 11, SAS), the model for optimal synthesis condition to maximize iodide sodalite yield was designed. All the variables were input as continuous variables. Among the five process variables, Al/Si ratio was not used because it was determined to be less significant according to the software algorithm. The model predicted optimal conditions for maximum iodide sodalite yield was at 11 M NaOH concentration, 20-d aging time, 155°C processing temperature, and without dilution. The interaction profile diagram at the optimal condition is shown in Fig. 7.

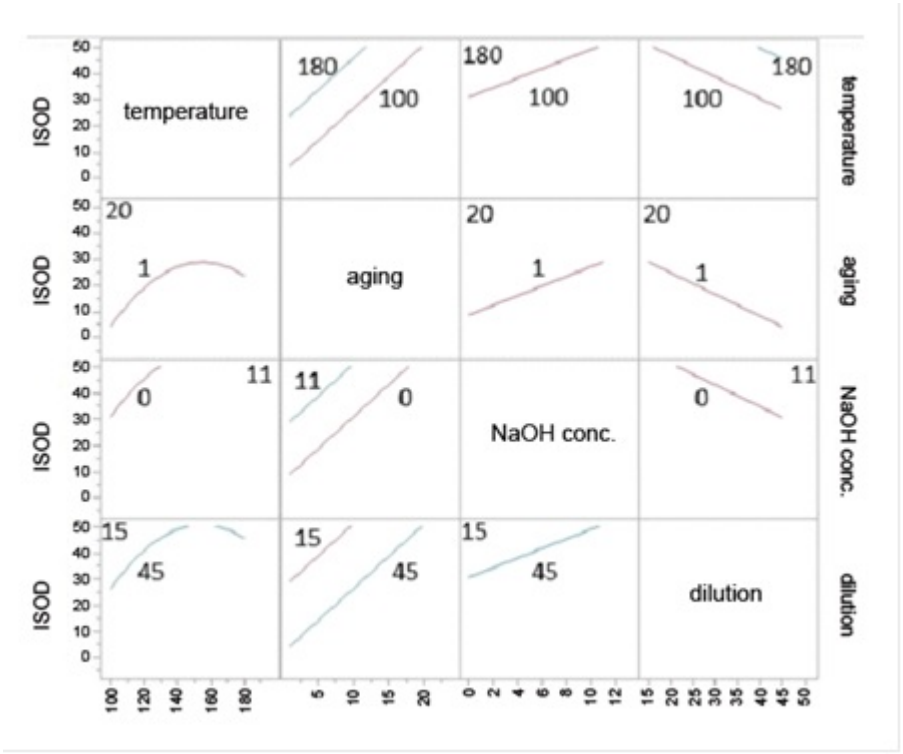

Fig. 7. Interaction profile diagram for the optimal hydrothermal condition when using $NaAlO_2$, SiO_2, NaI, and NaOH within given experiment ranges.

CONCLUSIONS

Five process variables were investigated to determine their relationship to iodide sodalite formation. Increased in NaOH concentration, temperature, and aging time, in general, resulted in higher iodide sodalite yield. Excess Si/Al favored cancrinite formation whereas excess sodium and aluminum favored hydrosodalite formation. Lowering precursor concentration yielded the nepheline hydrate 1 phase at the 180°C synthesis temperature. The synthesis without NaOH at 100°C favored zeolite A formation. The formation of zeolite A before sodalite in the aging experiments suggests that zeolite A is a precursor phase. High NaOH concentration, longer aging time, and higher precursor concentration produced higher overall crystalline fraction (lower amorphous content). By contrast, temperature and Al/Si affected the crystalline phase distribution but not so much the overall crystal fraction within

the tested range. A model for optimal conditions for iodide sodalite was designed, and it agreed with the general trends seen in one-at-a-time variation experiments. This model can be helpful for hydrothermal synthesis when using $NaAlO_2$, SiO_2, and NaI precursors with NaOH.

REFERENCES

1 L.L. BURGER, R.D. SCHEELE, and K.D. WIEMERS, "Selection of a form for fixation of iodine-129," PNL-4045, Pacific Northwest Labratory, Richland, WA (1981).

2 P. TAYLOR, "A review of methods for immobilizing iodine-129 arising from a nuclear fuel recycle plant, with emphasis on waste-form chemistry," AECL-10163, Whiteshell Nuclear Research Establishment, Pinawa, Manitoba, Canada (1990).

3 M.I. OJOVAN and W.E. LEE, *An Introduction to Nuclear Waste Immobilisation*. Elsevier Science, Amsterdam (2005).

4 T.J. GARINO, T.M. NENOFF, J.L. KRUMHANSL, and D.X. RADEMACHER, "Low-Temperature Sintering Bi–Si–Zn-Oxide Glasses for Use in Either Glass Composite Materials or Core/Shell 129I Waste Forms," *Journal of the American Ceramic Society*, 94(8), 2412-2419 (2011).

5 J.L. KRUMHANSL and T.M. NENOFF, "Hydrotalcite-like layered bismuth–iodine–oxides as waste forms," *Applied Geochemistry*, 26(1), 57-64 (2011).

6 J. MATYÁŠ and R. ENGLER, "Assessment of Methods to Consolidate Iodine-Loaded Silver-Functionalized Silica Aerogel," *Pacific Northwest National Laboratory, PNNL-22874*, (2013).

7 B. ASSFOUR, T. ASSAAD, and A. ODEH, "In silico screening of metal organic framework for iodine capture and storage," *Chemical Physics Letters*, 610, 45-49 (2014).

8 F. AUDUBERT and J. LARTIGUE, "Iodine immobilization in apatites," Proc. 4 Atalante Conference (2000).

9 F. AUDUBERT, J. CARPENA, J. LACOUT, and F. TETARD, "Elaboration of an iodine-bearing apatite Iodine diffusion into a Pb 3 (VO 4) 2 matrix," *Solid State Ionics*, 95(1), 113-119 (1997).

10 T. NAKAZAWA, H. KATO, K. OKADA, S. UETA, and M. MIHARA, "Iodine immobilization by sodalite waste form," Proc. Cambridge Univ Press 663 MRS Proceedings, 51 (2000).

11 I. BARDEZ, L. CAMPAYO, D. RIGAUD, M. CHARTIER, and A. CALVET, "Investigation of sodalites for conditioning halide salts (NaCl and NaI): Comparison of two synthesis routes," Proc. ATALANTE 2008, O4_19 (2008).

12 E. MADDRELL, A. GANDY, and M. STENNETT, "The durability of iodide sodalite," *Journal of Nuclear Materials*, 449(1-3), 168-172 (2014).

13 W.L. EBERT, "Testing to Evaluate the Suitability of Waste Forms Developed for Electrometallurgically Treated Spent Sodium-Bonded Nuclear Fuel for Disposal in the Yucca Mountain Repository," ANL-05/43, Argonne National Laboratory, Argonne, Illinois (2005).

14 K. BATEMAN, C. KNIGHT, and C. SOLBRIG, "Current Status of Ceramic Waste Form Development," INL/INT-06-11736, (2007).

15 E.R. MADDRELL and P.K. ABRAITIS, "A comparison of wasteforms and processes for the immobilization of iodine-129," *Mater. Res. Soc. Symp. Proc.*, 807(Scientific Basis for Nuclear Waste Management XXVII), 261-266 (2004).
16 T. NAKAZAWA, H. KATO, K. OKADA, S. UETA, and M. MIHARA, "Iodine immobilization by sodalite waste form," *Mater. Res. Soc. Symp. Proc.*, 663(Scientific Basis for Nuclear Waste Management XXIV), 51-57 (2001).
17 W.I. WINTERS, "The Effect of Hot-Pressing Conditions on the Properties of Iodide Sodalite," RHO-LD-153, Rockwell International-Rockwell Hanford Operations, Richland, WA (1980).
18 D. STRACHAN and H. BABAD, "Iodide and Iodate Sodalites for the Long-Term Storage of Iodine-129," RHO-SA-83, Rockwell International-Rockwell Hanford Operations, Richland, WA (1979).
19 D. HIRABAYASHI, Y. TANADA, T. SUGIYAMA, Y. ENOKIDA, and K. SAWADA, "Low-temperature conversion of spent adsorbent to iodine sodalite by a mechanochemical route," *AIChE J.*, 58(8), 2441-2447 (2012).
20 N.C. NIELSEN, H. BILDSØE, H.J. JAKOBSEN, and P. NORBY, "^{7}Li, ^{23}Na, and ^{27}Al quadrupolar interactions in some aluminosilicate sodalites from MAS NMR spectra of satellite transitions," *Zeolites*, 11(6), 622-632 (1991).
21 B. BEAGLEY, C. HENDERSON, and D. TAYLOR, "The crystal structures of aluminosilicate-sodalites: X-ray diffraction studies and computer modelling," *Mineralogical Magazine*, 46(341), 459-464 (1982).
22 Q. LIU and A. NAVROTSKY, "Synthesis of nitrate sodalite: An in situ scanning calorimetric study," *Geochimica et cosmochimica acta*, 71(8), 2072-2078 (2007).
23 M.E. BRENCHLEY and M.T. WELLER, "Synthesis and structures of $M_8[AlSiO_4]_6\cdot(XO_4)_2$, M= Na, Li, K; X= Cl, Mn Sodalites," *Zeolites*, 14(8), 682-686 (1994).
24 C. RIOS REYES, C. DENVER WILLIAMS, and C. ROBERTS, "Synthesis and Characterisation of SOD-, CAN-AND JBW-Type Structures by Hydrothermal Reaction of Kaolinite at 200°C," *Dyna*, 78(166), 38-47 (2011).
25 H. TRILL, H. ECKERT, and V.I. SRDANOV, "Mixed Halide Sodalite Solid Solution Systems. Hydrothermal Synthesis and Structural Characterization by Solid State NMR," *The Journal of Physical Chemistry B*, 107(34), 8779-8788 (2003).
26 S. HANSEN and L. FÄLTH, "X-ray study of the nepheline hydrate I structure," *Zeolites*, 2(3), 162-166 (1982).
27 T. HOFS and J.-C. BUHL, "Synthesis, hydrothermal stability and thermal reaction behavior of nepheline hydrate I (NH I)," *Reaction Kinetics and Catalysis Letters*, 84(2), 375-382 (2005).

ACKNOWLEDGEMENTS

This research is funded by the U.S. Department of Energy in support of the Nuclear Energy University Program – Advanced Waste Forms program. The authors also thank Jamie Weaver for assistance with the hydrothermal synthesis, Jose Marcial for help with X-ray diffraction, and Ashutosh Goel for general comments.

Received: 22 August 2016 | Accepted: 30 December 2016

DOI: 10.1111/jace.14772

ORIGINAL ARTICLE

Journal of the American Ceramic Society

Synthesis and characterization of iodosodalite

Saehwa Chong[1] | Jacob Peterson[2,3] | Junghune Nam[4] | Brian Riley[1,3] | John McCloy[1,3,4]

[1]Materials Science and Engineering Program, Washington State University, Pullman, Washington

[2]School of Chemical Engineering and Bioengineering, Washington State University, Pullman, Washington

[3]Pacific Northwest National Laboratory, Richland, Washington

[4]School of Mechanical and Materials Engineering, Washington State University, Pullman, Washington

Correspondence
John McCloy, Materials Science and Engineering Program, Washington State University, Pullman, WA
Email: john.mccloy@wsu.edu

Funding information
Nuclear Energy University Programs, Grant/Award Number: DE-NE0008257; U.S. Department of Energy, Grant/Award Number: DE-NE0008257.

Abstract

The effects of six process variables were investigated on the hydrothermal growth of iodosodalite, $Na_8Al_6Si_6O_{24}I_2$: pH (NaOH concentration), aging time, temperature, Al/Si ratio, precursors used (i.e., zeolite 4A, kaolinite, meta-kaolin, colloidal silica, and sodium aluminate), and precursor concentration. Powder X-ray diffraction (XRD) with Rietveld refinements, X-ray photoelectron spectroscopy (XPS), Fourier transform infrared spectroscopy (FTIR), and scanning electron microscopy (SEM) were performed to characterize the structures, phase fractions, chemical state, and surface morphology of the synthesized products. Iodosodalite yield increased as aging time and pH increased. The crystallization of iodosodalite was favored in the temperature range 140°C-180°C. Decreasing the Al/Si ratio by half increased the crystallization of basic cancrinite. Lowering the precursor concentration by adding water revealed the crystallization of nepheline hydrate I and a decrease in the sodalite fraction. Among the tested precursors, zeolite 4A yielded the highest mass fraction of iodosodalite in the synthesized powders. From the aging time and temperature variation experiments, the phase transformation of zeolite A→sodalite→cancrinite was observed. XPS and FTIR results showed the presence of only iodide but not iodate in the synthesized product. The crystallization of various minerals suggests that mechanisms for transport of the ions and formation of the aluminosilicate frameworks vary with hydrothermal conditions.

KEYWORDS
FTIR, hydrothermal, iodosodalite, sodalite, XPS, XRD

1 | INTRODUCTION

Sodalite is a microporous material with a cage-like structure that can incorporate various ions, and it has been studied for many industrial applications including nuclear waste forms,[1–4] optical data storage,[5,6] and semiconductor quantum dots.[7,8] Sodalite has a generic chemical formula of $M_8Al_6Si_6O_{24}X_2$ often written as $M_8(AlSiO_4)_6X_2$, where M represents a cation (eg, Na^+, Ag^+, Ca^+, Li^+) and X represents an anion (eg, Cl^-, I^-, OH^-, IO_3^-). In the general sodalite structure, AlO_4 and SiO_4 tetrahedra are connected through shared oxygen atoms and form four-membered and six-membered rings that comprise the aluminosilicate framework known as the β-cage as shown in Figure 1. Tetrahedra of the β-cage formed by other 3+ and 4+ ions (eg, B^{3+}, P^{3+}, G^{3+}, Ge^{4+}) with oxygen are also reported in the literature.[9,10] The β-cage typically incorporates four cations that are tetrahedrally coordinated to an anion at the center of the cage. However, anion-free β-cages have been observed, such as in hydrosodalite, $Na_6(AlSiO_4)_6{\cdot}8H_2O$, which contains only three sodium cations to balance the charge. The lattice constant of sodalite, which is directly related to the size of the β-cage, is dependent on the elements of the framework, sizes of cations and anions, and temperature.[11]

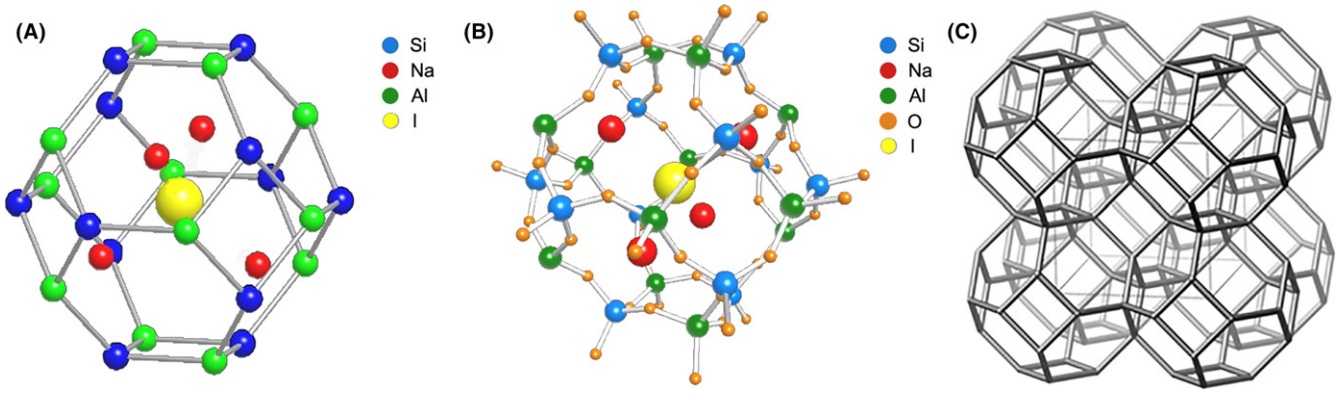

FIGURE 1 A, Structure of the β-cage for iodosodalite shown without oxygen atoms. B, The β-cage of iodosodalite shown with oxygen atoms forming tetrahedra around Al and Si. C, The stacked structure of sodalite with respect to the unit cell.[42] Note that the radii of atoms are not to scale [Color figure can be viewed at wileyonlinelibrary.com]

1.1 | Iodosodalite

Since I^- incorporates into sodalite, the nuclear waste community has considered sodalite as a vehicle for immobilizing radioactive iodine-129 in the β-cage.[3,12–14] This is an attractive option because of the feasibility of synthesis at low temperatures (<200°C) to control iodine volatility and because the aluminosilicate framework of the sodalite is compatible with glass matrices used to encapsulate the sodalite crystallites. In addition, chlorosodalite, $Na_8Al_6Si_6O_{24}Cl_2$, has been studied extensively and has been proposed as the baseline mineral for the spent electrochemical salt waste that would be produced when reprocessing used nuclear fuel via the pyrochemical method.[15,16] Iodosodalite, $Na_8Al_6Si_6O_{24}I_2$, has an iodide and four sodium cations in the β-cage with a lattice constant of 9.009 Å. A discrepancy exists in the symmetry of the cubic space group reported for iodosodalite in the literature, such that one study showed the disordered positions of Al and Si resulting in $I\bar{4}3m$ symmetry,[17] whereas most other studies favored the ordered positions of Al and Si with $P\bar{4}3n$ symmetry,[18,19] the space group usually proposed for other sodalites.

Iodosodalite is typically synthesized by high-temperature solid-state routes or lower temperature aqueous routes, such as hydrothermal or wet chemistry methods. Typical solid-state synthesis requires around 800°C,[2] but the volatility of iodine occurs at similar temperature resulting in substantial loss of iodine.[2,20] Also, longer synthesis times at 850°C showed the transformation of sodalite to nepheline in the case of chlorosodalite.[21]

The formation of aluminosilicate frameworks under hydrothermal conditions involves gelation, dissolution, nucleation, and crystallization as shown in Figure 2.[22] The precursors form amorphous hydrogels and subsequently dissolve in the presence of a mineralizing agent such as

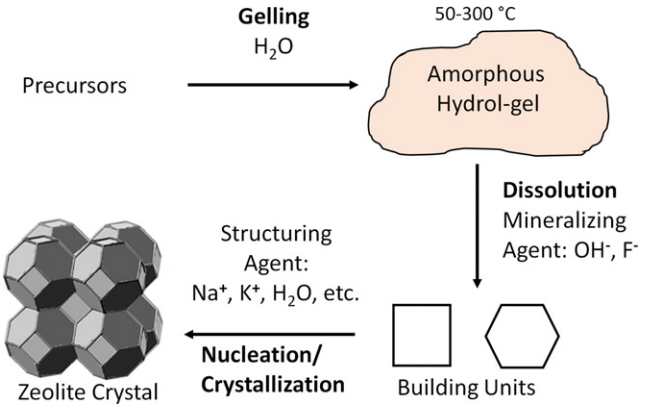

FIGURE 2 Hydrothermal synthesis of zeolite crystal (modified from Derouane et al.[22]) [Color figure can be viewed at wileyonlinelibrary.com]

OH^-. Various species separated in the solution will form into different sizes of nuclei and reach critical size during an induction period. After the induction period, crystallization occurs rapidly.[23] Structuring agents such as Na^+ ions and water influence the formation of various crystals depending on the process variables.[22] Therefore, a small variation of synthesis conditions when using the hydrothermal processing route can yield various pure or co-crystallized zeolitic framework minerals such as sodalite, cancrinite $[Na_8(AlSiO_4)_6(OH)_2{\cdot}3H_2O]$, nepheline hydrate I $[Na_3(AlSiO_4)_3{\cdot}H_2O]$, and zeolite A $[Na_{12}(AlSiO_4)_{12}{\cdot}27H_2O]$.[1,24–27]

1.2 | Competing minerals to iodosodalite

Previous studies have shown that the hydrothermal route with a stoichiometric ratio of the precursors usually yields iodosodalite with other minerals including hydroxysodalite $[Na_8(AlSiO_4)_6(OH)_2{\cdot}2H_2O]$, cancrinite, nepheline hydrate I,

zeolite A, and analcime [$NaAlSi_2O_6{\cdot}H_2O$], depending on the synthesis condition;[14] the framework structures of these minerals are shown in Figure 3. Cancrinite and sodalite are classified as feldspathoids, which have the same aluminosilicate framework structure as some zeolites but without water.[23,28] Analcime and nepheline hydrate I are zeolites which are defined as crystalline and hydrated aluminosilicates typically containing group I and II elements and composed of AlO_4 and SiO_4 tetrahedra.[23] Although there is a distinction between zeolite and feldspathoid, water-containing sodalite such as hydroxysodalite is sometimes considered a zeolite in the literature.[29,30] Feldspathoids containing water can be fit in the definition of zeolite if they have ion exchange properties.[23]

When performing the hydrothermal synthesis route for making iodosodalite, the most competing mineral is hydroxysodalite. Since hydrothermal synthesis involves NaOH and water, OH^- anions and H_2O can be incorporated into the β-cages. The "hydro-sodalite" system has several different chemical formulas associated with the name including $Na_8(AlSiO_4)_6(OH)_2{\cdot}xH_2O$ with $2{\leq}x{\leq}4$, $Na_6(AlSiO_4)_6{\cdot}xH_2O$ with $6<x{\leq}8$, and $Na_8(AlSiO_4)_6(OH)_x$ with x=2 or 4,[31–34] where they are often distinguished as hydroxysodalite, hydrosodalite, and hydroxylsodalite, respectively. Buhl[35] reported the presence of OH^- and water in the β-cages regardless of an excessive amount of $NaIO_3$ precursor in their hydrothermal synthesis of iodate sodalite.

The generic chemical formula of the basic cancrinite is $Na_8(AlSiO_4)_6(OH)_2{\cdot}3H_2O$. However, various alternative compositions have been reported in the literature including $Na_8(AlSiO_4)_6(OH)_{2.04}(H_2O)_{2.66}$,[36] $Na_{7.14}(AlSiO_4)_6(H_2O)_{4.87}$,[37] $Na_{7.34}(AlSiO_4)_6(OH)_{1.68}(H_2O)_{7.56}$,[38] and $Na_{7.62}(AlSiO_4)_6(OH)_{1.62}(H_2O)_{2.5}$.[39] The cancrinites are hydrothermally synthesized in a wide range of temperature between 90°C and 500°C.[40] Studies have shown that sodalite transforms into cancrinite with longer aging time, higher temperature, and higher precursor concentration.[1,24,39,41]

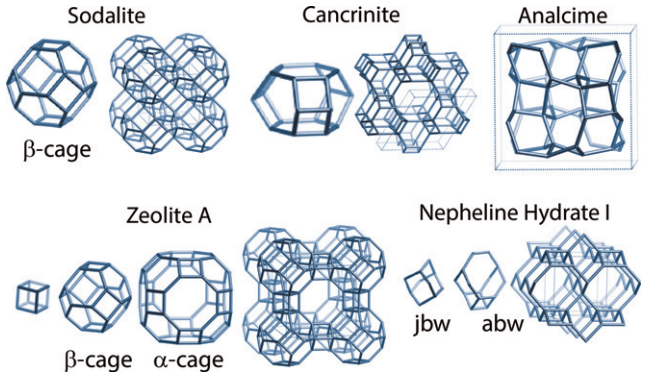

FIGURE 3 Building units and frameworks of sodalite, cancrinite, analcime, zeolite A, and nepheline hydrate I (modified from Baerlocher et al.[42]) [Color figure can be viewed at wileyonlinelibrary.com]

Nepheline hydrate I, also known as JBW, after Na-J with Barrer & White,[42] is often co-crystallized with more stable products such as cancrinite and sodalite.[28] The general chemical formula of nepheline hydrate I, $Na_3(AlSiO_4)_3{\cdot}xH_2O$, with different amount water as x=1, 1.5, 1.8, and 2, has been reported in the literature[43–45] but the transformation path has not been clearly established yet. Lin et al.[24] reported the phase transformation from zeolite A to nepheline hydrate I, whereas Rios et al.[27] proposed the possibility of transformation from cancrinite to nepheline hydrate I.

Zeolite A, also known as LTA for Linde Type A,[42] is known to be an intermediate phase between an amorphous gel and sodalite, and its formation requires relatively low temperature (<90°C).[1,41] Analcime can have a variety of crystallographic structures under different hydrothermal conditions including triclinic, monoclinic, orthorhombic, tetragonal, cubic, and hexagonal systems. Ghobarkar et al.[46] showed that analcime with different crystal symmetries can be controlled by using specific temperature ranges between 80°C and 650°C at a constant pressure.

2 | EXPERIMENTAL PROCEDURE

2.1 | Materials

Sodium iodide (NaI certified grade, Fisher, Waltham, MA, USA), sodium aluminate ($NaAlO_2$, Strem Chemicals, Newburyport, MA, USA), colloidal silica (SiO_2 LUDOX HS-40, Sigma Aldrich, St. Louis, MO, USA), sodium hydroxide (NaOH certified ACS grade, Fisher), zeolite 4A ($Na_{12}Al_{12}Si_{12}O_{48}$ xH_2O, W.R Grace & Co., Columbia, MD, USA), and kaolinite ($Al_2Si_2O_5(OH)_4$ natural, Sigma Aldrich), were used as-received. Meta-kaolin ($Al_2Si_2O_7$) was synthesized by heat-treating kaolinite at 850°C for 17 hours. The water content in zeolite 4A was found to be 7.5 mass% by thermogravimetric analysis. Deionized water was used for all experiments.

Colloidal silica was selected as the silica source over powdered silica based on preliminary hydrothermal synthesis experiments of iodosodalite. The colloidal silica contained some NaOH and has pH of ~9. All the precursors were analyzed under XRD showing the dried colloidal silica as amorphous, meta-kaolin as mostly amorphous, and other precursors as crystalline and phase-pure.

2.2 | Hydrothermal synthesis

For the pH, aging time, temperature, Al/Si ratio, and precursor concentration variation experiments, NaI, $NaAlO_2$, and colloidal SiO_2 were used as precursors, and NaOH was used as a mineralizing agent. The stoichiometric molar

ratio of NaI:$NaAlO_2$:SiO_2 was 1:3:3 for iodosodalite synthesis. In general, initial solutions were prepared by mixing 0.500 ± 0.007 g of NaI, 0.823 ± 0.006 g of $NaAlO_2$, and 0.601 ± 0.008 g of SiO_2 from colloidal silica in 10.75 mL of water. One-variable-at-a-time experiments were conducted to investigate the effect of each variable as shown in Table 1.

Detailed synthesis conditions of the $NaAlO_2$ experiments are as follows. For the pH variation experiment, 0, 0.6, 1.2, or 1.65, all ±0.006 g, of NaOH were dissolved in 3.75 mL of water, then these solutions were added and mixed into the initial solutions of sodalite precursors, resulting in total precursor solution pH of 13.2, 13.6, 13.9, and 14.0, respectively. Approximately 15 mL of the mixed solution was poured into an autoclave (200 mL acid digestion vessel, Parr Instrument Company, Moline, IL) and placed in an oven at 180°C for 2 days. For the aging time variation experiment, two sets of solutions with or without NaOH (1.65 g) were prepared. Four solutions were placed in an oven at 100°C for 1, 5, 10, and 20 days for each set. For the temperature variation experiment, four solutions were prepared and placed in an oven at 100°C, 140°C, 180°C, and 200°C for 2 days, covering typical hydrothermal process temperature for sodalite minerals.[1,9,27,47] For the Al/Si ratio experiment, the excess amount of $NaAlO_2$ or SiO_2 was added to the initial stoichiometric solution to make the Al/Si ratio equal to 1.5 or 0.5. Therefore, in obtaining the Al/Si ratio of 1.5, it resulted in excess Al and Na. For the precursor concentration experiment, the total amount of water was adjusted to 7.5, 14.5, 29.5, or 44.5 mL of DIW, and the solutions were placed in an oven at 180°C for 2 days.

To compare the yield of iodosodalite synthesized from the commonly used precursors in the literature, four samples of iodosodalite were hydrothermally grown using kaolinite, meta-kaolin, zeolite 4A, or sodium aluminate plus colloidal silica, all under the same process conditions. The synthesis conditions include the stoichiometric ratio of precursors, temperature of 180°C, 2 days of aging,

TABLE 1 Hydrothermal synthesis conditions for parameter variation experiments (pH, aging time, temperature, Al/Si ratio, and precursor concentration). "ND" means that the data for that entry was not determined

		Molar composition of reactants								
No.	Experiment	NaI	$NaAlO_2$	SiO_2	Excess NaOH	H_2O (mL)	pH	Aging time (d)	*T* (°C)	Si/Al
1	pH (NaOH) Variation	1.0	3.0	3.0	0.0	14.5	13.2	2	180	1
2		1.0	3.0	3.0	4.5	14.5	13.6	2	180	1
3		1.0	3.0	3.0	9.1	14.5	13.9	2	180	1
4		1.0	3.0	3.0	12.5	14.5	14.0	2	180	1
5	Aging time variation with NaOH	1.0	3.0	3.0	12.5	14.5	ND	1	100	1
6		1.0	3.0	3.0	12.5	14.5	ND	5	100	1
7		1.0	3.0	3.0	12.5	14.5	ND	10	100	1
8		1.0	3.0	3.0	12.5	14.5	ND	20	100	1
9	Aging time variation without NaOH	1.0	3.0	3.0	0.0	10.8	ND	1	100	1
10		1.0	3.0	3.0	0.0	10.8	ND	5	100	1
11		1.0	3.0	3.0	0.0	10.8	ND	10	100	1
12		1.0	3.0	3.0	0.0	10.8	ND	20	100	1
13	Temperature variation	1.0	3.0	3.0	12.5	14.5	ND	2	100	1
14		1.0	3.0	3.0	12.5	14.5	ND	2	140	1
15		1.0	3.0	3.0	12.5	14.5	ND	2	180	1
16		1.0	3.0	3.0	12.5	14.5	ND	2	200	1
17	Al/Si Ratio variation	1.0	3.0	3.0	12.5	14.5	ND	2	180	1
18		1.0	3.0	6.0	12.5	14.5	ND	2	180	0.5
19		1.0	4.5	3.0	12.5	14.5	ND	2	180	1.5
20	Precursor concentration variation	1.0	3.0	3.0	12.5	7.5	ND	2	180	1
21		1.0	3.0	3.0	12.5	14.5	ND	2	180	1
22		1.0	3.0	3.0	12.5	29.5	ND	2	180	1
23		1.0	3.0	3.0	12.5	44.5	ND	2	180	1

10.75 mL of water, and addition of 3.75 mL of 11 mol·L^{-1} NaOH solution. After the hydrothermal process, all the synthesized samples were washed three times for 5 minute each using a microcentrifuge at 9000 rpm then subsequently dried at 90°C overnight.

2.3 | Characterization methods

XRD (X'Pert Pro MPD, PANalytical, Almelo, Netherlands) spectra were obtained for phase identification and quantification. Three consecutive XRD scans were performed with a Cu-K_α X-ray source at 45 kV and 40 mA in the range of 5° to 90° 2θ with 0.008° 2θ step and 11 seconds of dwelling time per step, and the intensities added. For Rietveld analysis, samples were doped with ~10 mass% of NIST SRM-674b ZnO as an internal standard to quantify phases and crystalline fraction, and subsequently analyzed using Highscore software (PANAlytical). The refined parameters include U, V, and W for the width, preferred orientation for the relative peak heights for different planes, the unit cell, and the sample height (see Supplementary for more details). The weighted profile R values ranged from 5.68% to 11.17%, and the goodness-of-fit values ranged from 0.89 to 3.06 (see Supplementary). SEM (XL-30 field emission SEM and Quanta 200F, FEI, Hillsboro, OR, USA; JSM-7001F field emission, JEOL, Tokyo, Japan) micrographs were obtained to observe the surface morphology. The secondary electron and through the lens detectors were used with the acceleration voltage of 5-15 kV. XPS (Axis 165, Kratos, Manchester, UK) spectra were obtained to understand the chemical state of elements in sodalite. An Al-K_α X-ray source was used at 156 W with 0.15 eV step and 0.3 seconds of dwell time per step, and spectra from two repeated scans were added. FTIR (Thermo Nicolet 6700 spectrometer, ThermoFisher, Waltham, MA, USA) spectra were obtained from 400-4000 cm^{-1} using 64 co-adds with a resolution of 4 cm^{-1}. Sample was added to KBr at a concentration of ~0.5 mass% and pressed into pellets for measurement.

3 | RESULT AND DISCUSSION

3.1 | Products

The products from the hydrothermal synthesis were usually co-crystallized minerals depending on the process conditions. Although the pure iodosodalite within the crystalline fraction was synthesized, it was not possible to synthesize pure iodosodalite without amorphous fraction using the methods described here. The amorphous fraction of the hydrothermally grown sodalite is often ignored in the literature, but this study showed that all the synthesized products contained >40 mass% of the amorphous fraction. Among all the synthesized powders, Sample 8 (see Table 1) had the highest iodosodalite fraction of 54.5 mass% with the rest being amorphous. The mass% of various phases synthesized in process variable experiments are summarized in Figure 4. The error on the phase mass% was estimated to be ±0.06 × the mass% value for major phases (~40-50 mass%) and ±0.076 × the mass% for minor phases (~12-15 mass%) (see Supplementary for details). Most of the products contained some fraction of hydroxysodalite suggesting the presence of β-cages that were empty or filled with OH^- and H_2O. It is not clear from the XRD analysis if the iodosodalite and hydroxysodalite are in the mixed phase such that I^- and OH^- are randomly distributed in the β-cages, or whether they are separate microscopic phases, and further investigation will be performed to confirm. Other mixed sodalites have been reported in the literature, but the experimental evidence is unclear as to how these guest anions are distributed,[47–49] particularly since evidence in mixed halide sodalites indicates the presence of both near ideal miscibility (Cl/Br and Br/I) and domain segregation (Cl/I).[47] It should be noted that the XRD patterns of iodosodalite and hydroxysodalite have several similar peak positions such as near 14° and 24°. The coexistence of the β-cages containing either OH^- or I^- was observed in two ways. First, XRD patterns showed that increase in the peak intensity around 14°, the second major peak position of hydroxysodalite, was observed with increase in hydroxysodalite fraction in pH and aging variation experiments (see Supplementary for details). Second, a refinement test showed that fitting with both iodosodalite and hydroxysodalite resulted in better weighted R and goodness-of-fit values compared to fitting only with iodosodalite or hydroxysodalite. Figure 5 shows an example of fitted peaks using both iodosodalite and hydroxysodalite. For iodosodalite, the crystallographic information files used to refine the data in this study utilized the $P\bar{4}3n$ space group because it provided a better fit to the data. Other phases, including analcime, cancrinite, zeolite A, and nepheline hydrate I, were observed within the tested range as shown in Figure 6, and conditions promoting their formation are discussed in the next section.

The morphology of iodosodalite has polycrystalline features as shown in images in Figure 7. This suggests that iodosodalite nucleates and crystallizes on pre-existing crystallites under suitable conditions. The crystallite size of iodosodalite was estimated to be 25-80 nm by XRD analysis, but as seen with SEM analysis, these crystallites tend to agglomerate into larger clusters. The sodalite crystallites observed with SEM show various sizes, generally <500 nm. All the iodosodalite synthesized with different precursors show the same polycrystalline morphology. Maddrell et al.[3] observed similar morphologies in their hydrothermally grown iodosodalite. The characteristic features of sodalite, cancrinite, and zeolite A are shown in

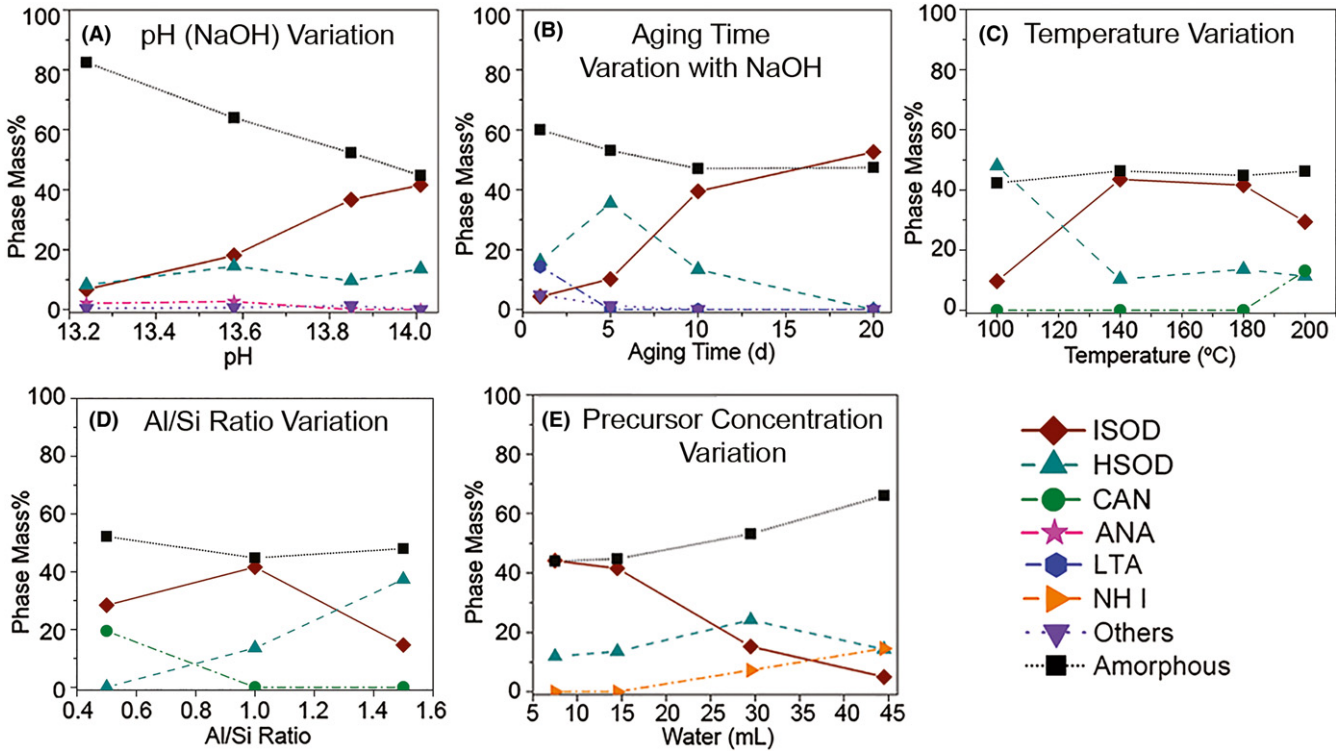

FIGURE 4 Phase mass% distribution of variable experiments. The abbreviation for mineral names and associated ICSD numbers are the following: iodosodalite as ISOD (71434), hydroxysodalite as HSOD (413496), cancrinite as CAN (28521), analcime as ANA (40451), nepheline hydrate as NH I (17069), and zeolite A as LTA (263084) [Color figure can be viewed at wileyonlinelibrary.com]

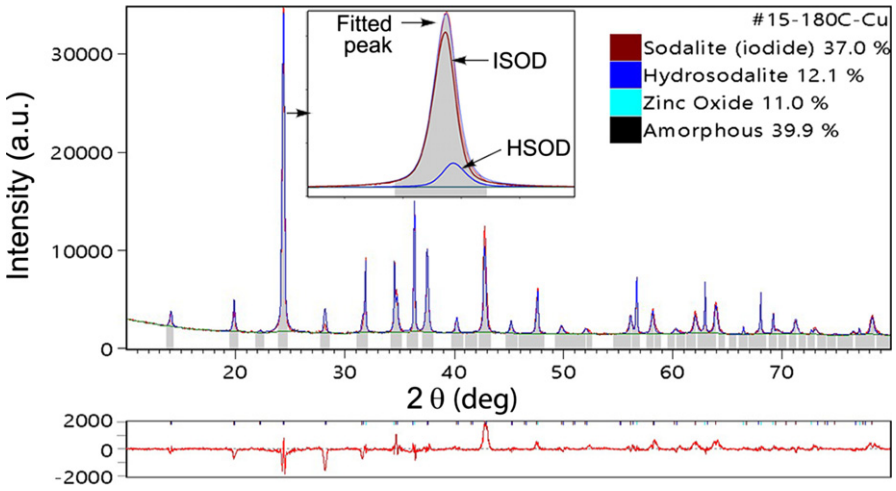

FIGURE 5 Quantification of phase fractions in sample 15 using Rietveld method [Color figure can be viewed at wileyonlinelibrary.com]

Figure 7. The cubic crystallite of zeolite A[27,50,51] and elongated[24,39] or lephispheric[27] crystallites of cancrinte have also been observed in other hydrothermal studies.

3.2 | Effects of process variables on the synthesis

The pH (NaOH concentration) variation study revealed that pH is a crucial variable in the crystallization of iodosodalite. Higher pH yielded higher mass% of iodosodalite and overall crystalline fraction. Although there is no specific study on the effect of pH on the crystallization of iodosodalite to the best of our knowledge, other studies on the zeolites have shown pH as one of the main variables affecting the type and composition of crystallizing material.[23,28,52] The pH value influences the kinetics and the polymerization equilibrium of the aluminosilicate reactant. High pH decreases the induction period in the crystallization

of zeolites.[53] Higher crystalline fraction of sodalite with higher pH suggests that faster dissolution of the initial amorphous gel occurs, followed by polycondensation of the aluminosilicate framework and transformation from the previous phase, possibly zeolite A, to sodalite. NaOH is often used as a mineralizing agent to synthesize zeolite framework minerals such as sodalite, cancrinite, and nepheline hydrate I[1,27,31,38,54] where the OH^- aids in the dissolution of the hydro-gel and reactants, and Na^+ strongly reorganizes surrounding water molecules.[22] Walton et al.[55] reported that higher NaOH concentration resulted in faster transformation of zeolite A to hydroxysodalite in their hydrothermal synthesis. In our study, besides sodalite, analcime with cubic symmetry was precipitated at pH of 13.2 and 13.6; however, only a small fraction was observed indicating that sodalite is more stable within the given condition.

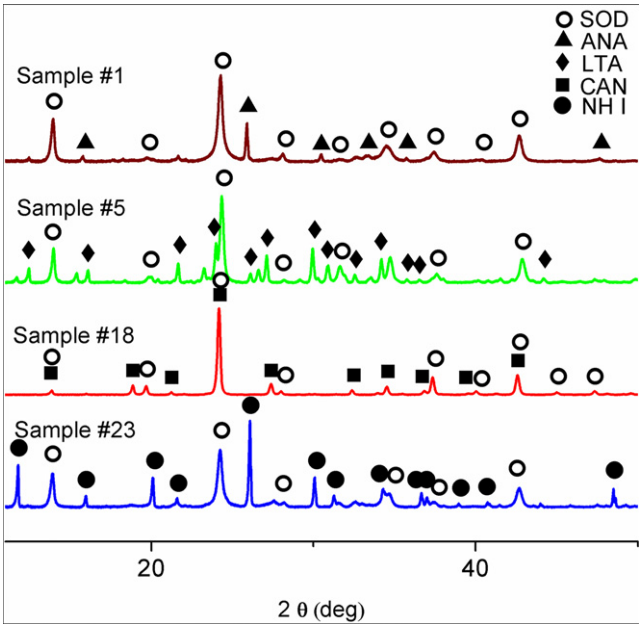

FIGURE 6 XRD patterns of synthesized samples showing co-crystallization of sodalite and other phases. SOD, ANA, LTA, CAN, and NH I denote sodalite, analcime, zeolite A, and nepheline hydrate I respectively [Color figure can be viewed at wileyonlinelibrary.com]

The effect of aging time variation was investigated on the two sets of samples synthesized at 100°C for 1-20 days, with or without the addition of NaOH. The samples synthesized with NaOH showed higher mass% of iodosodalite with longer aging time. The 20 days sample had ~50 mass% of iodosodalite with the other half amorphous. This trial achieved the highest iodosodalite fraction among the synthesized powders, suggesting that aging time is a critical variable. Between the 1 and 5 days samples, the transformation of zeolite A to sodalite phase was observed. Our results showed the co-crystallization of zeolite A as the major phase and sodalite as the minor phases in the 1 day sample, and that mostly sodalite phase was

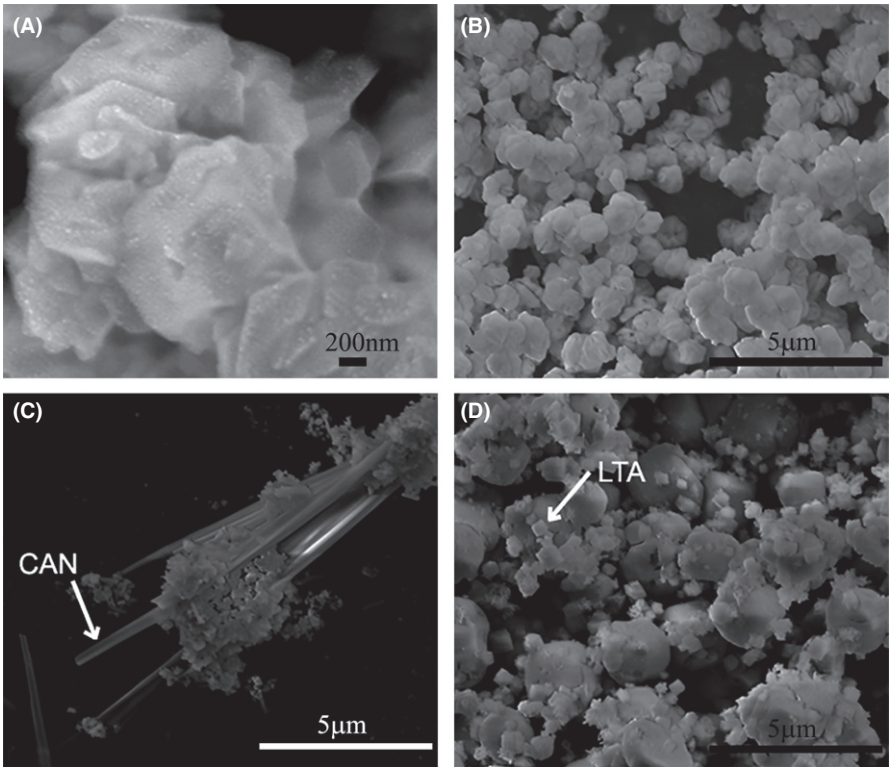

FIGURE 7 SEM micrographs of (A) iodosodalite with higher magnification, (B) iodosodalite, (C) cancrinite, and (D) LTA

formed by the 5 days sample. This indicated that transformation of zeolite A to sodalite occurred within 1 day and almost completed by 5 days. Liu et al.[1] observed the transformation of zeolite A to sodalite phase within 8 hours at 90°C. Rios et al.[41] observed the transformation of zeolite A→sodalite→cancrinite in the samples synthesized at 100°C for 6-120 hours. Our result along with previous studies in the literature shows that transformation from amorphous gel to zeolite A is an intermediate phase between amorphous gel and sodalite. Iodosodalite phase fraction increased while the hydroxysodalite fraction decreased as aging time increased. This indicates that there is possible anion exchange occurring between OH^- and I^-. Once a larger I^- anion is positioned inside the β-cage, it would be less likely to be replaced by smaller OH^- anion. This will cause increase in iodosodalite fraction with aging time. More investigation will be performed to verify this anion exchange. The powder samples synthesized without addition of NaOH contained mainly zeolite A and zeolite P1, $Na_6(Al_6Si_{10}O_{32})(H_2O)_{12}$, as the major phases, and almost no sodalite was present regardless of aging time.

To investigate the effect of temperature, four samples were synthesized at 100°C, 140°C, 180°C, and 200°C soak temperatures. The XRD results showed the highest iodide fraction was obtained at 140°C and 180°C. At the 100°C, the formation of hydroxysodalite was favored, whereas at 200°C the formation of cancrinite was observed along with sodalite. This suggests that iodosodalite formation would be maximized between 140°C and 180°C. Higher yield of sodalite from 100°C to 140°C is due to the solubility of zeolite A and sodalite. The solubility of both phases increases as the temperature increases, and zeolite A has higher solubility than sodalite.[55] This will result in faster dissolution of zeolite A and nucleation of sodalite. The crystallization of cancrinite at 200°C indicates the phase transformation of sodalite to cancrinite at higher temperature. Although the sodalite is more thermodynamically stable than cancrinite,[40] the transformation of sodalite to cancrinite at the higher temperature and longer aging time has been observed in the literature.[1,24,39,41] The phase transformation of sodalite to cancrinite is believed to be a slow solution-based mechanism involving the dissolution of sodalite and subsequent formation of cancrinite in a liquid medium.[56] The effect of the Al/Si ratio in the precursors was investigated using three samples synthesized with Al/Si ratio of 0.5, 1, and 1.5. The Al/Si ratio of 0.5 resulted in the formation of the cancrinite and a decrease in sodalite fraction. The excess $NaAlO_2$ was added to make the Al/Si ratio of 1.5, and the results showed that the excess Na and Al favored the formation of hydroxysodalite. The Al/Si ratio is known to control the equilibrium state of precursors during synthesis, and the composition of the crystallizing materials.[53] Oleksiak et al.[57] reported that the Al/Si ratio influenced the nucleation and the initial crystalline phase. A low Al/Si ratio in the precursor is reported to help the crystallization of basic cancrinite in hydrothermal synthesis, even though basic cancrinite has a Al/Si molar ratio of 1.[58]

The precursor concentration was varied by adding different volumes of water, and four samples were synthesized with the water volume equal to 7.5, 14.5, 29.5, or 44.5 mL. Lowering the water amount increased the fraction of iodosodalite, whereas increasing the water amount revealed the formation of nepheline hydrate I, which was consistent with Buhl et al.[25] who showed that lower NaOH concentration favored the formation of nepheline hydrate I in their hydrothermal synthesis at 200°C. Rios et al.[27] reported the formation of nepheline hydrate I at 200°C but none at 100°C. Lin et al.[24] observed the transformation of zeolite A to nepheline hydrate I within 3 hours at 200°C. Our NaOH concentration study at 180°C did not show the presence of nepheline hydrate I at the lowest tested NaOH concentration; however, lowering the overall precursor concentration, including NaOH, and synthesizing at 180°C showed the formation of nepheline hydrate I. Comparatively, the samples synthesized without any NaOH at 100°C favored the formation of zeolite A. These observations suggest that the crystallization of both zeolite A and nepheline hydrate I favor the low precursor concentration, but zeolite A is shown to crystallize at relatively low temperatures, whereas nepheline hydrate I is only observed at ≥180°C.

Four iodosodalite samples were synthesized using different commonly used precursors including sodium aluminate, colloidal silica, zeolite 4A, kaolinite, and meta-kaolin, under the same conditions (180°C, 2 days of aging, and Al/Si=1), and the resulting phase distributions were compared. All the precursors except meta-kaolin were used as-received. Meta-kaolin was synthesized by heat-treating kaolinite at 850°C for 17 hours. The XRD pattern of meta-kaolin showed mostly amorphous with partial crystalline phases. The sodalite powder synthesized from the zeolite 4A precursor had the highest iodosodalite mass fraction among the four tested precursors as shown in Figure 8. In all cases, the major crystalline phase was iodosodalite, followed by hydroxysodalite; a small fraction of cancrinite was observed in the samples synthesized with zeolite 4A, kaolinite, and meta-kaolin.

3.3 | Chemistry of sodalite

XPS was performed on two samples with high iodosodalite (sample 8) and high hydroxysodalite (sample 13) fractions to understand the chemical state of sodalite. The measured

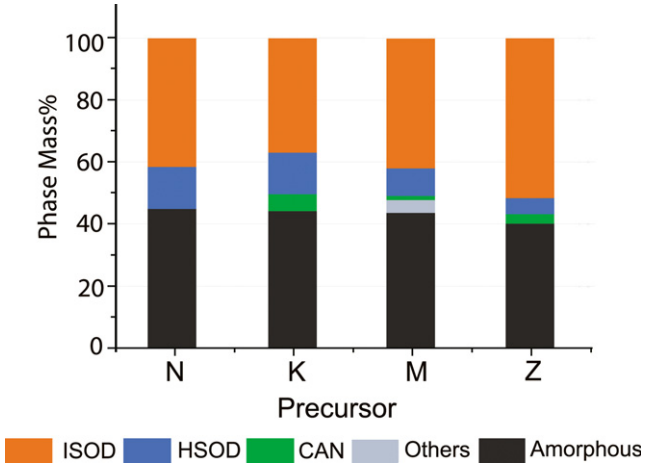

FIGURE 8 Phase mass% of the product synthesized with different precursors (N: $NaAlO_2$+SiO_2+NaOH+NaI, K: Kaolinite+NaOH+NaI, M: Meta-kaolin+NaOH+NaI, and Z: Zeolite 4A+NaOH+NaI). Here, "ISOD" denotes iodosodalite, "HSOD" denotes hydroxysodalite, and "CAN" denotes cancrinite [Color figure can be viewed at wileyonlinelibrary.com]

peaks were adjusted according to C (1*s*) reference peak at 248.6 eV. The binding energy of I (3*d*5/2) was measured at 619.1 eV which indicates I^- (618.4 eV[59] and 618.7 eV[60]) but not I^{5+} (623.5 eV[59]) nor I^{7+} (624.0 eV[59]) as shown in Figure 9 (see also Supplementary). This result confirmed that the oxidation number of iodine in iodosodalite samples is −1 as it should be. However, the measured binding energy for I (3*d*5/2) was 0.4 to 0.7 eV higher than published iodine data for NaI. In order to check the instrumental error, XPS on NaI precursor was performed and showed the peak position of I (3*d*5/2) at 618.4 eV. The higher binding energy for I (3*d*5/2) in sodalite can be due to the difference in the structure. In

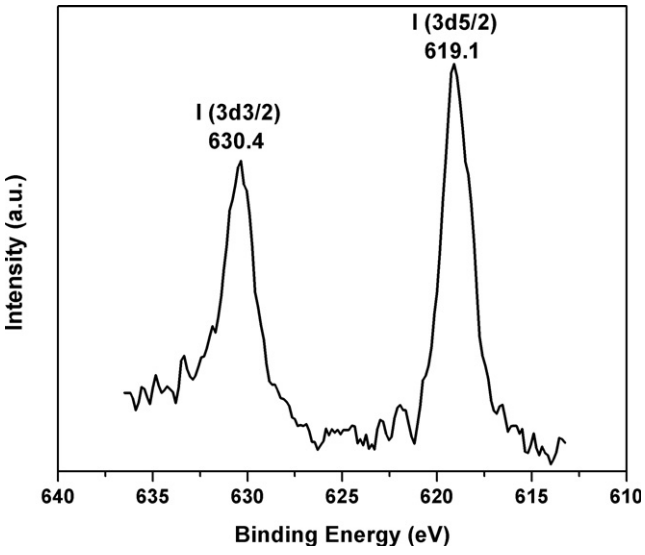

FIGURE 9 XPS spectra of I (3d) in sample 8

iodosodalite, I^- is surrounded by four Na^+ cations forming a tetrahedron at the center of the negatively charged β-cage, whereas I^- in salt NaI is surrounded by six Na^+ cations forming an octahedron. The distance between Na and I in the β-cage is 3.12 Å compared to 2.71 Å for salt NaI, which implies that the electrostatic force between Na and I in sodalite is weaker than that of salt NaI. This will result in higher binding energy for the electrons of iodide in the sodalite as the less attraction force is exerted from Na^+ cation. In addition, the scanning step size makes the accuracy of the measurement ±0.15 eV. Although no specific XPS study has been performed on iodosodalite to the best of our knowledge, studies on zeolites have shown that different structures resulted in shift in binding energies for Si–O.[61] The measured binding energies of sodalite samples (Na, Al, Si, O, I) compared with published data are summarized in Table 2 (spectra are shown in Supplementary). The measured XPS result is valid for confirming the oxidation state of iodine as there is a significant difference (~5 eV) for the binding energies between iodide and iodate.

FTIR was performed on three samples with different iodosodalite and hydroxysodalite fractions as shown in Figure 10. The result was in good agreement with published data as shown in Table 3. O–H stretching bands from water were observed ~3000 to 3700 cm^{-1}, and higher water content was observed in the sample with higher hydroxysodalite fraction. The O-H deformation vibration was observed ~1642 cm^{-1}, and the hydroxyl OH^- absorption band were observed ~3634 cm^{-1} for samples with hydroxysodalite. These water and hydroxyl absorption bands have been reported in the literature.[20,34] The absorption bands due to impurity of CO_3^{2-} were observed at 841 and 1440 cm^{-1}. The peak between 840 and 880 cm^{-1} is typically observed in CO_3^{2-} bearing cancrinite,[62] and the CO_3^{2-} band ~1450 cm^{-1} region has been shown in hydrothermally grown sodalite.[20,63] This suggests that there may be a small fraction of cancrinite phase in the samples. In agreement with XPS, FTIR showed that there is no iodate in the synthesized product. Buhl[35] reported that a significant vibration of iodate was observed at 775 cm^{-1} for iodate sodalite, and this band was not observed in any FTIR spectrum.

3.4 | Implications for nuclear waste management

This study was focused on the effects of process variables on the iodosodalite yield, and the result can be helpful to optimize the iodosodalite yield using a hydrothermal method. In a future study, the synthesized powders will be mixed with glass binders and sintered to form a glass-bonded waste form. The iodine fraction and chemical

TABLE 2 XPS binding energies of sample 8, 13 and published data for hydroxysodalite. The measured binding energies were referenced to C (1s) at 284.6 eV. "NA" means that data for that entry is not applicable

	Phase mass%			Binding energy (eV)				
Material	**ISOD**	**HSOD**	**Amorphous**	**Na (1*s*)**	**Al (2*p*)**	**Si (2*p*)**	**O (1*s*)**	**I (3*d*5/2)**
Sample 8	52.6	0.0	47.4	1070.5	74.2	102.1	531.0	619.1
Sample 13	9.7	48.0	42.3	1070.5	74.5	102.1	530.9	618.8
HSOD[61]	NA			Not stated	73.6	101.5	530.9	NA
HSOD[64]	NA			1070.3	73.8	101.5	530.2	NA

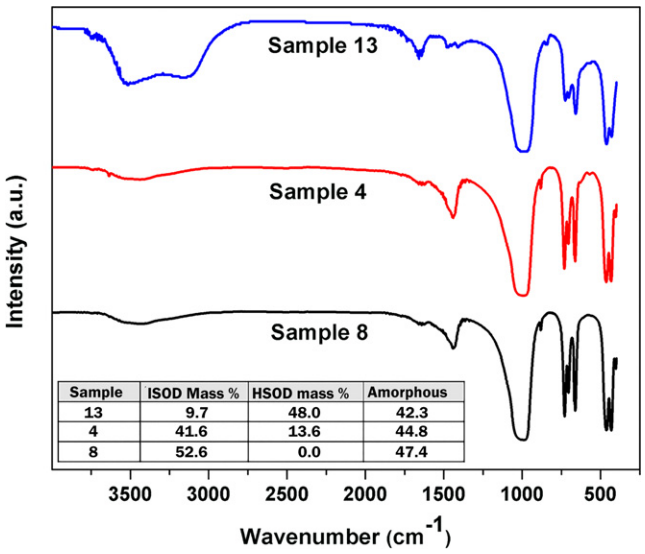

FIGURE 10 FTIR spectra of sodalite samples with different amount of iodosodalite (ISOD) and hysdroxysodalite (HSOD) fractions, as shown in inset [Color figure can be viewed at wileyonlinelibrary.com]

durability of the glass-bonded waste form will be characterized and compared to other iodine containing waste forms. Though the focus in this study was to obtain the highest fraction of iodosodalite in washed powders, the focus of the latter study will be to obtain the highest incorporation of iodine in iodosodalite in unwashed powders after consolidation and heat treatment at low temperatures to prevent iodine volatilization.

4 | CONCLUSION

The effect of six variables (pH, aging time, temperature, Al/Si ratio, differing precursors, and precursor concentration) on the hydrothermal synthesis of iodosodalite was investigated. Higher pH and longer aging time increased the iodosodalite yield along with the overall crystalline fraction within the tested range. The crystallization of iodosodalite was favored in the temperature range between 140°C and 180°C. A lower water amount and Al/Si molar ratio of unity yielded a higher mass% of iodosodalite (up to ~50 mass%, with the remainder being X-ray amorphous). From aging time and temperature variation experiments, the phase transformation of zeolite A→sodalite→cancrinite was observed with longer aging time and higher temperature, respectively. Among the tested precursors, the product synthesized via zeolite 4A had the highest mass% of iodosodalite. XPS and FTIR verified the presence of iodide but not iodate.

TABLE 3 IR absorption bands of sample 4, 8, 13 and published data for several sodalite. "NA" means that data for that entry is not applicable

	Phase mass%			Vibration Frequency of T–O bands (cm^{-1})		
Material	**ISOD**	**HSOD**	**Amorphous**	**ν_{as} (T–O)**	**ν_s (T–O)**	**δ (O–T–O)**
Sample 13	9.7	48.0	42.3	994	725, 702, 663	461, 430
Sample 4	41.6	13.6	44.8	995	730, 704, 661	462, 432
Sample 8	52.6	0.0	47.4	996	729, 704, 661	461, 431
ISOD[65]	NA			997	728, 701, 661	462, 431
ISOD[20]	NA			961	730, 697, 661	455, 420
HSOD[63]	NA			not stated	731, 705, 660	465, 430
HSOD[66]	NA			1096, 986	729, 701, 660	not stated
ClSOD[65]	NA			981	738, 713, 671	469, 437
BrSOD[65]	NA			986	733, 708, 667	465, 434

ACKNOWLEDGMENTS

This research was supported by the U.S. Department of Energy in support of the Nuclear Energy University Program-Advanced Waste Forms program, award # DE-NE0008257. The authors also thank Grant Norton, Min Kyu Song, Ashutosh Goel, Denis Strachan, Ewan Maddrell, John Dickson, and the anonymous reviewers for helpful comments, José Marcial for help with XRD, Young Jay Ryu for help with SEM, Jared Kroll for help with FTIR, and Louis Scudiero for help with XPS.

REFERENCES

1. Liu Q, Navrotsky A. Synthesis of nitrate sodalite: an in situ scanning calorimetric study. *Geochim Cosmochim Acta*. 2007;71: 2072-2078.
2. Nakazawa T, Kato H, Okada K, Ueta S, Mihara M. Iodine immobilization by sodalite waste form, 1-8 in Proc. Materials Research Society. 663. MRS Proceedings;2000
3. Maddrell E, Gandy A, Stennett M. The durability of iodide sodalite. *J Nucl Mater*. 2014;449:168-172.
4. Lepry WC, Riley BJ, Crum JV, Rodriguez CP, Pierce DA. Solution-based approaches for making high-density sodalite waste forms to immobilize spent electrochemical salts. *J Nucl Mater*. 2013;442:350-359.
5. Stein A, Ozin GA, Stucky GD. Silver sodalites. A chemistry approach towards reversible optical data storage. *J. Soc. Photogr. Sci. Technol. Japan*. 1990;53:322-328.
6. Bolwijn P, Schipper D, Van Doorn C. Cathodrochromic properties of sodalite. *J Appl Phys*. 1972;43:132-137.
7. Marder S, Sohn JE, Stucky GD. *Materials for Nonlinear Optics (ACS Symposium Series 455)*. Washington D. C: American Chemical Society; 1991.
8. Jelinek R, Chmelka B, Stein A, Ozin G. Multinuclear magicangle spinning and double-rotation NMR study of the synthesis and assembly of a sodalite semiconductor supralattice. *J Phys Chem*. 1992;96:6744-6752.
9. Brenchley ME, Weller MT. Synthesis and structures of $M_8[AlSiO_4]_6{\cdot}(XO_4)_2$, M= Na, Li, K; X= Cl Mn Sodalites.. *Zeolites*. 1994;14:682-686.
10. Fechtelkord M. Influence of Sodium Ion Dynamics on the 23Na Quadrupolar Interaction in Sodalite: A High-Temperature ^{23}Na MAS NMR Study. *Solid State Nucl Mag Res*. 2000;18:70-88.
11. Borhade A, Wakchaure S, Dholi A. One pot synthesis and crystal structure of aluminosilicate mixed chloro-iodo sodalite. *Ind. J. Phys*. 2010;84:133-141.
12. Babad H, Strachan DM. Method for immobilizing radioactive iodine. USPTO, US4229317 A. The United States of America as Represented by the United States Department of Energy; 1980.
13. Maddrell ER, Vance ER, Gregg DJ. Capture of iodine from the vapour phase and immobilisation as sodalite. *J Nucl Mater*. 2015;467:271-279.
14. Chong S, Peterson J, Riley B,McCloy J. Hydrothermal synthesis and analysis of iodine-containing sodalite, 16153 in Proc. Waste Management. WM2016; 2016.
15. Ebert WL. Testing to evaluate the suitability of waste forms developed for electrometallurgically treated spent sodium-bonded nuclear fuel for disposal in the Yucca Mountain repository, ANL-05/43. Argonne, Illinois: Argonne National Laboratory; 2006.
16. Bateman K, Knight C, Solbrig C. Current status of ceramic waste form development, Idaho National Laboratory, Idaho Falls, ID, INL/INT-06-11736; 2007.
17. Beagley B, Henderson C, Taylor D. The crystal structures of aluminosilicate-sodalites: x-ray diffraction studies and computer modelling. *Miner Mag*. 1982;46:459-464.
18. Nielsen NC, Bildsøe H, Jakobsen HJ, Norby P. ^{7}Li, ^{23}Na, and ^{27}Al quadrupolar interactions in some aluminosilicate sodalites from MAS NMR spectra of satellite transitions. *Zeolites*. 1991;11:622-632.
19. Hamilton WC. Significance tests on the crystallographic R factor. *Acta Cryst*. 1965;18:502-510.
20. Bardez I, Campayo L, Rigaud D Chartier M, Calvet A.Investigation of sodalites for conditioning halide salts (NaCl and NaI): Comparison of two synthesis routes, O4_19 in. ATALANTE 2008; 2008.
21. Novembre D, Gimeno D, Pasculli A, Di Sabatino B. Synthesis and characterization of sodalite using natural kaolinite: an analytical and mathematical approach to simulate the loss in weight of chlorine during the synthesis process. *Fresn Environ Bull*. 2010;19:1109-1117.
22. Derouane EG, Lemos F, Naccache C, Ribeiro FR, *Zeolite Microporous Solids: Synthesis, Structure, and Reactivity*, Vol. 352.Berlin, Germany Springer Science & Business Media; 2012.
23. Breck DW. *Zeolite Molecular Sieves: Structure, Chemistry, and Use* , Vol. 4.New York City, New York, Wiley; 1974.
24. Lin D-C, Xu X-W, Zuo F, Long Y-C. Crystallization of JBW, CAN, SOD and ABW type zeolite from transformation of metakaolin. *Microp Mesop Mater*. 2004;70:63-70.
25. Hofs T, Buhl J-C. Synthesis, hydrothermal stability and thermal reaction behavior of nepheline hydrate i (NH I). *React Kinet Catal Lett*. 2005;84:375-382.
26. Rios CA, Williams CD, Maple MJ. Synthesis of zeolites and zeotypes by hydrothermal transformation of kaolinite and metakaolinite. *Bistua*. 2007;5:15-26.
27. Reyes CR, Williams CD, Roberts C. Synthesis and characterisation of SOD-, CAN-and JBW-type structures by hydrothermal reaction of kaolinite at 200°C. *Dyna*. 2011;78:38-47.
28. Barrer RM. *Hydrothermal Chemistry of Zeolites* Amsterdam, Netherlands: Academic Press; 1982.
29. Nabavi MS, Mohammadi T, Kazemimoghadam M. Hydrothermal synthesis of hydroxy sodalite zeolite membrane: Separation of H_2/CH_4. *Ceram. Intern*. 2014;40:5889-5896.
30. Xu X, Bao Y, Song C, Yang W, Liu J, Lin L. Microwaveassisted hydrothermal synthesis of hydroxy-sodalite zeolite membrane. *Microp Mesop Mater*. 2004;75:173-181.
31. Kendrick E, Dann S. Synthesis, properties and structure of ion exchanged hydrosodalite. *J Solid State Chem*. 2004;177:1513-1519.
32. Felsche J, Luger S, Baerlocher C. Crystal structures of the hydrosodalite $Na_6[AlSiO_4]_6{\cdot}8H_2O$ and of the anhydrous sodalite $Na_6[AlSiO_4]_6$. *Zeolites*. 1986;6:367-372.
33. Hassan I, Grundy H. Structure of basic sodalite, $Na_8Al_6Si_6O_{24}(OH)_2{\cdot}2H_2O$. *Acta Cryst C*. 1983;39:3-5.
34. Engelhardt G, Felsche J, Sieger P. The hydrosodalite system $Na_{6+\ x}[SiAlO_4]_6(OH)_x{\cdot}nH_2O$: formation, phase composition, and de-and rehydration studied by ^{1}H, ^{23}Na, and ^{29}Si MAS-NMR

spectroscopy in tandem with thermal analysis, x-ray diffraction, and IR spectroscopy. *J Am Chem Soc*. 1992;114:1173-1182.
35. Buhl J-C. The properties of salt-filled sodalites. Part 4. Synthesis and heterogeneous reactions of iodate-enclathrated sodalite $Na_8[AlSiO_4]_6(IO_3)_{2-x}(OH{\cdot}H_2O)_x$; 0.7< x< 1.3. *Thermochim Acta*. 1996;286:251-262.
36. Hassan IN, Grundy HD. The crystal structure of basic cancrinite, ideally Na8[Al6Si6O24](OH)2·3H2O. *Canad Miner*. 1991;29: 377-383.
37. Barrer R, Cole J, Villiger H. Chemistry of soil minerals. Part VII. Synthesis, properties, and crystal structures of salt-filled cancrinites. *J Chem Soc A*. 1970;1523-1531.
38. Fechtelkord M, Posnatzki B, Buhl J-C. Characterization of basic cancrinite synthesized in a butanediol-water system. *Eur J Miner*. 2003;15:589-598.
39. Vaughan DE, Yennawar HP, Perrotta AJ, Benesi AJ. Structure comparison of co-crystallized 6-and 12-sided large cancrinite crystals. *Microp Mesop Mater*. 2009;123:274-279.
40. Fechtelkord M, Posnatzki B, Buhl J-C. Synthesis of basic cancrinite in a butanediol-water system. *Chem Mater*. 2001;13:1967-1975.
41. Reyes CAR, Williams C, Alarcón OMC. Nucleation and growth process of sodalite and cancrinite from kaolinite-rich clay under low-temperature hydrothermal conditions. *Mater Res*. 2013;16: 424-438.
42. Baerlocher C, McCusker LB, Olson DH. *Atlas of Zeolite Framework Types*. Amsterdam, Netherlands: Elsevier; 2007.
43. Hansen S, Fälth L. X-ray study of the nepheline hydrate I structure. *Zeolites*. 1982;2:162-166.
44. Edgar A. Note on lattice parameters of nepheline hydrate I. *Am Miner*. 1964;49:1139-1141.
45. Guth JL. Properties of foreign anions in sodium aluminosilicates with three-dimensional framework. *Rev Chim Minerale*. 1965;2:127-144.
46. Ghobarkar H, Schäf O. Effect of temperature on hydrothermal synthesis of analcime and viseite. *Mater Sci Eng, B*. 1999;60: 163-167.
47. Trill H, Eckert H, Srdanov VI. Mixed halide sodalite solid solution systems. Hydrothermal synthesis and structural characterization by solid state NMR. *J Phys Chem B*. 2003;107:8779-8788.
48. Dickson JO, Harsh JB, Lukens WW, Pierce EM. Perrhenate incorporation into binary mixed sodalites: The role of anion size and implications for technetium-99 sequestration. *Chem Geol*. 2015;395:138-143.
49. Dickson JO, Harsh JB, Flury M. W. W. Lukens WW, Pierce EM. Competitive Incorporation of Perrhenate and Nitrate into Sodalite. *Environ Sci Technol*. 2014;48:12851-12857.
50. Hashemian S, Houssini SH, Salehifar H, Salari K. Adsorption of Fe(III) from Aqueous Solution by Linde Type-A Zeolite. *Amer. J. Analy. Chem*. 2013;4:123-126.
51. Kuwahara Y, Ohmichi T, Kamegawa T, Mori K, Yamashita H. A novel conversion process for waste slag: synthesis of a hydrotalcite-like compound and zeolite from blast furnace slag and evaluation of adsorption capacities. *J Mater Chem*. 2010;20: 5052-5062.
52. Occelli ML, Robson HE. *Zeolite Synthesis*, Washington, D.C., USA: American Chemical Society;1989.
53. Bhatia S. *Zeolite Catalysts: Principles and Applications*. Boca Raton, Florida, USA; CRC press; 1989.
54. Healey AM, Johnson GM, Weller MT. The synthesis and characterisation of JBW-type zeolites.: part A: sodium/potassium aluminosilicate, $Na_2K[Al_3Si_3O_{12}]{\cdot}0.5H_2O$. *Microp Mesop Mater*. 2000;37:153-163.
55. Walton RI, Millange F, O'Hare D, Davies AT, Sankar G. Catlow CRA. An in situ energy-dispersive X-ray diffraction study of the hydrothermal crystallization of zeolite A. 1. Influence of reaction conditions and transformation into sodalite. *J Phys Chem B*. 2001;105:83-90.
56. Barnes MC, Addai-Mensah J, Gerson AR. The mechanism of the sodalite-to-cancrinite phase transformation in synthetic spent Bayer liquor. *Microp Mesop Mater*. 1999;31:287-302.
57. Oleksiak MD, Soltis JA, Conato MT, Penn RL, Rimer JD. Nucleation of FAU and LTA Zeolites from heterogeneous aluminosilicate precursors. *Chem Mater*. 2016;28:4906-4916.
58. Yuan J, Yang J, Ma H, Liu C, Zhao C. Hydrothermal synthesis of analcime and hydroxycancrinite from K-feldspar in Na_2SiO_3 solution: characterization and reaction mechanism. *RSC Adv*. 2016;6:54503-54509.
59. Sherwood PM. X-ray photoelectron spectroscopic studies of some iodine compounds. *J Chem Soc, Faraday Trans*. 1976;2:1805-1820.
60. Morgan WE, Van Wazer JR, Stec WJ. Inner-orbital photoelectron spectroscopy of the alkali metal halides, perchlorates, phosphates, and pyrophosphates. *J Am Chem Soc*. 1973;95:751-755.
61. Herreros B, He H, Barr TL, Klinowski J. ESCA studies of framework silicates with the sodalite structure: 1 Comparison of purely siliceous sodalite and aluminosilicate sodalite.. *J Phys Chem* 1994;98:1302-1305.
62. Pekov IV, Olysych LV, Chukanov NV, et al. Crystal chemistry of cancrinite-group minerals with an AB-type framework: a review and new data I. Chemical and structural variations.. *Canad Miner*. 2011;49:1129-1150.
63. Buhl J-C, Hoffmann W, Buckermann W, Müller-Warmuth W. The crystallization kinetics of sodalites grown by the hydrothermal transformation of kaolinite studied by ^{29}Si MAS NMR. *Solid State Nucl Magn Res*. 1997;9:121-128.
64. Wagner C, Passoja D, Hillery H, et al. Auger and photoelectron line energy relationships in aluminum–oxygen and silicon–oxygen compounds. *J Vac Sci Techn*. 1982;21:933-944.
65. Stein A, Ozin GA, MacDonald PM, Stucky GD, Jelinek R, Pines A. *Class A sodalites: silver, sodium, halosodalites*, DTIC document; 1992.
66. Hermeler G, Buhl J-C, Hoffmann W. The influence of carbonate on the synthesis of an intermediate phase between sodalite and cancrinite. *Catal Today*. 1991;8:415-426.

How to cite this article: Chong S, Peterson J, Nam J, Riley B, J McCloy. Synthesis and characterization of iodosodalite. *J Am Ceram Soc*. 2017;100:2273–2284.

Glass-bonded iodosodalite waste form for immobilization of I-129

Saehwa Chong,[1] Jacob A. Peterson, [3] Brian J. Riley,[3] Diana Tabada,[4] Donald Wall,[4] John S. McCloy[1, 2, 3]

[1]Materials Science and Engineering Program, Washington State University, Pullman, WA 99164

[2]School of Mechanical and Materials Engineering, Washington State University, Pullman, WA 99164

[3]Pacific Northwest National Laboratory, Richland, WA 99354

[4]Nuclear Science Center, Washington State University, Pullman, WA 99164

Corresponding author – John S. McCloy, john.mccloy@wsu.edu, School of Mechanical and Materials Engineering, Washington State University, PO BOX 642920, Pullman, WA 99164-2920

Highlights

- Waste forms for radioactive iodine synthesized and tested
- Hydrothermal iodosodalite ($Na_8(AlSiO_4)_6I_2$) glass-bonded using borosilicate glasses
- Iodine quantified by neutron activation analysis, volumetric, and Rietveld XRD
- ASTM C1308 chemical durability test measured release rate of iodine and cations

Glass-bonded Iodosodalite

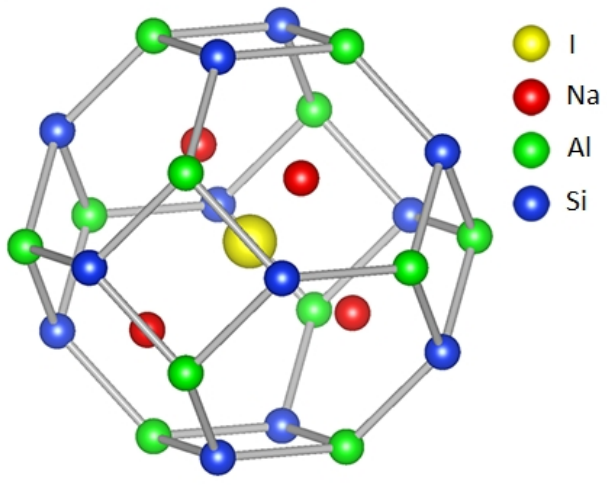

Characterization

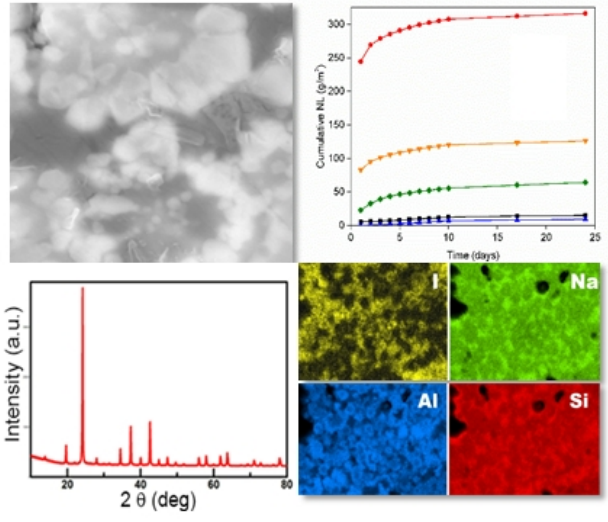

- XRD
- SEM/EDS
- FTIR
- NAA
- TGA/DSC
- ICP-MS
- Porosity

Glass-bonded iodosodalite waste form for immobilization of I-129

Saehwa Chong,[1] Jacob A. Peterson, [3] Brian J. Riley,[3] Diana Tabada,[4] Donald Wall,[4] John S. McCloy[1, 2, 3]

[1]Materials Science and Engineering Program, Washington State University, Pullman, WA 99164

[2]School of Mechanical and Materials Engineering, Washington State University, Pullman, WA 99164

[3]Pacific Northwest National Laboratory, Richland, WA 99354

[4]Nuclear Science Center, Washington State University, Pullman, WA 99164

Abstract

Immobilization of radioiodine (e.g., ^{129}I, ^{131}I) is an important need for current and future nuclear fuel cycles. For the current work, iodosodalite [$Na_8(AlSiO_4)_6I_2$] was synthesized hydrothermally from metakaolin, NaI, and NaOH. Following hydrothermal treatment, dried unwashed powders were used to make glass-bonded iodosodalite waste forms by heating pressed pellets at 650, 750, or 850 °C with two different types of sodium borosilicate glass binders, i.e., NBS-4 and SA-800. These heat-treated specimens were characterized with X-ray diffraction, Fourier-transform infrared spectroscopy, scanning electron microscopy, energy dispersive spectroscopy, thermal analysis, porosity and density measurements, neutron activation analysis, and inductively-coupled plasma mass spectrometry. The pellets mixed with 10 mass% of NBS-4 or SA-800 and heat-treated at 750 °C contained ~44-47 % retention of batched iodine with relatively low porosities, while other pellets with higher iodine retention either contained higher porosity or were not completely sintered. ASTM C1308 chemical durability tests of monolithic specimens showed a large initial release of Na, Al, Si, and I on the first day, possibly from water-soluble salt crystals or non-durable amorphous phases. Release rates of Na and Si were higher than for Al and I, probably due to a poorly durable Na-Si-O phase from the glass bonding matrix. The cumulative normalized releases of iodine for the identical specimens with different *S*/V values of 80 or 8 m^{-1} were 12.5 and 91.9 g/m^2 for the first 10

1-d exchanges, suggestive of coherent dissolution. The average release rates of iodine from 10-24 days during the 7-d exchange intervals were 0.23 and 1.29 $g/m^2/d$ for 80 or 8 m^{-1} respectively.

Keywords

Iodosodalite; sodalite; glass ceramic waste form; glass composite material

1. Introduction

The disposal of radionuclides in stable waste forms is of great importance to the long-term safety of humans and environment. These radionuclides can be released from a variety of processes including medical isotopes, legacy nuclear wastes from Cold War weapons production, and reprocessing of used nuclear fuel. During nuclear fuel reprocessing, several radionuclides are released from the fuel and some enter the off-gas stream such ^{129}I, which is very problematic due to its long half-life of 15.7 million years, high mobility in the earth's environment, easy incorporation into the human thyroid, and difficulty to immobilize using traditional vitrification methods [1-5].

A process from generation to disposal of ^{129}I requires both capture and immobilization. Several methods have been proposed to capture iodine using solid sorbents and wet scrubbing. For solid sorbents, currently planned or deployed methods to capture iodine are focused on usage of silver-loaded zeolite (AgZ) [6], silver nitrate-loaded silica (AgS) [7], and silver nitrate-loaded alumina (AgA) [8]. For wet scrubbing methods, commonly studied methods for iodine capture involve caustic scrubbing, Mercurex, electrolytic scrubbing, and Iodox [9]. Among these methods, hydrothermal synthesis of iodine-containing minerals in high pH solution can be useful for capturing iodine in the caustic scrubber solution. However, the caustic scrubber solution contains various radionuclides, halides, and dissolved hydroxide-scrubbable species, e.g., Cl^-, CO_2, and NO_x^-. Finally, it is a challenge to separate iodine effectively from other anionic species and incorporate into a waste form structure with good chemical durability.

In this study, we demonstrate the immobilization of iodine in iodosodalite [$Na_8(AlSiO_4)_6I_2$] and provide characterization of the waste forms. Waste form characterizations performed include X-ray diffraction

(XRD), Fourier-transform infrared (FTIR) spectroscopy, scanning electron microscopy (SEM), energy dispersive spectroscopy (EDS), thermal analysis, porosity and density measurements, as well as chemical durability using ASTM C1308-14 tests [10]. For iodine quantification, neutron activation analysis (NAA) and inductively-coupled plasma mass spectrometry were utilized (ICP-MS).

2. Background

2.1 Sodalite

Sodalite is a microporous mineral, similar to zeolites, with an aluminosilicate β-cage in which various ions can incorporate. The general chemical formula of sodalite is $M^{1+}_{8}(A^{3+}B^{4+}O^{2-}_{4})_{6}X^{1-}_{2}$ where *M* and *X* represent a cation and anion inside the β-cage, *A* represents the 3+ cations (typically Al^{3+}), and B represents the 4+ cations (typically Si^{4+}), where *A* and *B* form the framework (through oxygen bridges), as shown in Fig. 1. The *M* cations (e.g., Na^{+}, Ag^{+}, Cs^{+}, Li^{+}) [11-13] form a tetrahedron around the *X* anion (e.g., I^{-}, Cl^{-}, OH^{-}, Br^{-}) [14, 15] at the center of the β-cage. In addition, 2+ cations (e.g., Mg^{2+}, Ca^{2+}, Sr^{2+}, Zn^{2+}) and 2- anions (e.g., SO_4^{2-}, CO_3^{2-}, MoO_4^{2-}, CrO_4^{2-}) have been documented [11, 16]. For the β-cage framework, 3+ and 4+ ions (e.g., Al^{3+}, Ga^{3+}, Si^{4+}, Ge^{4+}) [14, 17, 18] form AO_4 or BO_4 tetrahedra that comprise the four- and six-membered rings through shared oxygen atoms. Sodalite is classified as a feldspathoid, although water-containing sodalite such as basic sodalite, $Na_8(AlSiO_4)_6(OH)_2(H_2O)_2$, can be considered as a zeolite [19, 20]. The symmetry of the elements in the sodalite structure is generally described with either the $I\bar{4}3m$ or, more commonly, $P\bar{4}3n$ space groups.

Sodalite can be synthesized through a variety of techniques such as hydrothermal and solid-state methods. Hydrothermal synthesis is typically done in a basic solution at temperatures around 90-200 °C, whereas the solid-state synthesis requires temperatures > 700 °C. For the hydrothermal method, controlling the crystallization of a pure sodalite phase and the undesired incorporation of OH^{-} into the β-cage is a challenge [14]. The formation of hydroxysodalite can be avoided in the solid-state synthesis, but the volatility of iodine and transformation of iodine to nepheline can occur [5, 21].

Iodosodalite has been considered as a potential mineral to immobilize ^{129}I due to the ability to incorporate halides in the β-cage, the viability of low temperatures (<200 °C) synthesis, and the compatibility of the aluminosilicate framework with glass matrices. In addition, chlorosodalite [$Na_8(AlSiO_4)_6Cl_2$] is currently the proposed baseline mineral for the spent electrochemical salt waste in a pyrochemical nuclear fuel recycling process [22, 23].

2.2 Glass ceramic waste forms

The glass-bonded iodosodalite waste form is a glass ceramic in which the iodine remains immobilized within the crystalline sodalite phase contained within a sintered glass matrix. These types of glass ceramics are sometimes called glass composite materials (GCMs) [24]. These waste forms generally require low sintering temperature to avoid iodine volatility. Garino et al. developed a GCM using Bi-Zn-B-oxide glass for AgI and AgI-zeolite [25] and Bi-Si-Zn-oxide glasses for AgI and AgI-mordenite [26] that were heat-treated at 500 and 550 °C, respectively. The glass binder helps to reduce the porosity, immobilize the radionuclide in its amorphous environment, and induce the crystallization of the targeted phase or phases that encapsulate the radionuclide(s) [22, 27].

2.3 Glass binder selection

For the glass-bonded iodosodalite waste form, it is crucial to mix with a proper glass binder to form a chemically durable GCM waste form at a sufficiently low sintering temperature to minimize the volatility of iodine. Glass binders for sodalite-based waste forms have been developed and studied for immobilization of Cl^- in glass-bonded chlorosodalite [28, 29].

In one study by Riley et al. [29], a series of SA-### (where ### = temperature, °C) glass binders with only Na_2O, B_2O_3, and SiO_2 as components where composition-property models were used to predict the temperature at which the viscosity was ~ 100 Pa·s. The SA-### glass binders were designed for low viscosities compared to NBS glass binders, to aid the densification of the waste form at lower temperature. The glass-bonded waste form synthesized with SA-### glass binders had high sodalite fractions with maximum densification occurring at 750-850 °C [29].

In a subsequent study, Riley et al. [28] developed a series of Na_2O-B_2O_3-SiO_2 (NBS)-based glass binders with additions of Al_2O_3, CaO, Li_2O, and/or ZrO_2 and showed that the resulting glass-bonded waste form contained high amounts of chlorosodalite. Each component of NBS glass binders was added for specific reasons, including ~20 mass% Na_2O to aid sodalite formation, ~5 mass% of Al_2O_3 to increase the chemical durability, ~5 mass% of ZrO_2 to have greater change in viscosity as a function of temperature [28, 30, 31]. The amount of B_2O_3, Na_2O, CaO, and Li_2O were selected to control the transition temperature, thermal expansion, viscosity, and chemical durability based on composition-property models [28, 32]. In the current study, one NBS glass binder (i.e., NBS-4) and one SA glass binder (i.e., SA-800) were selected for evaluation with iodosodalite to form glass-bonded iodosodalite for immobilization of I^-.

3. Experimental methods

3.1 Hydrothermal synthesis of iodosodalite

Iodosodalite was hydrothermally synthesized using the stoichiometric ratio of precursors. The respective molar ratio of sodium iodide (NaI, Fisher, Waltham, MA, USA), metakaolin ($Al_2Si_2O_7$), sodium hydroxide (NaOH, Fisher), and deionized water was 1:1.5:3:21, according to the reaction shown in Equation (1). Metakaolin was synthesized by heat-treating kaolinite [$Al_2Si_2O_5(OH)_4$, Sigma-Aldrich, St. Louis, MO, USA] at 850 °C for 17 h. The precursor solution was magnetic stirred for 10 min, poured into an autoclave (125 mL acid digestion vessel, Parr Instrument Company, Moline, IL), and placed in an oven at 180 °C for 48 h. After the hydrothermal process, the solution was dried at 90 °C overnight. Unlike previous work with hydrothermal sodalite synthesis [14, 33, 34], the syntheses in the current work were done without using excess NaOH or washing of the final powder, to avoid the effect of extra Na^+ and OH^- during synthesis and losing unreacted iodine and other residuals, respectively.

$$2NaI + 3Al_2Si_2O_7 + 6NaOH + xH_2O \rightarrow Na_8(AlSiO_4)_6I_2 + 6OH^- + xH_2O \quad (1)$$

3.2 Synthesis of NBS-4 and SA-800 glass binders

Two borosilicate glasses, NBS-4 and SA-800, were synthesized as glass binders; the compositions are listed in Table 1. This selection was based on the previous studies in which NBS-4 showed the best result

for chemical durability while having the same loading capacity as other NBS glass binders for a previous chlorosodalite study [28], and SA-800 allowed for lower viscosities and sintering temperatures [29]. For the synthesis of NBS-4, a platinum crucible half-filled with precursors was placed in a furnace at 650 °C, and the temperature was ramped to 1150 °C at 10 °C min^{-1}. The additional precursors were charged at 1150 °C, and the furnace was ramped up to 1550 °C at 10 °C min^{-1}. The melt was held for 2 h at 1550 °C and then water quenched. The glass was ground in a tungsten carbide mill, and the melting and quenching process was repeated. For the synthesis of SA-800, the similar steps to NBS-4 were taken, and the precursors were charged at 875 °C and ramped to 1050 °C at 10 °C min^{-1}. The melt was held for 40 min and poured.

3.3 Pellet preparation and firing

Both iodosodalite and glass powders were sieved to 63-125 μm particle size fraction to aid in more homogeneous mixing. These powders were initially mixed with a vortex mixer and then with a mortar and pestle. The experimental matrix with sample names is shown in Table 2. For sample names, the notation P##-YY(N/S)-ZZZC was used where ## was the pellet number, YY was the mass% of glass binder, ZZZ was the heat-treatment temperature (°C), and N and S denote NBS-4 and SA-800 respectively (where only one was used per sample), and 0GB denotes pellets sintered without glass binder. First, 10 or 20 mass% of glass binders were mixed into the iodosodalite powder with a mortar and pestle, and ~1 g of each sample was pressed into a pellet with a uniaxial press at $\sim 4.3 \times 10^7$ Pa (~6200 psi) for 1 min, resulting in a pellet that was ~20 mm diameter and ~2 mm thick. The pellets were placed on alumina sintering plates in three furnaces, heated to 650, 750, and 850 °C at 10°C min^{-1}, dwelled for 8 h, and then furnace cooled. Two identical pellets were synthesized for a given condition due to insufficient quantity of powder from a single pellet for all the characterization; a full pellet was preferred for the chemical durability tests.

3.4 Characterization

3.4.1. Physical characterization

X-ray diffraction (XRD) using a diffractometer (X'Pert Pro MPD, PANalytical, Netherlands) was used to obtain the diffraction patterns, and the phase identification and quantification were done with HighScore

150 software (PANalytical) using Rietveld analysis. Five consecutive XRD scans for each sample were
151 performed and the spectra added. Either a Co tube at 40 kV or a Cu tube at 45 kV were used, both at 40
152 mA, and samples were scanned in the range of 10 to 90° 2θ with a 0.05° 2θ step and 14-s dwells per step.
153 For Rietveld analysis, specimens were mixed with 30 to 40 mass% of zinc oxide (ZnO, Sigma-Aldrich) as
154 an internal standard. The refined parameters include U, V, and W for fitting the width, peak shape, peak
155 asymmetry, preferred orientation for fitting the intensities, and unit cell.
156 Portions of sample pellets were vacuum-impregnated with resin and polished in glycol-based diamond
157 suspensions to a 250-nm finish. Then, SEM analysis was performed on the polished cross-sections with a
158 JSM-7001F field-emission gun microscope (JEOL USA, Inc. Peabody, MA) using a backscattered electron
159 (BSE) detector for atomic number contrast. All samples were first sputter-coated with Pt (Polaron Range
160 SC7640, Quorum Technologies Ltd., East Sussex, England). The EDS analysis was performed with a
161 Bruker xFlash® 6|60 (Bruker AXS Inc., Madison, WI) and dot mapping was performed at ~100 k counts s^{-1}
162 with a ~51-min collection time over 1024×768 pixels at a 16-µs dwell time per pixel.
163 Fourier transform infrared (FTIR, Nicolet iS10 spectrometer, ThermoFisher, USA) spectra were
164 obtained 550-4000 cm^{-1} with a resolution of 4 cm^{-1} using a diamond attenuated total reflectance (ATR)
165 plate. Samples were dried at 90 °C overnight before the measurement. Four background scans were taken
166 and averaged before the sample measurement, and 20 scans were averaged for the sample measurement.
167 The peaks of resulting spectra were analyzed using OriginPro 8 (v8.0724) and compared with published
168 data.
169 Simultaneous thermo-gravimetric analysis (TGA) and differential scanning calorimetry (DSC) (SDT
170 Q600, TA Instrument, USA) were performed to study the transition and decomposition of sodalite structure
171 and volatility of iodine. All the samples were dried at 90 °C overnight before TGA/DSC measurement. ~50
172 mg of each specimen was filled into an alumina crucible and heated to 1000 °C at 10 °C min^{-1}.
173 Densities of pellets were calculated using a He pycnometer (AccuPyc II 1340, Micromeritics, USA).
174 Prior to the volume measurement, the masses of ground pellets were measured. Subsequently, 1-cm^3 sample
175 holder was filled with ~0.5 g of ground pellets, and 5 consecutive measurements of volume were taken and

averaged. The measured masses and volumes were used to calculate the densities of pellets, and the porosities of the pellets were calculated with the Equation (2).

$$\phi\ (vol\%)\ =\ (\rho_P\ -\ \rho_g)\ /\ \rho_P\ \times\ 100 \quad (2)$$

where □ is the porosity, ρ_p is the pycnometric density, and ρ_g is the geometric density.

3.4.2. Iodine quantification methods

The NAA characterization was performed at the Washington State University Nuclear Science Center. Four calibration standard solutions with different concentration of NaI were prepared. The samples were packaged in polyethylene vials, heat sealed, and irradiated with the standards in the reactor at 100 kW with for 10 min. The peak intensity of γ-rays from the samples was measured with an EG&G Ortec HPGe detector, Model 0195. The data was processed with the Genie 2000 Gamma Acquisition and Analysis Software (Canberra v3.2.1).

Iodine quantification by volumetric method was performed at Galbraith Laboratory, Inc. Iodine in the samples were oxidized to iodate in an oxygen flask. The resulting solution was treated with excess potassium iodide liberating free iodine that was titrated with thiosulfate using starch as an indicator. The final mass% of iodine was calculated with an empirical formula shown in Equation (3).

$$I(wt\%) = \frac{(sample\ titration,\ mL - blk\ titration, mL)(N\ Na_2S_2O_3)(21.5)(100)}{Sample\ weight, mg} \quad (3)$$

For volumetric and Rietveld analysis, two additional pellets for each of P10-10NBS4-750C and P22-10SA800-750 were synthesized under the same conditions, and three measurements were performed on three pellets for each analysis for statistical calculations, accounting for any variability due to the synthesis reproducibility and measurement uncertainties (e.g., weighing of internal standards, fitting procedures). For the NAA analysis, the linear calibration line was drawn using NaI standard, and the slope with the uncertainty was calculated. Two sets of counting data were collected at different time intervals after cessation of irradiation, and the one with a smaller percent of the dead time for detector response was used. The linear equation was used to calculate the iodine mass in the samples.

3.4.3. Chemical durability

The dissolution behaviors of P10-10N-750C samples were evaluated using a modified ASTM C1308-14 test procedure. Two samples prepared under the same conditions, one a cylindrical pellet and the other a quadrant, were used for the tests of the effect of different surface areas. All experiments were conducted at 90 °C in Teflon® vessels (Savillex, Eden Prairie, MN) in the same convection oven. The surface area-to-volume (S/V) ratio of 80 m^{-1} for a whole pellet and 8 m^{-1} for a quadrant were attained by controlling the amount of leachant (i.e., deionized water). The samples were set on top of a Teflon support grid so that it was elevated off the bottom inner surface of the vessel and readily accessible to the solution on all sides.

For each sampling, vessels were removed from the oven and weighed. Then, the solutions from the vessels were removed without cooling. The sample was taken out of the vessel to allow all solution to be removed. Excess water was wicked off the sample, but the sample was not dried. The sample was placed back into the vessel and fresh solution was added to match the original mass of the vessels. The very small amount of test solution wetting the sample was carried over into the next test interval. The vessels were recapped and then placed back into the oven. Each solution exchange procedure only required a few minutes. The concentration of elements in the leachate solutions were measured using inductively-coupled plasma mass spectrometry (ICP-MS).

The incremental normalized mass loss, $NL_{i,n}$, for each test interval was calculated using Equation (4) where $C_{i,n}$ is the concentration of species i measured in the test solution during the n-th test interval, S is the geometric surface area of the specimen, V is the volume of solution, and f_i is the mass fraction of the i-th species in the test specimen. The cumulative dissolution over a series of n-test intervals, $NL_{i,c}$, was calculated as the sum of incremental $NL_{i,n}$ values using Equation (5).

$$NL_{i,n} = \frac{C_{i,n}}{S/V * f_i} \quad (4)$$

$$NL_{i,c} = \sum_{i=1}^{N} NL_{i,n} \quad (5)$$

4. Results and discussion

4.1 Structure and morphology

The XRD phase analysis of heat-treated pellets are presented in Fig. 2 showing the change in phase fraction of crystalline and amorphous phases depending on sodalite and glass binder fractions and heat-treatment temperature. The weighted profile R values ranged from 2.43 to 4.77 %, and the goodness of fit values ranged from 1.55 to 4.84. The heat-treated pellets contained ~15-54 mass% of iodosodalite along with ~4–31 mass% of aluminosilicate phases [i.e., ~4-31 mass% of nepheline ($Na_{7.85}Al_{7.85}Si_{8.15}O_{32}$) [35] or ~8-13 mass% of interstitial carnegieite ($Na_6Al_4Si_4O_{17}$) [36]], with the rest being amorphous. In general, higher heat-treatment temperatures resulted in lower iodosodalite and higher amorphous fractions.

The structures of the resulting phases are shown in Fig. 3. Iodosodalite and carnegieite phases have the cubic crystal systems with $P\bar{4}3n$ and $F\bar{4}3m$ space groups, respectively, whereas nepheline has the hexagonal crystal system with $P6_3$ space group. The synthesized NBS-4 and SA-800 glasses were transparent with no bubbles and showed the amorphous characteristic spectra under XRD. XRD analysis showed that fractions of sodalite and/or the amorphous phase transform into nepheline phase as the firing temperature increased from 650 to 850 °C. Fig. 4 shows the XRD spectra of P8-10N-650C, P10-10N-750C, and P12-10N-850C, revealing the crystallization of nepheline as temperature increased. The transition of chlorosodalite to nepheline at ~700 or 850 °C has been observed in the literature [21, 28], and the results of the current study show evidence of the same process. As shown by Novembre et al. [21], the reaction kinetics showed that the rate of sodalite → nepheline transformation was a slow process at a constant temperature.

The amorphous fraction in the samples heat-treated at 850 °C was higher than those of 650 and 750 °C and this is attributed to the decomposition of sodalite into nepheline and NaI, where the NaI appears to decompose within the sample, according to the results shown in this study – see Equation (6) below. One proposed reaction is that, as NaI enters the matrix of sodalite and nepheline within the amorphous melt, it decomposes; here, the Na enters the glass (as Na_2O) and the iodine evolves as a gas [i.e., $I_2(g)$] – see

Equation (7). This is evidenced by the presence of I-free aluminosilicate phases, the absence of NaI in the diffraction patterns, and the iodine deficiencies measured in heat-treated pellets.

$$Na_8(AlSiO_4)_6I_2 \xrightarrow{\Delta} 6\ NaAlSiO_4 + 2\ NaI \quad (6)$$

$$2\ NaI + O_2(g) \xrightarrow{\Delta} 2\ Na_2O + I_2(g) \quad (7)$$

This result agrees with TGA and DSC results (discussed later in section 4.2) in which there is a large mass loss and an endothermic reaction at ~800 °C. The resulting fractions of sodalite and nepheline phases were not significantly affected by the addition of NBS-4 and SA-800 glass binders according to Rietveld analysis. Sodalite fractions were higher in the NBS-4 pellets than SA-800 pellets following heat treatment at 750°C. The SA-800 pellets heat-treated at 650 °C contained relatively higher iodosodalite fractions but were weakly sintered and brittle, and those heat-treated at 850 °C contained high amorphous fractions. Therefore, 750 °C was determined to be the optimal sintering temperature for these pellets.

FTIR spectra of P4-0GB-750C, P10-10N-750C, and P22-10S-750C are shown in Fig. 5. The frequencies of asymmetric stretching (v_{as}) of *T*-O (*T* = Si or Al) band at 965 cm^{-1} and symmetric stretching (v_s) of *T*-O bands at 657, 700, and 725 cm^{-1} of sodalite are labeled in Fig. 5, according to the literature [5, 14, 37]. The frequency of *T*-O vibrational bands from the β-cages with different anions are similar [37, 38]. Peaks at ~880 and 1450 cm^{-1} were absorption bands due to impurity of CO_3^{2-} [5, 38]. Samples heat treated at 750 °C contained minor nepheline phases according to XRD analysis, but it is difficult to differentiate nepheline from iodosodalite with FTIR because *T*-O bands of nepheline at ~690 and 960 cm^{-1} [39] overlap with iodosodalite bands and this discernment is especially difficult when the fraction of nepheline is small.

SEM-EDS analysis results performed on the polished cross-section of P18-20N-850C and P22-10S-750C pellets are shown in Fig. 6. The sintered pellets were porous and elements were heterogeneously distributed. The variability of iodine concentration shows that iodine is only present in one phase (i.e., iodosodalite) and absent from the other phase(s) (i.e., aluminosilicate and amorphous phases). Less iodine distribution in the sample heat-treated at 850 °C compared to that of 750 °C is due to iodine volatility as the β-cage decomposed. These results corroborate the XRD results showing a decrease in iodosodalite

fraction and an increase in amorphous fraction as the heat-treatment temperature increased from 750 to 850 °C. Small amounts of K and Ca were found and are considered to be impurities in the kaolinite precursor which was used to synthesize the baseline powder for the pellets; some of the signal for Ca was from the NBS-4 glass binder.

4.2 Thermal analysis

TGA and DSC were performed on the baseline iodosodalite powder, P4-0GB-750C, P10-10N-750C, and P22-10S-750C as shown in Fig. 7. TGA shows that there are two stages of mass loss. For the heat-treated samples, decrease in 2-3 mass% occurs at 600 to 670 °C due to transition of sodalite to nepheline or other sodium aluminosilicate phases. The water in the structure was removed during the heat treatment, and no significant loss due to water dehydration was observed for the heat-treated pellets. Above 800 °C, the sodalite structure decomposed to amorphous material or nepheline, and the iodine volatilized resulting in significant decrease in mass% of iodine. These transitions are supported by the XRD results. For the baseline iodosodalite, the major loss from 600 to 800 °C is due to dehydration of water in the structure in addition to phase transitions, and the mass loss continued at higher temperatures due to the iodine volatility and sodalite decomposition.

Hydrothermally-grown iodosodalite typically contains a minor amount of basic sodalite phase that contains water. The evidence of these water-containing phases can be seen with FTIR at ~3000 to 3600 cm^{-1} regions, which disappear after heat treatment above 650 °C. DSC does not show the significant change in heat flow around 800 °C for heat-treated pellets, indicating that the sodalite → nepheline transition is likely a slow process, and consequently the heat flow signal will be spread out over time. For the baseline iodosodalite powder, two clear endothermic peaks at 640 and 811 °C represent the water loss from the structure and decomposition of sodalite with iodine volatility, respectively.

4.3 Density and porosity

Densities were measured on heat-treated pellets. All the samples contained iodosodalite, nepheline, NBS-4, and/or SA-800 with similar densities of 2.62 (ICSD 71434), 2.61 (ICSD 108352), 2.53 [28], and 2.51 g/cm^3 [29], respectively. In general, firing to 750 °C increased the density of the pellets, but as the

300 temperature increased to 850 °C, the densities of pellets with NBS-4 increased whereas ones with SA-800
301 decreased as shown in Fig. 8. XRD showed that pellets with SA-800 contained higher amorphous fractions
302 compared to those with NBS-4 after firing at 850 °C, resulting in relatively lower densities for pellets made
303 with SA-800.

304 Porosities decreased substantially for the pellets with SA-800 as the heat-treatment temperature
305 increased, whereas only a slight decrease was observed for ones with NBS-4. As for the densities, addition
306 of glass binders resulted in higher sample densities compared to baseline iodosodalite powder alone when
307 heat-treated at 650 and 750 °C, but samples with SA-800 heat-treated at 850 °C resulted in substantially
308 lower densities. Overall, the pellets with NBS-4 contained higher crystalline fractions but with higher
309 porosities compared to the pellets with SA-800. Smaller porosities of the pellets with SA-800 are attributed
310 to lower viscosity with this glass at the sintering temperatures than for NBS-4, which resulted in more
311 effective means to close porosity within the pellets during the heat-treatment process.

312 4.4 Iodine quantification

313 The iodine masses in P10-10N-750C and P22-10S-750C were determined with the NAA, volumetric,
314 and Rietveld methods and are compared in Fig. 9. The quantification results from these methods for P22-
315 10S-750 agree well, but there is some discrepancy for P10-10N-750C. It should be noted that iodine
316 quantification with Rietveld analysis only accounts for iodine in the crystalline fraction and not any which
317 might be in the amorphous fraction, which is expected to be low based on the low solubility of iodine in
318 borosilicate glass [40]. According to Fig. 9, only 38-47% of the as-batched iodine remained in these pellets,
319 and the rest volatilized during the heat-treatment. A similar iodine retention was observed previously during
320 solid state synthesis of iodosodalite, in which ~53 mass% of iodine remained after synthesis at 800 °C,
321 whereas ~94 mass% of chlorine remained in the case of chlorosodalite [41].

322 4.5 Chemical durability

323 The cumulative normalized mass loss ($NL_{i,c}$) values for Na, Al, Si, B, and I of P10-10N-750C samples
324 with S/V of 8 and 80 m^{-1} are shown in Fig. 10. A large release of these elements, especially Na and Si, was
325 observed in the first day, possibly from water-soluble salt crystals and non-durable amorphous phases. The

326 $NL_{I,c}$ values were 91.9 and 12.5 g/m^2 for 8 and 80 m^{-1} for the 10 1-d exchanges with a linear trend,
327 respectively. When the exchange interval was changed to 7-d, the release rate decreased, which has been
328 observed in previous studies with glass-bonded sodalite [42]. Despite the slope change after 10 days, the
329 overall linear loss behavior indicated congruent dissolution of iodine over time. The release rate of iodine,
330 shown by the slope, is lower than sodium and silicon. Incongruent dissolution of the different elements is
331 indicative of a multi-phase materials, which was expected since sodalite and glass are both present. Since
332 Na, Al, and Si are present in the NBS-4 glass as well as in the sodalite phase, but the release of Al was
333 much lower than that of Na and Si, it is more likely that a separate amorphous phase was present containing
334 Na and Si following the hydrothermal synthesis. For all the elements, the release rate decreased when
335 measured at longer intervals. For iodine, the release rates during the 7-d exchange intervals (i.e., 10-24 days
336 of the test) were 0.23 and 1.29 g/m^2/d for 80 or 8 m^{-1} respectively. The nearly linear releases of I and Si
337 from NBS-4-bonded iodosodalite is likely due to dissolution of iodosodalite. The sensitivity to the S/V ratio
338 and much faster releases in the 8 m^{-1} test compared with the 80 m^{-1} test is consistent with a solution affinity
339 mechanism controlled by sodalite solubility. The linear release of B in the 7-d exchanges suggests the non-
340 linear release of B seen in the initial three or four 1-d exchanges is probably an artifact of the surface.
341 According to previous studies [42], it is known that NBS-4 glass dissolves by surface dissolution. Based
342 on different release behaviors of B and I, it is likely that the response is dominated by sodalite dissolution,
343 not glass. This release rate is an order of magnitude higher than a reported value for hot isostatically pressed
344 iodosodalite [43]; however, there are differences in sample preparation and chemical durability test between
345 the P10-10N-750C sample and those from the study by Maddrell et al. (i.e., hot isostatic pressed sample
346 and static solution test) [43]. The release behaviors presented here for P10-10N-750C are similar to the
347 ASTM C1308 test result for glass-bonded chlorosodalite ceramic waste forms [42].

348 **5. Conclusions**

349 Glass-bonded iodosodalite waste forms were synthesized by mixing iodosodalite powder with
350 NBS-4 or SA-800 borosilicate glass binders, and firing pellets at different temperatures of 650, 750, or

850 °C. The effects of firing temperature and glass loading (i.e., 0, 10, and 20 mass%) were investigated. Heat-treatment at 750 °C resulted in the best waste form as the pellets heat-treated at 650 °C were not well sintered, and ones at 850 °C contained low fractions of iodosodalite and high amorphous content. As the temperature increased from 650 to 850 °C, higher nepheline fractions were observed. The sintered pellets of P10-10N-750C and P22-10S-750C both had similar and relatively high iodine fractions, i.e., 9.3 and 8.6 mass% (volumetric), respectively. The pellets mixed with NBS-4 had higher iodosodalite phase compared SA-800 under the same heat-treatment temperature and mixed amount of glass binder after heat-treatment at 750 °C. P22-10S-750C was less porous than P10-10N-750C, indicating that SA-800 was better at closing pores as it had lower viscosity at the sintering temperatures. The iodine masses in P10-10N-750C and P22-10S-750C showed that ~38-44% of the as-batched iodine remained in these pellets. The chemical durability test on P10-10N-750C showed that iodine release rate was lower than sodium and silicon during the first 10 days and decreased significantly to 0.23 and 1.29 $g/m^2/d$ for 80 or 8 m^{-1} in the 10-24 d interval, respectively. The linear release behavior of iodine indicated congruent dissolution of iodosodalite.

Acknowledgements

This research was supported by the U.S. Department of Energy in support of the Nuclear Energy University Program – Advanced Waste Forms program, award # DE-NE0008257. Pacific Northwest National Laboratory (PNNL) is operated by Battelle Memorial Institute for the DOE under contract DE-AC05-76RL01830. The authors also thank Grant Norton, Min-Kyu Song, and Ashutosh Goel for helpful comments. The authors also thank Benjamin Williams and Michelle Snyder for help with chemical durability experiments and William Ebert for help with interpretation of the chemical durability data.

References

1. Taylor, P., A review of methods for immobilizing iodine-129 arising from a nuclear fuel recycle plant, with emphasis on waste-form chemistry, 1990, Atomic Energy of Canada Ltd.
2. Goldsmith, J.R., C.M. Grossman, W.E. Morton, R.H. Nussbaum, E.A. Kordysh, M.R. Quastel, R.B. Sobel, and F.D. Nussbaum, *Juvenile hypothyroidism among two populations exposed to radioiodine.* Environmental health perspectives, 1999. **107**(4): p. 303.
3. Hou, X., V. Hansen, A. Aldahan, G. Possnert, O.C. Lind, and G. Lujaniene, *A review on speciation of iodine-129 in the environmental and biological samples.* Analytica Chimica Acta, 2009. **632**(2): p. 181-196.
4. Yang, J.H., J.M. Shin, J.J. Park, G.I. Park, and M.S. Yim, *Novel synthesis of bismuth-based adsorbents for the removal of 129 I in off-gas.* Journal of Nuclear Materials, 2015. **457**: p. 1-8.
5. Bardez, I., L. Campayo, D. Rigaud, M. Chartier, and A. Calvet. *Investigation of sodalites for conditioning halide salts (NaCl and NaI): Comparison of two synthesis routes*. in *ATALANTE 2008*. 2008. Montpellier (France).
6. Jubin, R., Airborne Waste management technology applicable for use in reprocessing plants for control of iodine and other off-gas constituents, 1988, Oak Ridge National Laboratory, TN.
7. Herrmann, F., B. Herrmann, and V. Hoeflich, Removal efficiency of silver impregnated filter materials and performance of iodie filters in the off-gas of the Karlsruhe reprocessing plant WAK, 1997, Harvard Univ., Boston, MA.
8. Takeshita, K. and Y. Azegami, *Development of thermal swing adsorption (TSA) process for complete recovery of iodine in dissolver off-gas.* Journal of Nuclear Science and Technology, 2004. **41**(1): p. 91-94.
9. Riley, B.J., J.D. Vienna, D.M. Strachan, J.S. McCloy, and J.L. Jerden, *Materials and processes for the effective capture and immobilization of radioiodine: A review.* Journal of Nuclear Materials, 2016. **470**: p. 307-326.
10. *Standard Test Method for Accelerated Leach Test for Diffusive Releases from Solidified Waste and a Computer Program to Model Diffusive, Fractional Leaching from Cylindrical Waste Forms*, in *Standard Test Method for Accelerated Leach Test for Diffusive Releases from Solidified Waste and a Computer Program to Model Diffusive, Fractional Leaching from Cylindrical Waste Forms*. 2014, American Society for Testing and Materials International, ASTM International Book of Standards Volume 12.01: West Conshohocken, PA.
11. Brenchley, M.E. and M.T. Weller, *Synthesis and Structures of $M_8[AlSiO_4]_6{\cdot}(XO_4)_2$, M= Na, Li, K; X= Cl, Mn Sodalites.* Zeolites, 1994. **14**(8): p. 682-686.
12. Mon, J., Y. Deng, M. Flury, and J.B. Harsh, *Cesium incorporation and diffusion in cancrinite, sodalite, zeolite, and allophane.* Microporous and Mesoporous Materials, 2005. **86**(1): p. 277-286.
13. Mikuła, A., M. Król, and A. Koleżyński, *Experimental and theoretical spectroscopic studies of Ag-, Cd-and Pb-sodalite.* Journal of Molecular Structure, 2016. **1126**: p. 110-116.
14. Chong, S., J. Peterson, J. Nam, B. Riley, and J. McCloy, *Synthesis and characterization of iodosodalite.* Journal of the American Ceramic Society, 2017. **100**(5): p. 2273-2284.

15. Trill, H., H. Eckert, and V.I. Srdanov, *Topotactic transformations of sodalite cages: Synthesis and NMR study of mixed salt-free and salt-bearing sodalites.* Journal of the American Chemical Society, 2002. **124**(28): p. 8361-8370.

16. Antao, S.M., I. Hassan, and J.B. Parise, *Chromate Aluminate Sodalite, $Ca_8[Al_{12}O_{24}](CrO_4)_2$: Phase Transitions and High-temperature Structural Evolution of the Cubic Phase.* The Canadian Mineralogist, 2004. **42**(4): p. 1047-1056.

17. Borhade, A. and S. Wakchaure, *Synthesis and characterization of gallosilicate halide sodalites using organic solvent.* Indian Journal of Chemistry. Section A, Inorganic, Bio-inorganic, Physical, Theoretical & Analytical Chemistry, 2010. **49**(8): p. 1047.

18. Borhade, A.V., A.G. Dholi, D.R. Tope, and S. Wakchaure, *Solvothermal synthesis and crystal structure of aluminogermanate halide sodalites using organic solvent.* Indian Journal of Pure and Applied Physics, 2012. **50**(8): p. 576-582.

19. Nabavi, M.S., T. Mohammadi, and M. Kazemimoghadam, *Hydrothermal synthesis of hydroxy sodalite zeolite membrane: Separation of H 2/CH 4.* Ceramics International, 2014. **40**(4): p. 5889-5896.

20. Henmi, T., *Synthesis of hydroxy-sodalite ("zeolite") from waste coal ash.* Soil Science and Plant Nutrition, 1987. **33**(3): p. 517-521.

21. Novembre, D., D. Gimeno, A. Pasculli, and B. Di Sabatino, *Synthesis and characterization of sodalite using natural kaolinite: an analytical and mathematical approach to simulate the loss in weight of chlorine during the synthesis process.* Fresenius Environmental Bulletin, 2010. **19**(6): p. 1109-1117.

22. Ebert, W., Testing to evaluate the suitability of waste forms developed for electrometallurgically treated spent sodium-bonded nuclear fuel for disposal in the Yucca Mountain reporsitory, 2005, ANL-05/43, Argonne National Laboratory, Lemont, IL.

23. Bateman, K., C. Knight, and C. Solbrig, Current Status of Ceramic Waste Form Development, 2007, INL/INT-06-11736, Idaho National Laboratory, Idaho Falls, ID.

24. McCloy, J.S. and A. Goel, *Glass-ceramics for nuclear-waste immobilization.* MRS Bulletin, 2017. **42**(3): p. 233-240.

25. Garino, T.J., T.M. Nenoff, J.L. Krumhansl, and D.X. Rademacher, *Development of Waste forms for Radioactive Iodine.* Ceramics for Environmental and Energy Applications, 2010: p. 35-42.

26. Garino, T.J., T.M. Nenoff, J.L. Krumhansl, and D.X. Rademacher, *Low-Temperature Sintering Bi–Si–Zn-Oxide Glasses for Use in Either Glass Composite Materials or Core/Shell 129I Waste Forms.* Journal of the American Ceramic Society, 2011. **94**(8): p. 2412-2419.

27. Lepry, W.C., B.J. Riley, J.V. Crum, C.P. Rodriguez, and D.A. Pierce, *Solution-based approaches for making high-density sodalite waste forms to immobilize spent electrochemical salts.* Journal of Nuclear Materials, 2013. **442**(1): p. 350-359.

28. Riley, B.J., J.D. Vienna, S.M. Frank, J.O. Kroll, J.A. Peterson, N.L. Canfield, Z. Zhu, J. Zhang, K. Kruska, and D.K. Schreiber, *Glass binder development for a glass-bonded sodalite ceramic waste form.* Journal of Nuclear Materials, 2017. **489**: p. 42-63.

29. Riley, B.J., W.C. Lepry, and J.V. Crum, *Solution-derived sodalite made with Si-and Ge-ethoxide precursors for immobilizing electrorefiner salt.* Journal of Nuclear Materials, 2016. **468**: p. 140-146.

30. Vienna, J., P. Hrma, and M. Schweiger, Compositional dependence of elemental release from HLW glasses by the product consistency test: One-component-at-a-time study, 1996, American Ceramic Society, Westerville, OH.

31. Feng, X., P. Hrma, J. Westsik Jr, N. Brown, M. Schweiger, H. Li, J. Vienna, G. Chen, G. Piepel, and D. Smith, *Glass optimization for vitrification of Hanford Site low-level tank waste.* Pacific Northwest National Laboratory Report PNNL-10918, 1996.

32. Vienna, J.D., D.-S. Kim, and P.R. Hrma, Database and Interim Glass Property Models for Hanford HLW and LAW Glasses, 2002, Pacific Northwest National Laboratory, Richland, WA.

33. Liu, Q. and A. Navrotsky, *Synthesis of nitrate sodalite: An in situ scanning calorimetric study.* Geochimica et cosmochimica acta, 2007. **71**(8): p. 2072-2078.

34. Dickson, J.O., J.B. Harsh, M. Flury, and E.M. Pierce, *Immobilization and exchange of perrhenate in sodalite and cancrinite.* Microporous and Mesoporous Materials, 2015. **214**: p. 115-120.

35. Vuli, P. and V. Kahlenberg, *On the high temperature behaviour of monoclinic trinepheline.* Neues Jahrbuch für Mineralogie-Abhandlungen: Journal of Mineralogy and Geochemistry, 2012. **189**(2): p. 197-206.

36. Borchert, W. and J. Keidel, *Beiträge zur Reaktionsfähigkeit der Silikate bei niedrigen Temperaturen.* Heidelberger Beiträge zur Mineralogie und Petrographie, 1947. **1**(1): p. 2-16.

37. Stein, A., G.A. Ozin, P.M. MacDonald, G.D. Stucky, and R. Jelinek, *Class A Sodalites: Silver, Sodium, Halosodalites.* Journal of the American Chemical Society, 1992. **114**(13): p. 5171–5186.

38. Buhl, J.-C., W. Hoffmann, W. Buckermann, and W. Müller-Warmuth, *The crystallization kinetics of sodalites grown by the hydrothermal transformation of kaolinite studied by 29 Si MAS NMR.* Solid State Nuclear Magnetic Resonance, 1997. **9**(2): p. 121-128.

39. Markovic, S., V. Dondur, and R. Dimitrijevic, *FTIR spectroscopy of framework aluminosilicate structures: carnegieite and pure sodium nepheline.* Journal of Molecular Structure, 2003. **654**(1): p. 223-234.

40. Riley, B.J., M.J. Schweiger, D.-S. Kim, W.W. Lukens, B.D. Williams, C. Iovin, C.P. Rodriguez, N.R. Overman, M.E. Bowden, and D.R. Dixon, *Iodine solubility in a low-activity waste borosilicate glass at 1000° C.* Journal of Nuclear Materials, 2014. **452**(1): p. 178-188.

41. Nakazawa, T., H. Kato, K. Okada, S. Ueta, and M. Mihara. *Iodine immobilization by sodalite waste form*. in *MRS Proceedings*. 2000. Cambridge Univ Press.

42. Ebert, W.L. and C.T. Snyder, Corrosion Tests with Waste Forms Developed for EChem Salt Wastes, 2015, FCRD-MRWFD-2015-000145, Argonne National Laboratory, Lemont, IL.

43. Maddrell, E., A. Gandy, and M. Stennett, *The durability of iodide sodalite.* Journal of Nuclear Materials, 2014. **449**(1): p. 168-172.

Tables

Table 1. Compositions of NBS-4 [28] and SA-800 [29] glass binders.

Glass binder	Mass %					
	SiO_2	B_2O_3	Na_2O	Al_2O_3	CaO	ZrO_2
NBS-4	58.87	8.98	20.17	5.99	3.99	2.00
SA-800	42.50	24.60	32.88	-	-	-

Table 2. Experimental matrix with sample names.

T (°C)	ISOD pellet	ISOD+10 mass% NBS-4 pellet	ISOD+20 mass% NBS-4 pellet	ISOD+10 mass% SA-800 pellet	ISOD+20mass% SA-800 pellet
650	P2-0GB-650C	P8-10N-650C	P14-20N-650C	P20-10S-650C	P26-20S-650C
750	P4-0GB-750C	P10-10N-750C	P16-20N-750C	P22-10S-750C	P28-20S-750C
850	P6-0GB-850C	P12-10N-850C	P18-20N-850C	P24-10S-850C	P30-20S-850C

Figure Captions

Fig. 1. (a) Structure of the β-cage in sodalite and (b) the stacked structure with the unit cell shown as a cube. Oxygen atoms and bridges are removed for simplicity.

Fig. 2. Phase mass% distribution of samples.

Fig. 3. Structures of (a) iodosodalite, (b) sodium aluminosilicate (interstitial carnegieite), and (c) nepheline phases, all projected on (001).

Fig. 4. XRD spectra of P8-10N-650C, P10-10N-750C, and P12-10N-850C. Sodium aluminosilicate is also known as the interstitial carnegieite or ($Na_6Al_4Si_4O_{17}$) [36].

Fig. 5. FTIR spectra of P4-0GB-750C, P10-10N-750C, and P22-10S-750C. See the text for details about the peak assignments.

Fig. 6. SEM of (a) P18-20N-850C and (b) P22-10N-750C and their EDS elemental maps (bottom). The bright and geometrically-shaped particles are iodosodalite and darker areas are nepheline and/or amorphous fractions.

Fig. 7. (a) TGA and (b) DSC plots of baseline powder, P4-0GB-750C, P10-10N-750C, and P22-10S-750C.

Fig. 8. (a) Densities and (b) porosities of heat-treated pellets. Lines are drawn as guide to the eye.

Fig. 9. Iodine quantification by different methods. Note that "maximum" is that from the batch assuming all of the iodine is in sodalite.

Fig. 10. Cumulative normalized releases ($NL_{i,c}$) of Na, Al, Si, B, and I from duplicate pellets of P10-10N-750C with S/V values of (a) 8 m^{-1} and (b) 80 m^{-1} as a function of time following ASTM C1308 experiment.

(a)

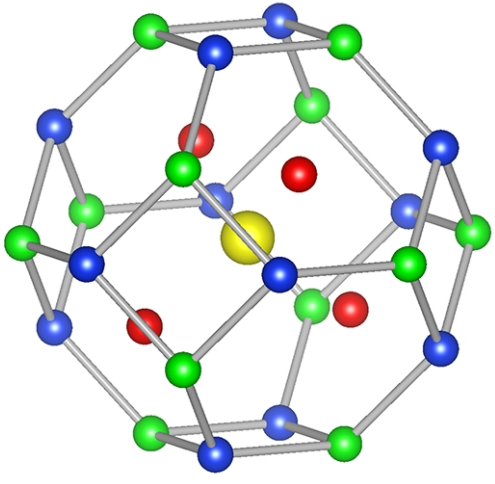

(b)

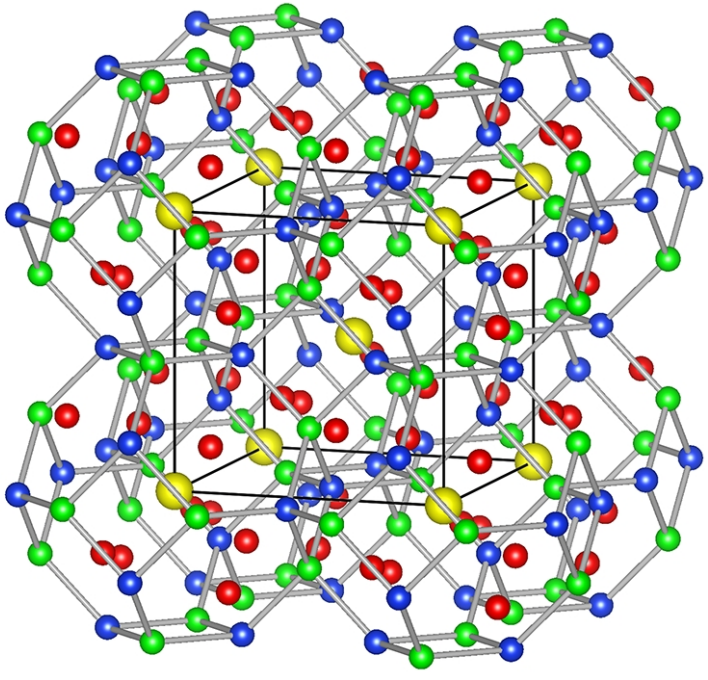

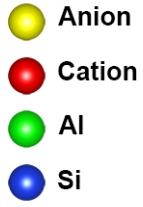

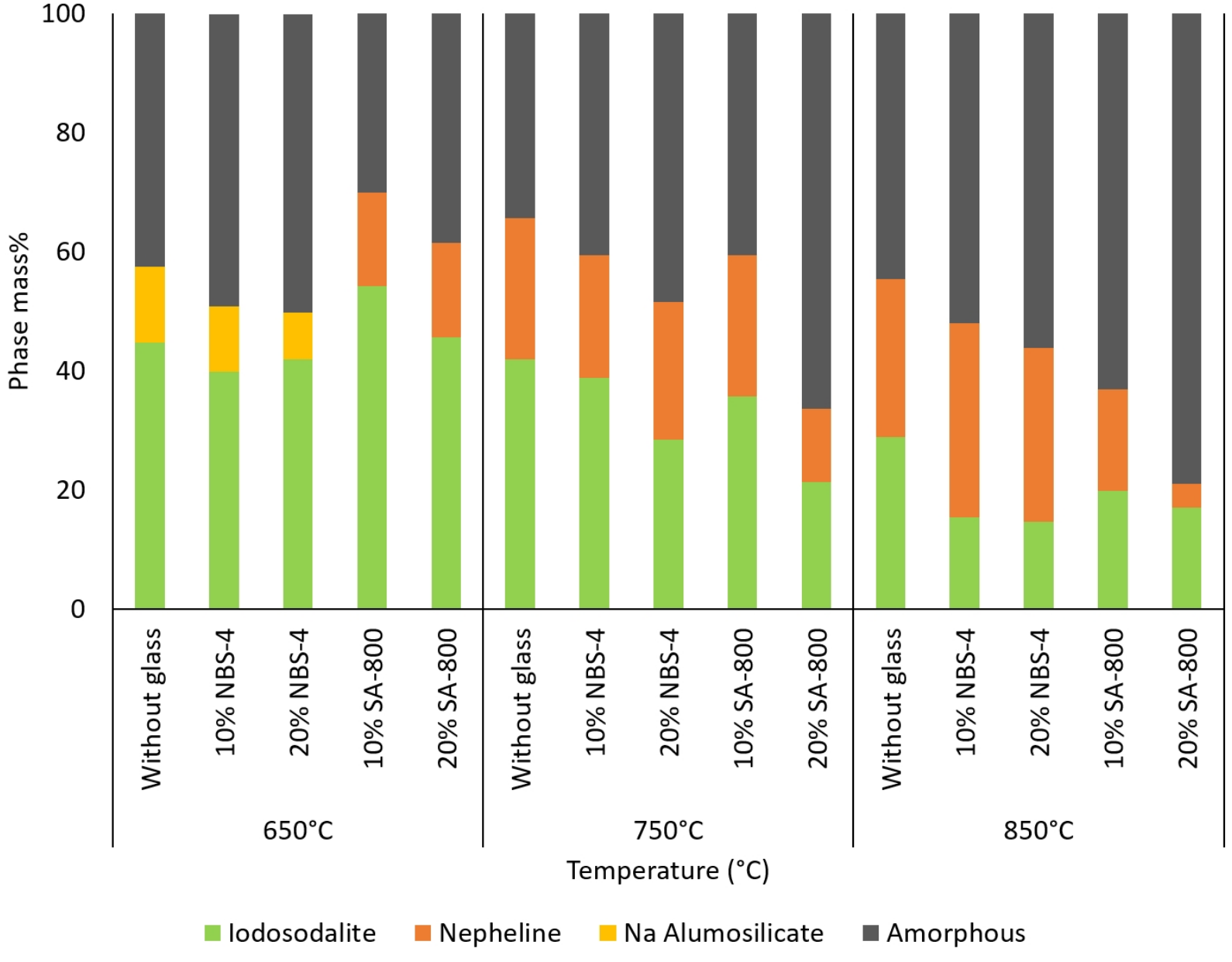
100
80
60
40
20
0
Phase mass%
Without glass
10% NBS-4
20% NBS-4
10% SA-800
20% SA-800
Without glass
10% NBS-4
20% NBS-4
10% SA-800
20% SA-800
Without glass
10% NBS-4
20% NBS-4
10% SA-800
20% SA-800
650°C
750°C
850°C
Temperature (°C)
Iodosodalite
Nepheline
Na Alumosilicate
Amorphous

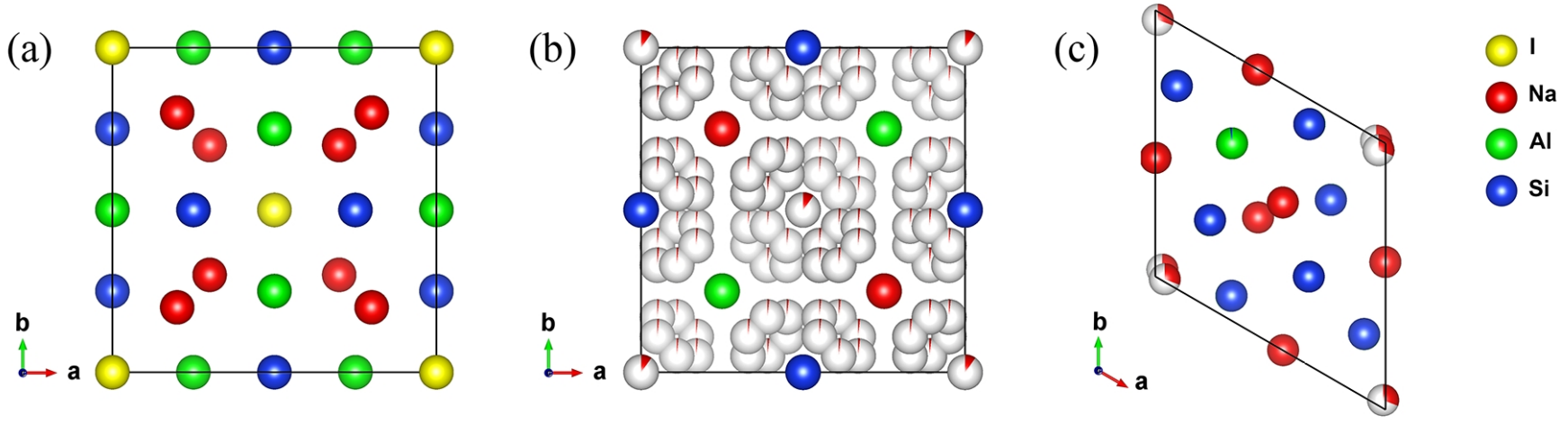
(a)
b
a
(b)
b
a
(c)
b
a
I
Na
Al
Si

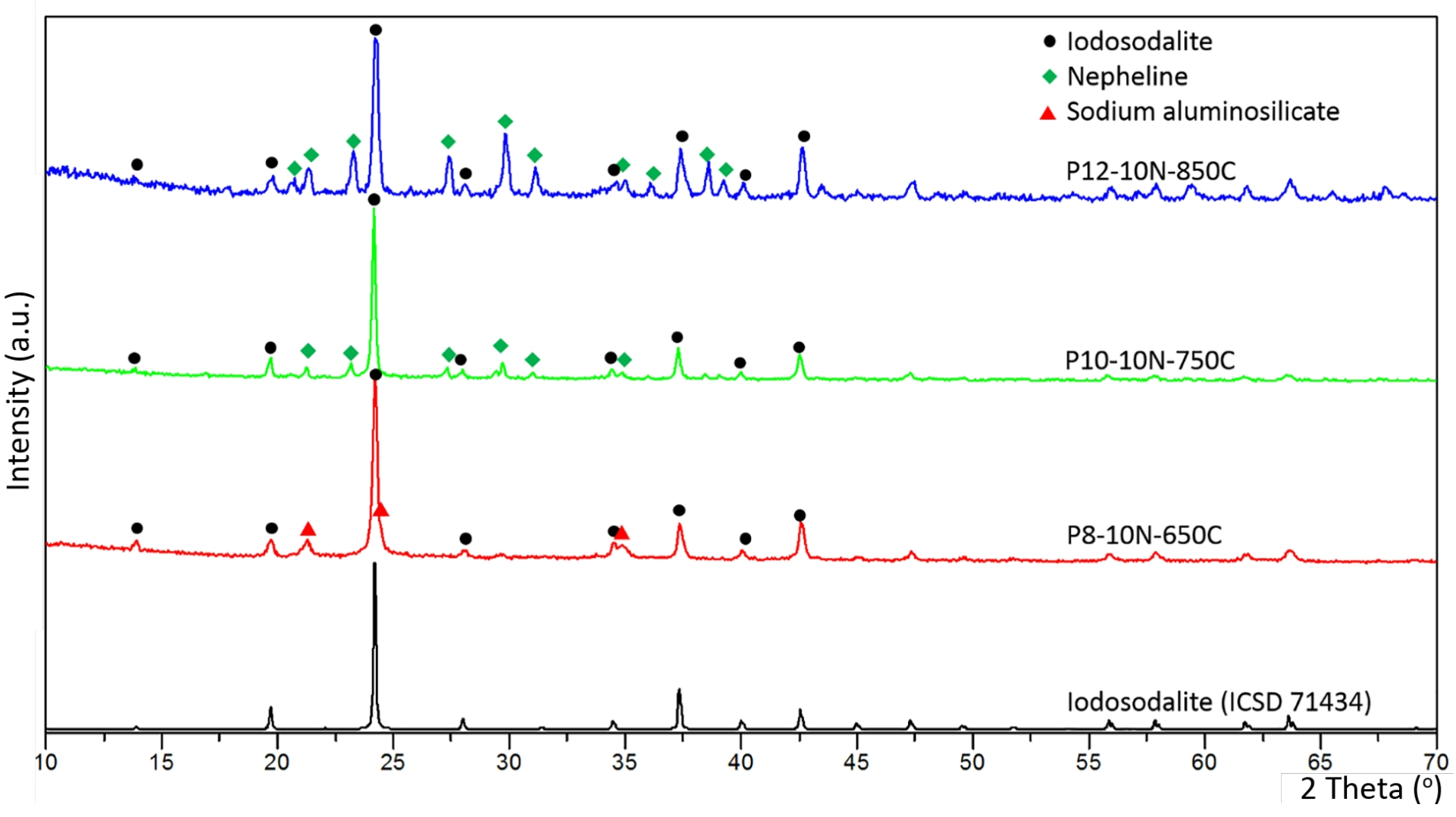
Iodosodalite
Nepheline
Sodium aluminosilicate
P12-10N-850C
P10-10N-750C
P8-10N-650C
Iodosodalite (ICSD 71434)
Intensity (a.u.)
10
15
20
25
30
35
40
45
50
55
60
65
70
2 Theta (°)

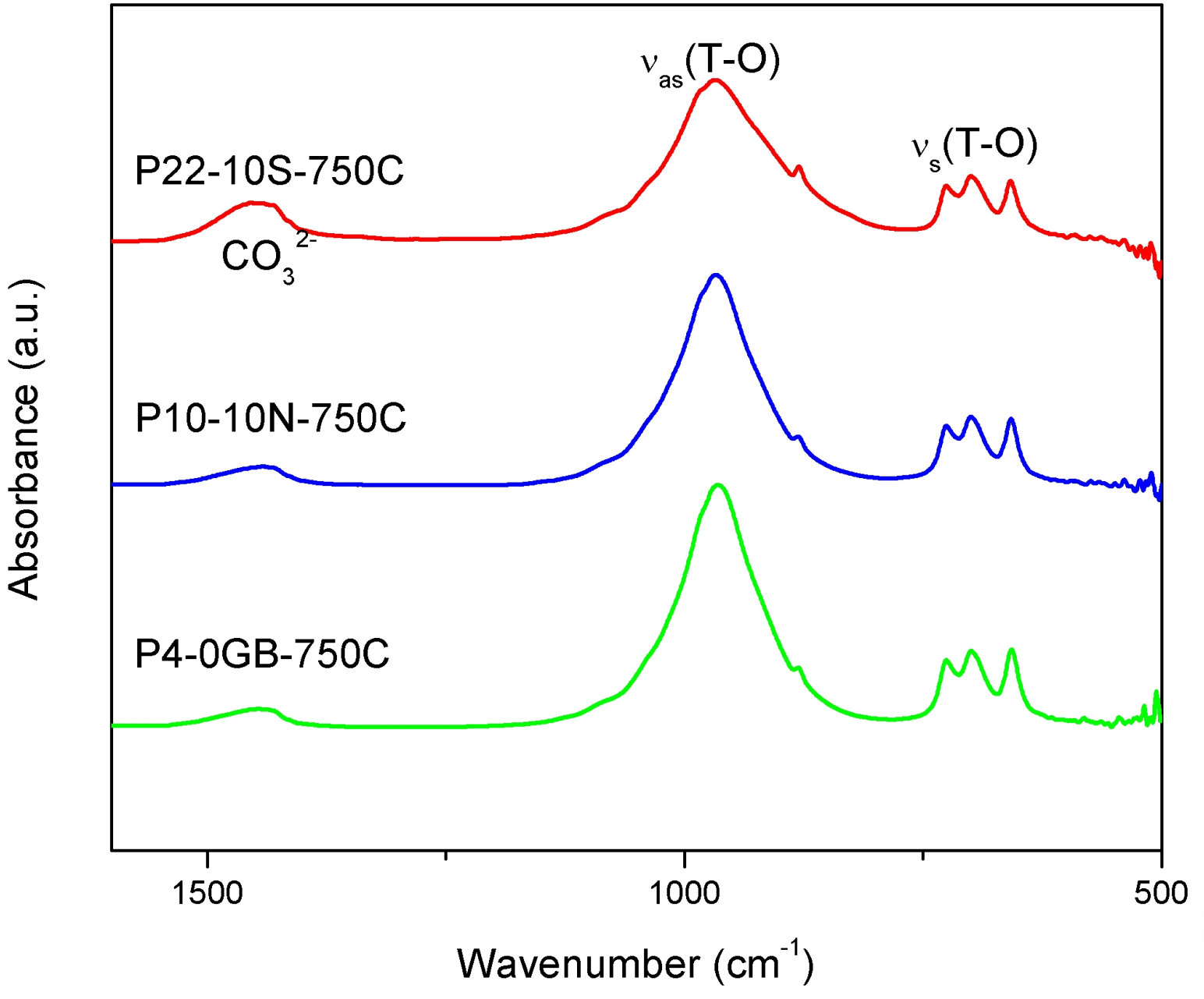
ν_{as}(T-O)
ν_{s}(T-O)
P22-10S-750C
CO_3^{2-}
P10-10N-750C
P4-0GB-750C
Absorbance (a.u.)
1500
1000
500
Wavenumber (cm^{-1})

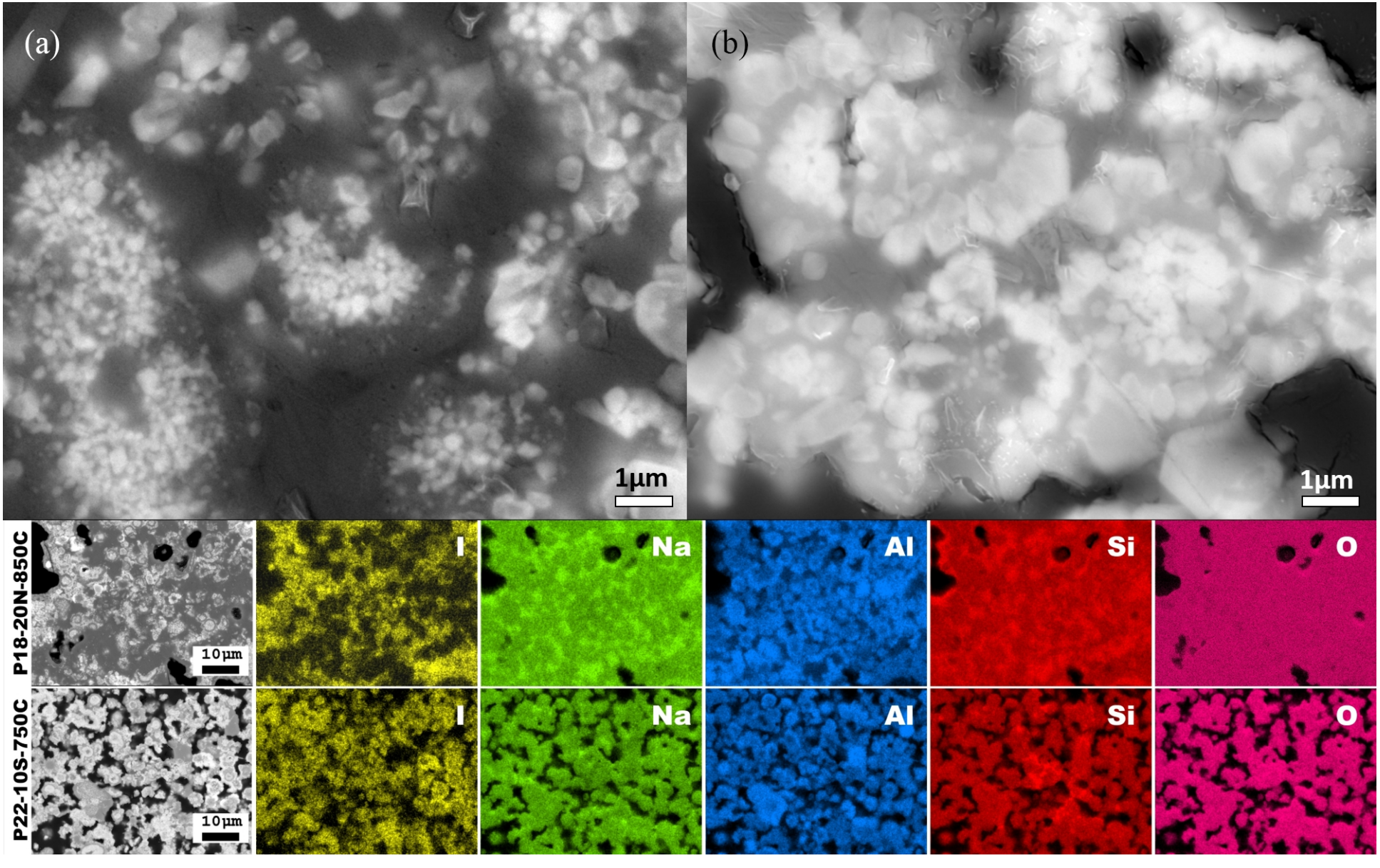
(a)
1μm
(b)
1μm
P18-20N-850C
10μm
I
Na
Al
Si
O
P22-10S-750C
10μm
I
Na
Al
Si
O

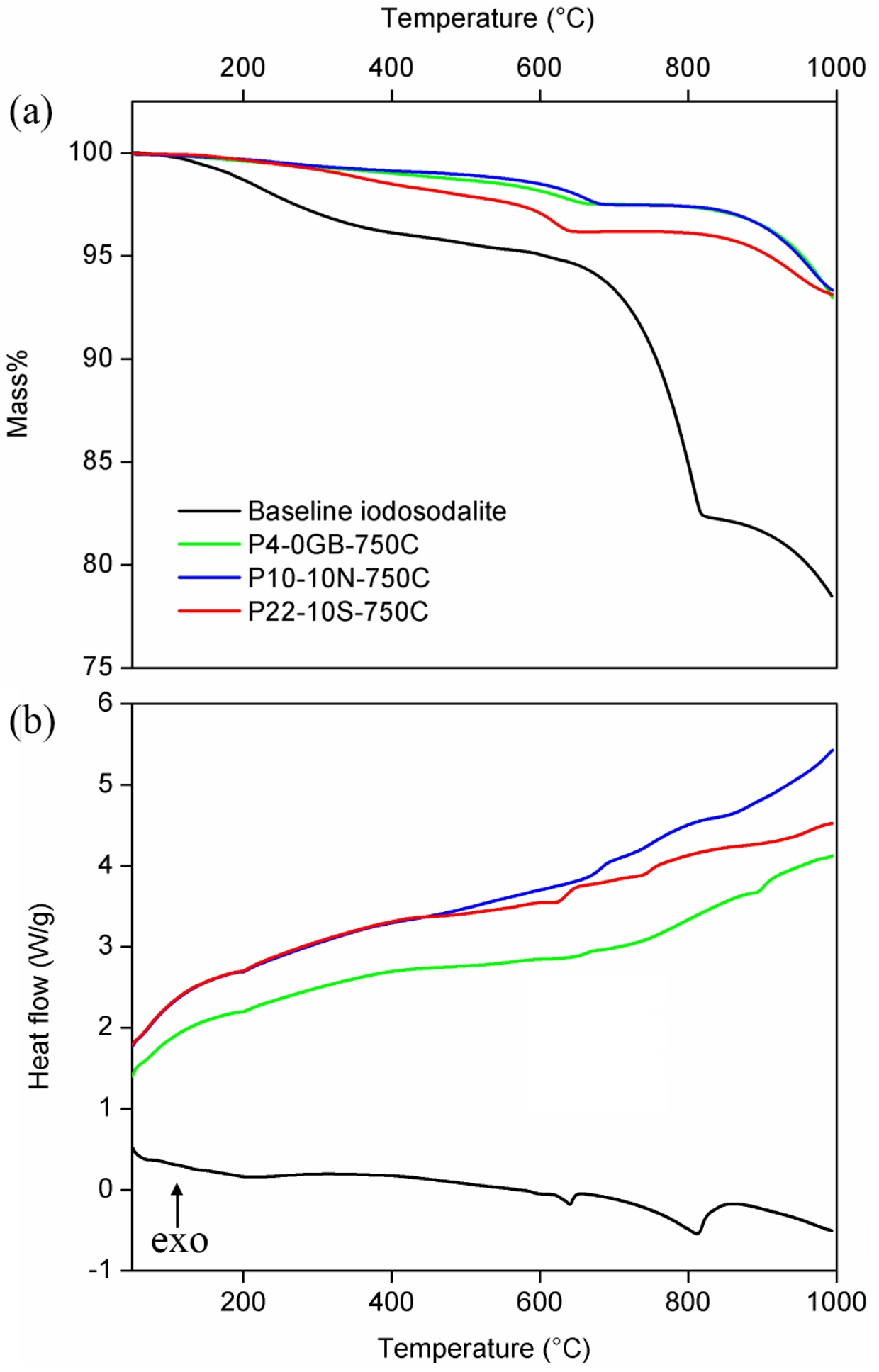
(a)
Temperature (°C)
200
400
600
800
1000
100
95
90
85
80
75
Mass%
Baseline iodosodalite
P4-0GB-750C
P10-10N-750C
P22-10S-750C
(b)
6
5
4
3
2
1
0
-1
Heat flow (W/g)
exo
200
400
600
800
1000
Temperature (°C)

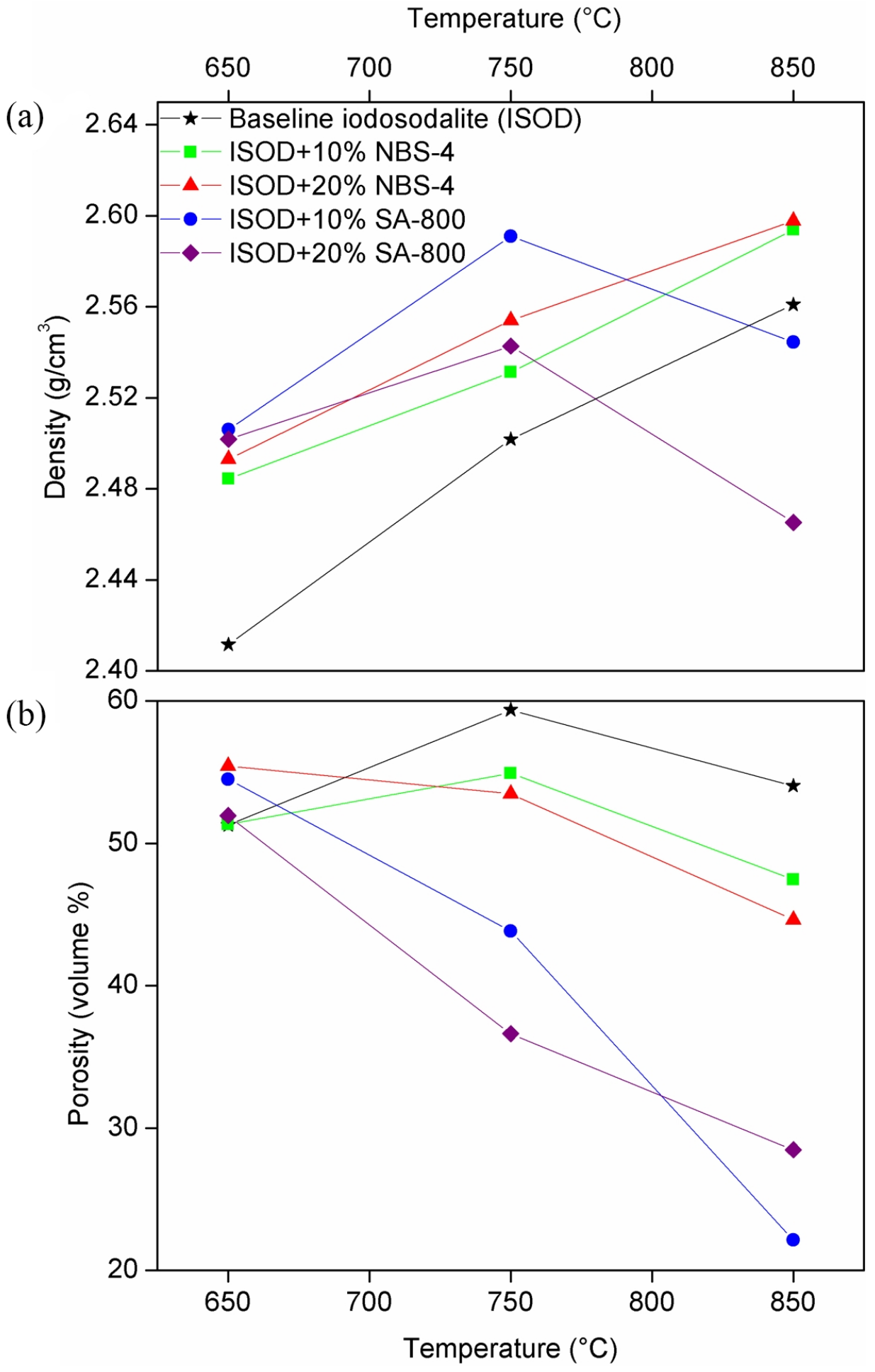
(a)
Temperature (°C)
650
700
750
800
850
Baseline iodosodalite (ISOD)
ISOD+10% NBS-4
ISOD+20% NBS-4
ISOD+10% SA-800
ISOD+20% SA-800
Density (g/cm3)
2.64
2.60
2.56
2.52
2.48
2.44
2.40
(b)
Porosity (volume %)
60
50
40
30
20
650
700
750
800
850
Temperature (°C)

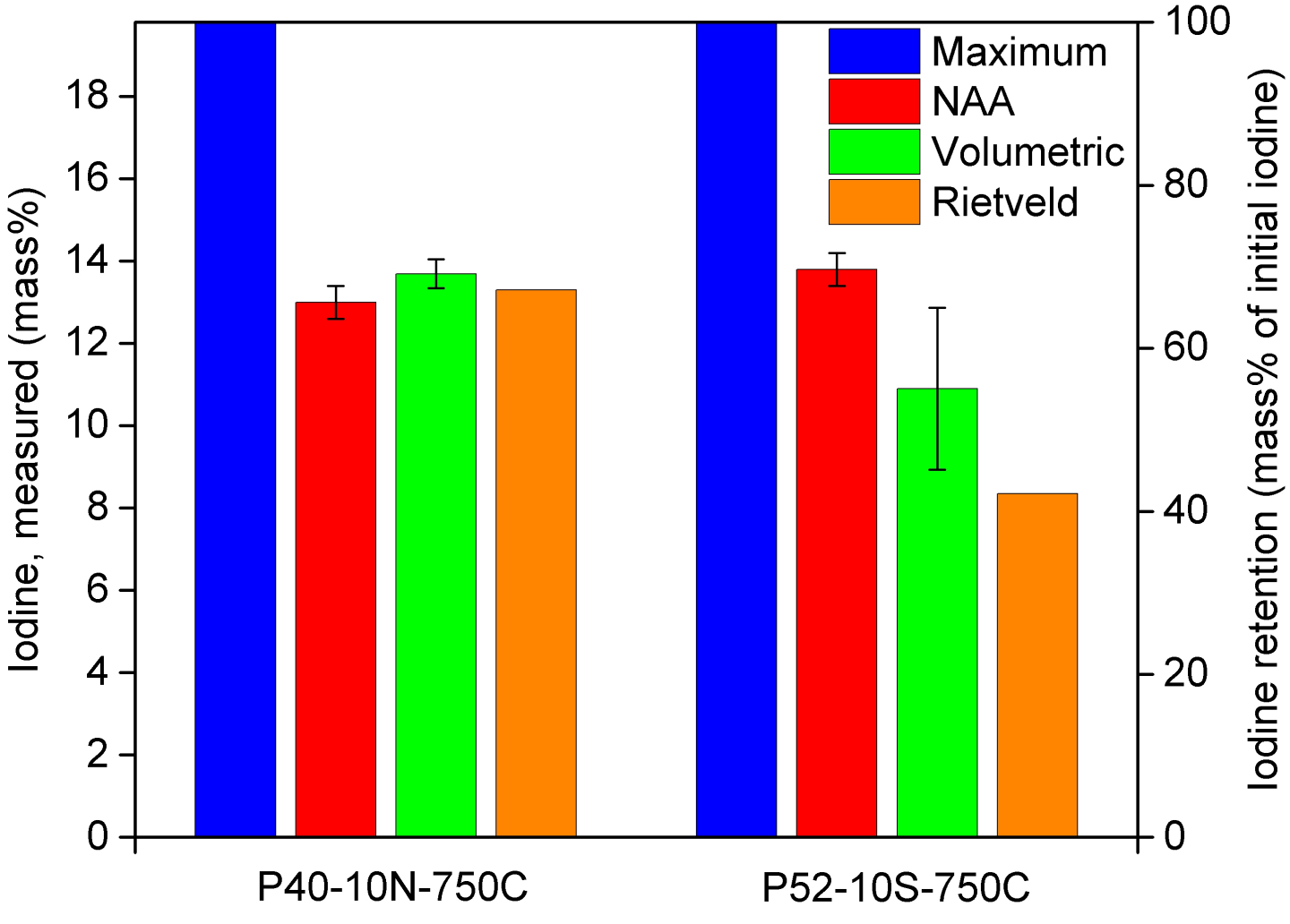
Maximum
NAA
Volumetric
Rietveld
Iodine, measured (mass%)
Iodine retention (mass% of initial iodine)
0
2
4
6
8
10
12
14
16
18
0
20
40
60
80
100
P40-10N-750C
P52-10S-750C

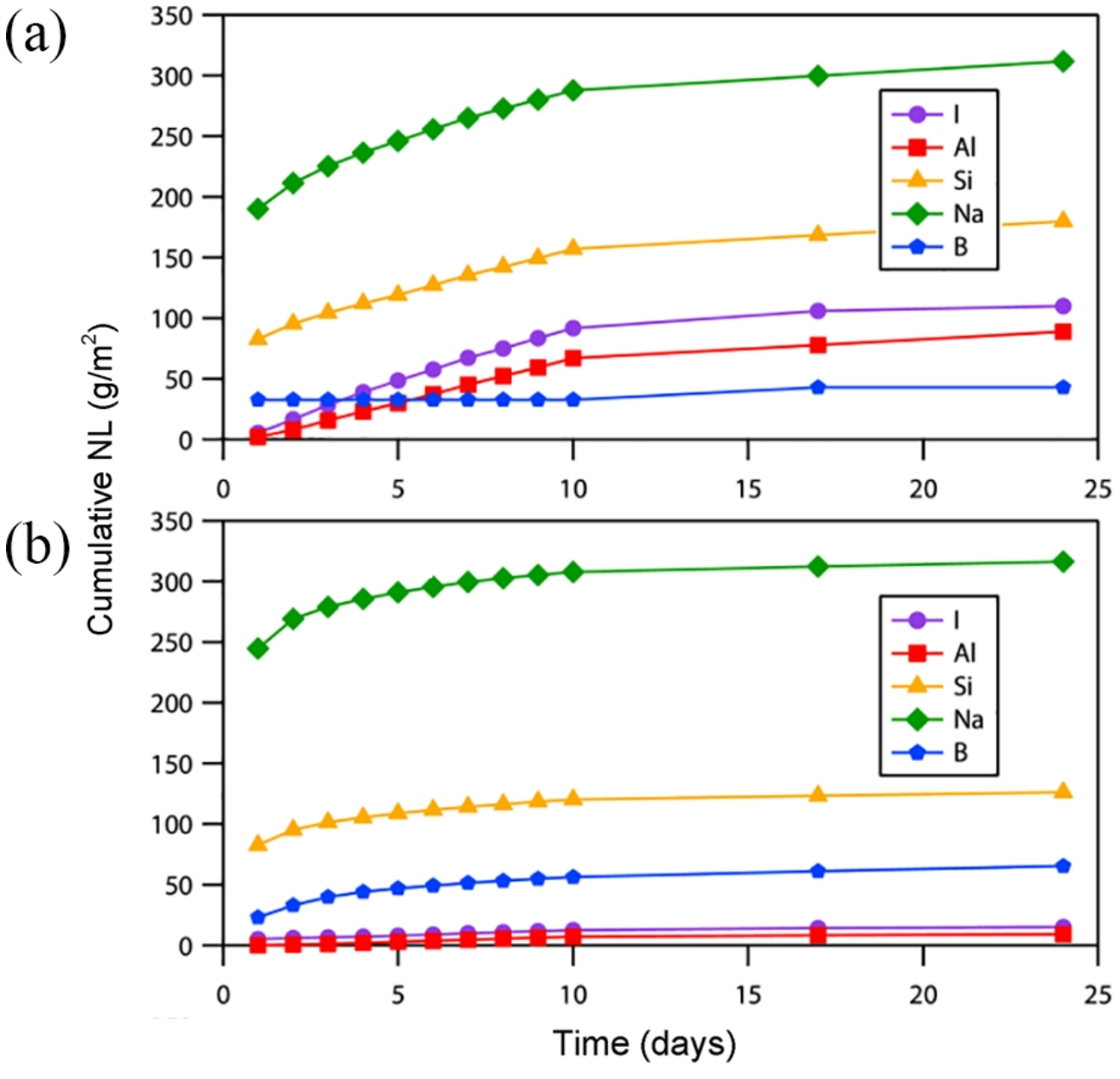
(a)
(b)
Cumulative NL (g/m^2)
Time (days)
I
Al
Si
Na
B
0
50
100
150
200
250
300
350
0
5
10
15
20
25

MRS Advances

Iodosodalite Waste Forms from Low-Temperature Aqueous Process

Junghune Nam,[1] Saehwa Chong,[2] Brian J. Riley,[3] John S. McCloy[1,2,3]

[1]*School of Mechanical & Materials Engineering, Washington State University, Pullman, WA 99164, USA*

[2]*Materials Science and Engineering Program, Washington State University, Pullman, WA 99164, USA*

[3]*Pacific Northwest National Laboratory, Richland, WA 99352, USA*

ABSTRACT

Nuclear energy is one option to meet rising electricity demands, although one concern of this technology is the proper capture and storage of radioisotopes produced during fission processes. One of the more difficult radioisotopes is ^{129}I due to its volatility and poor solubility in traditional waste forms such as borosilicate glass. Iodosodalite has been previously proposed as a viable candidate to immobilize iodine due to high iodine loading and good chemical durability. Iodosodalite was traditionally synthesized using solid state and hydrothermal techniques, but this paper discusses an aqueous synthesis approach to optimize and maximize the iodosodalite yield. Products were pressed into pellets and fired with glass binders. Chemical durability and iodine retention results are included.

INTRODUCTION

Iodine-129 (^{129}I) is a highly volatile radionuclide that is difficult to immobilize in a nuclear waste form using conventional vitrification processes [1]. It is highly water soluble and thus poses a serious concern for storage in geological repositories. It has a very long half-life of about 16 million years. Attempts have been made using vitrification processes and cements, but iodine typically has low solubility in typical borosilicate glass chemistries [2], and it is highly volatile at normal glass processing temperatures between 1000-1150°C. Iodine-containing mineral structures have received some attention as iodine waste form options, the more commonly studied being sodalite [3] and apatite [4].

Iodosodalite [$Na_8(AlSiO_4)_6I_2$], can be synthesized at temperatures below 200°C, and is the focus of this study. The structure of iodosodalite is shown in Figure 1. It consists of SiO_4 and AlO_4 tetrahedra arranged in rings, with a central "cage" containing a Na_4I tetrahedron. It is this so-called β-cage containing the iodide anion that makes sodalite attractive for immobilizing ^{129}I, because iodine is tightly bound within the cage and that reduces the tendency for release into the environment.

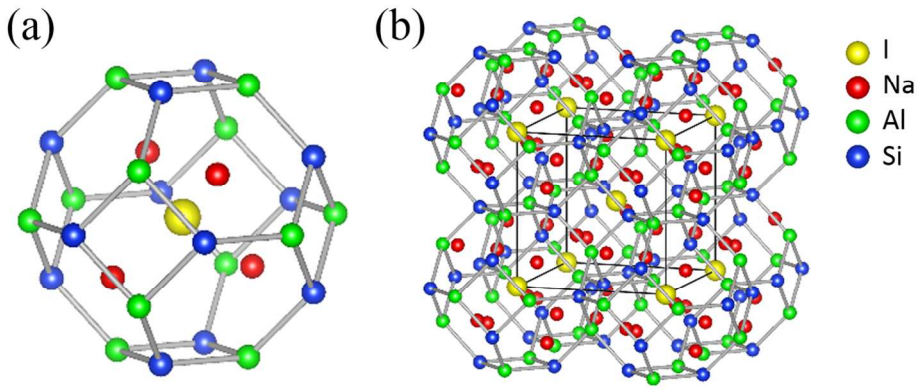

Figure 1. (a) Structure of the β-cage and (b) its arrangement in the sodalite unit cell. Oxygen atoms are not shown for better visualization.

Background on sodalite synthesis

Iodosodalite was first artificially synthesized using a solid state method in 1968 [5], where nepheline and NaI were mixed, sealed inside metal capsules, and heat treated to 500°C. In the years following, iodosodalite was mainly synthesized using hydrothermal methods [6, 7], where precursors were added to a solution heated inside a sealed autoclave to induce a higher pressure and encourage crystallization. The main disadvantage to the hydrothermal method, compared to an aqueous synthesis method that would occur in an open container, is that it would be difficult and expensive to scale hydrothermal synthesis up to industrial scale, since a large-volume, high-pressure environment would be necessary for this technique.

Strachan and Babad [13] compared two approaches for starting precursors for iodide sodalite: a kaolin clay mixture and an aluminosilicate gel. Both were cold pressed and fired to 1000°C and then vacuum hot pressed in graphite dies at 13.8 MPa with a die surface temperature of 1200°C. It was found that the samples made from the clay mixture had higher iodine content than those made from the gel mixture. Leach tests on these samples led to the proposal that iodosodalite should be a serious candidate for the immobilization of ^{129}I. Although these samples showed promise, there was difficulty in complete incorporation of the target iodine into the sodalite structure. Studies by Vance [14] and Dunn [15] have shown that at temperatures below 600°C, unreacted NaI remains after synthesis, while at higher temperatures between 600 and 1200°C, volatilization of iodine was observed along with the formation of a secondary glassy phase [14].

In 1980, Babad and Strachan [8] patented an aqueous synthesis method that involved simply stirring the precursors in water at 70°C in order to make a homogeneous solution. After stirring, the solution was dried in an oven overnight, pressed, and then sintered to form iodosodalite [8]. In 2008, Bardez [9] compared the low-temperature (75°C) aqueous method using kaolinite and a high temperature (i.e., up to 880°C) calcining method in air with nepheline as a precursor. Both methods yielded a "significant" amount of crystalline iodosodalite, which was not quantified. Thus, synthesis processes were not optimized in these prior studies. In 2013, Lepry et al. [10] compared crystalline chlorosodalite yields from 3 different aqueous synthesis precursor routes using either (1) $Al(OH)_3$ + NaOH + CS, (2) $NaAlO_2$ + CS, or (3) $Al_2Si_2O_7$ + NaOH (CS = colloidal silica) along with sintering aids, calcining, and pressure variation on pellet

pressing. The presented results and conclusions drawn from the aforementioned studies were used to develop the testing protocol used in the current work.

EXPERIMENTAL METHODS

The main objectives of this study were to: 1) identify an optimal low-temperature synthesis procedure for iodosodalite by choosing from several precursor options, drying temperatures, precursor concentrations, and NaOH concentrations; 2) characterize the iodosodalite powders using X-ray diffraction (XRD) and scanning electron microscopy (SEM); 3) produce and characterize glass-bonded iodosodalite waste forms from this process; and 4) perform chemical durability testing on the most promising glass-bonded waste form.

Baseline iodosodalite powder for the waste form study was synthesized using an aqueous method, and subsequently the resulting sodalite was separately combined with two different glass binders (i.e., NBS-4 and SA-800, described below) and sintered. Iodine quantification was performed using three methods. Finally, chemical durability tests were performed using the ASTM C1308 method.

Sodalite synthesis by aqueous method

The objective of this first phase of this work was to establish an optimized synthesis procedure for iodide sodalite. In an attempt to optimize the iodosodalite yield, parameters from hydrothermal synthesis were initially used which had shown success in increasing iodide sodalite yield, such as increased temperature, increased the amount of excess NaOH over stoichiometry, and optimized precursor concentration [3]. This optimization for the aqueous process was achieved by testing three different precursor routes as shown below, varying the synthesis conditions, and assessing the iodosodalite yield. The variables that were changed were drying temperature, NaOH concentration, and precursor concentration.

1.) Metakaolin + NaOH

$$2NaI + 3Al_2Si_2O_7 + 6NaOH \rightarrow Na_8(AlSiO_4)_6I_2 + 3H_2O$$

2.) Kaolinite + NaOH

$$2NaI + 3Al_2Si_2O_5(OH)_4 + 6NaOH \rightarrow Na_8(AlSiO_4)_6I_2 + 9H_2O$$

3.) $NaAlO_2$ + Colloidal Silica (Ludox 40 wt%)

$$2NaI + 6SiO_2 + 6NaAlO_2 \rightarrow Na_8(AlSiO_4)_6I_2$$

Precursors were sequentially added in stoichiometric amounts, based on 0.5 g of NaI, into 15 mL of deionized (DI) water in a Teflon vessel (Savillex, 60 mL) that was heated to 70°C in a water bath. The water bath provided uniform heating in the vessel on top of the hot plate, and the water temperature was monitored by a thermometer. Each precursor was added in stoichiometric amounts and stirred in the solution for 15 min before the next precursor was added. After the last precursor was added, the final solution was stirred for 1 hr for homogenization and then placed in an oven overnight for drying. The following day, the sample was washed with DI water 3 times in a centrifuge at 9000 rpm for 5 min cycles with DI water and dried overnight again at

95°C. This washing step was done only for the optimization study to eliminate phase contributions from unreacted salts.

As shown in the equations above, the first precursor for each synthesis route was NaI (Certified Grade, Fisher Chemical). This was followed by the Si-source, then the Na-source. The required Al was included in either the Si- or Na-source, depending on the precursor route.

The three different sources of Si were Ludox HS-40°colloidal silica (CS, Sigma Aldrich), kaolinite [$Al_2Si_2O_5(OH)_4$, natural, Sigma Aldrich], and metakaolin ($Al_2Si_2O_7$). Metakaolin was prepared by heat treating the kaolinite at 850°C for 17 hrs in an alumina crucible [11]. The Na-sources used were NaOH (ACS Certified Fisher Scientific) and $NaAlO_2$ (99.9%-Al, Strem Chemicals).

For the $Al_2Si_2O_7$, $Al_2Si_2O_5(OH)_4$, and CS precursor routes, different conditions were used to observe their effect on the yield of crystalline iodosodalite. As shown in Table 1, the conditions that were varied were the oven drying temperature, precursor concentration, and NaOH concentration in 15 mL of deionized (DI) water; these variables were chosen based on previous related hydrothermal synthesis results [3].

Table 1. Synthesis parameters that were investigated. Excess NaOH concentration is associated with the starting solution for synthesis before precursors are added into the Teflon vessel.

Precursor Concentration (mL of DI Water)	Drying Temperature (°C)	Excess NaOH (M)
7.5, 15, 22.5	65, 100, 135	0, 1, 2, 5

Glass binder synthesis method

Two borosilicate glass binders, NBS-4 and SA-800, were synthesized with the compositions shown in Table 2. These glass binders showed the best results during previous glass-bonded chlorosodalite studies [12, 13]. The best result for the chemical durability test of the glass itself was previously obtained using NBS-4 among the series of NBS glasses [12] , and the lowest porosity was observed with SA-800 among the series of SA glasses while having the similar sodalite fraction [13]. Since the chlorosodalite and iodosodalite have the same structure and cage composition except the anions, the hypothesis was that these glass binders would give a similar positive result with iodosodalite. For the synthesis of NBS-4 and SA-800, the precursors were mixed with a vortex mixer, poured into a platinum crucible, and melted at 1550°C for 2 hrs and 1050°C for 40 min, respectively. For NBS-4, the resulting glass was ground in a tungsten carbide mill, and the melting process was repeated as there were pores after the first melt.

Table 2. Compositions of NBS-4 and SA-800 glasses [12, 13].

Glass binder	Mass %					
	SiO_2	B_2O_3	Na_2O	Al_2O_3	CaO	ZrO_2
NBS-4	58.87	8.98	20.17	5.99	3.99	2.00
SA-800	42.50	24.60	32.88	-	-	-

Waste form synthesis method

Iodosodalite was synthesized using the stoichiometric ratio of NaI, $Al_2Si_2O_5(OH)_4$, and NaOH; the powder was unwashed after synthesis to avoid losing unreacted iodine and other residuals. The precursor selection and sodalite synthesis parameters were chosen based on the variable experiments showing the highest iodosodalite yield (see Results). Figure 2 shows the general procedures of waste form synthesis. Iodosodalite powder and glass binder were first mixed with a vortex mixer and then with a mortar and pestle. Approximately 1 g of mixed powder was pressed into a pellet using a 20-mm die with a uniaxial press at ~4.3×10^7 Pa (~6200 psi) and held under pressure for 1 min. The resulting pellets were heat-treated at 650, 750, or 850°C for 8 hrs.

For the sample names, PNN-YY glass binder-ZZZC was used where NN is the pellet number, YY is the mass% of glass binder, and ZZZ is the sintering temperature (°C). N, S, and 0GB represent NBS-4, SA-800, and no Glass Binder, respectively. Table 3 shows the investigated variables for the waste form study.

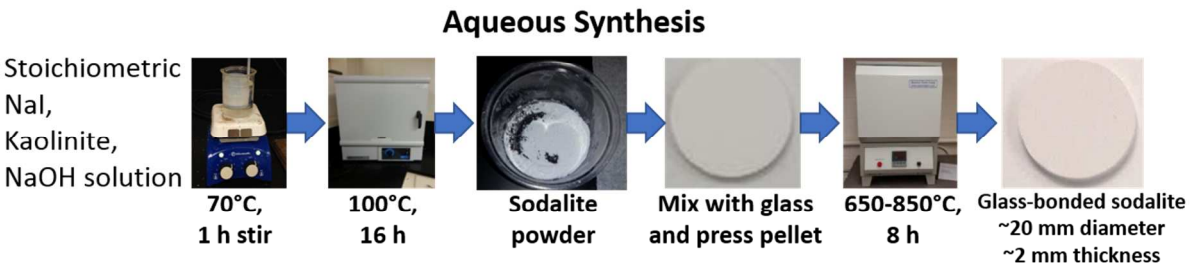

Figure 2. Schematic of process of aqueous synthesized iodosodalite glass-bonded waste forms.

Table 3. Synthesis parameters investigated.

Sintering Temperature (°C)	Glass binders (mass%)
650, 750, 850	0%, 10% NBS-4, 20% NBS-4, 10% SA-800, 20% SA-800

Characterization

X-ray diffraction (XRD) was performed with a PANalytical X'Pert Pro MPD with a Cu line x-ray source. Scans were performed at 45 keV and 40 mA through a range $2\theta = 5–90°$ with a 0.05° 2θ step size and 11-s dwell. Rietveld analysis was performed for phase identification and determination of the crystalline fraction for each phase on the PANalytical Highscore Plus software. For the amorphous phase fraction determination, 10 wt% of zinc oxide (ZnO, NIST SRM-674b) was mixed in as an internal standard using a planetary ball mill (Thinky ARE-310) with 5-mm yttrium-stabilized zirconia milling balls. The mill was spun for 3 min clockwise at 2000 rpm and 2 min counter-clockwise at 2200 rpm.

Scanning electron microscopy (SEM) on powders was performed using an FEI XL FEG Sirion by using carbon tape to adhere powder samples to the sample stage. Selected glass-bonded waste form pellets were impregnated with resin, cross-sectioned, and polished. SEM analysis (JSM-7001F field-emission gun microscope, JEOL USA, Inc. Peabody, MA) was then

performed in backscattered electron (BSE) mode with energy dispersive analysis (EDS) dot mapping (Bruker xFlash® 6|60,Bruker AXS Inc., Madison, WI).

An AccuPyc II 1340 (Micromeritics) was used to perform helium pycnometry in a 1 cm^3 sample cup. Each measurement consisted of 10 purges with helium gas, followed by 10 measurements of volume. The average density was calculated with the measured mass for each sample.

Iodine quantification was performed using neutron activation analysis (NAA), volumetric, and Rietveld methods. For NAA, the samples were packaged in heat-sealed polyethylene vials and irradiated with the standard in the reactor at 100 kW for 10 min at the Washington State University Nuclear Science Center. The peak intensity of γ-rays was measured with a high purity germanium detector (HPGe, EG&G Ortec, Model 0195), and the data was analyzed with the Genie 2000 Gama Acquisition and Analysis Software. For the volumetric method, iodine in the sample was titrated with thiosulfate using starch as an indicator, and the iodine mass was calculated using an empirical formula. For the Rietveld method, the width, peak shape, preferred orientation, and lattice parameters of reference phases were refined, and the mass% of iodosodalite and its chemical formula were used to calculate the iodine mass in the crystalline fraction.

Using the ASTM C1308-14 [14] chemical durability test, the dissolution behavior of one sample, P40-10N-750C, was investigated. The cylindrical pellet was placed in a DI water filled Teflon vessel at 90°C in a convection oven. The surface to area-to-volume (S/V) ratio of 80 m^{-1} was attained by controlling the volume of water. For each sampling, the solution was removed from the vessel after 1 day in the oven, and the same amount of water was refilled. The process was repeated for the 10 consecutive days (i.e., 1-d exchange interval), and then two additional exchanges were made at 7-d intervals (i.e., 17 d and 24 d into the test). Analytes present in the leachates were quantified with inductively-coupled plasma mass spectrometry (ICP-MS). The incremental normalized mass loss, $NL_{i,n}$, and the cumulative dissolution, $NL_{i,c}$, were calculated using Equation 1 and 2, respectively, where $C_{i,n}$ is the concentration of species i measured in the test solution during the n-th test interval, S is the geometric surface area of the specimen, V is the volume of solution, and f_i is the mass fraction of the i-th species in the test specimen.

$$NL_{i,n} = \frac{C_{i,n}}{S/V * f_i} \quad (1)$$

$$NL_{i,c} = \sum_{i=1}^{N} NL_{i,n} \quad (2)$$

RESULTS

Sodalite powder characterization

The trials for optimizing iodosodalite yield with aqueous processes are detailed elsewhere [15]. From the work on drying temperature, pH (NaOH concentration), and precursor variation, a baseline iodosodalite synthesis procedure was established with a maximum iodosodalite yield based on a $Al_2Si_2O_5(OH)_4$ precursor route synthesized in 15 mL of DI water and dried overnight at 100°C. This yielded ~95% crystalline iodosodalite with a measured density of 99.4% of the theoretical value. An SEM image of the optimum sodalite powder is shown in Figure 3.

The overall trends in variable effects on iodosodalite yield in aqueous synthesized samples seem to differ from those trends observed for hydrothermal synthesis, where an increased NaOH concentration was found to be favorable for sodalite formation with colloidal

silica in hydrothermal synthesis [16]. From experiments where the drying temperature was varied, 100°C was the optimal drying temperature for all three precursor routes based on the XRD quantification for iodosodalite fraction, and was the chosen drying temperature to perform the rest of the experiments. Increasing the pH clearly showed anion competition into the β-cages between the OH^- and I^- anions forming basic sodalite (i.e., "hydrosodalite") and iodosodalite respectively, especially between the 2 and 5 M NaOH samples for all three precursor routes. However, increasing the pH with up to 2 M NaOH did increase the iodosodalite yield for colloidal silica samples, showing the importance of NaOH on the crystallization of iodosodalite. However, this was not the case for $Al_2Si_2O_7$- and $Al_2Si_2O_5(OH)_4$-based samples. Densities decreased with increasing NaOH concentration with the exception of the colloidal silica 1 M and $Al_2Si_2O_5(OH)_4$ 2 M samples. Varying the precursor concentration from 15 mL of DI water negatively affected the iodosodalite yield and densities for both $Al_2Si_2O_5(OH)_4$ and $Al_2Si_2O_7$-based samples. Its effect was more significant for colloidal silica samples where increasing the concentration resulted in a largely amorphous sample, while decreasing the concentration resulted in no iodosodalite, but rather zeolite A, which is known to be a precursor for iodosodalite formation.

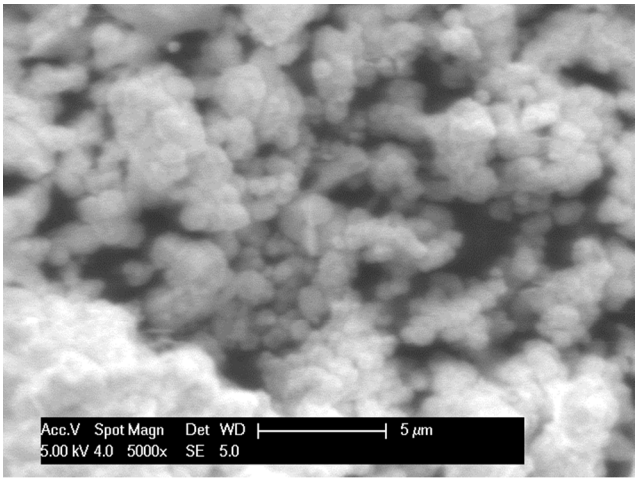

Figure 3. SEM image of iodosodalite polycrystals grown from aqueous synthesis with NaI + $Al_2Si_2O_5(OH)_4$ + NaOH in 15 mL DI water solution and then dried overnight at 100°C.

Waste form characterization

XRD phase analysis was performed on the glass-bonded waste form pellets as shown in Figure 4. As the temperature increased, the phase fraction of iodide sodalite decreased while the amorphous fraction increased. The nepheline (nominally $NaAlSiO_4$) phase was formed at 750 and 850°C. This indicates that iodosodalite transformed into nepheline or decomposed as the temperature increased. The transition of sodalite to nepheline at ~700–850°C has been reported with chlorosodalite [13, 17]. The samples heat-treated at 650°C had the highest iodosodalite fraction; however, due to incomplete sintering at 650°C, samples heat treated at 750°C appeared to be the waste form pellets produced with the most optimal properties. At 750°C, addition of NBS-4 resulted in higher sodalite fraction, but addition of SA-800 resulted in more effective closure of open porosity in fired pellets.

The results of SEM-EDS on the polished surfaces of P40-10N-750C and P52-10S-750C are shown in Figure 5. The elements are heterogeneously distributed in both samples. P40-10N-750C has more pores with larger particles, and this observation agrees with the porosity results. The brighter regions with particles represent the iodosodalite crystals, and the darker regions are glass or nepheline phases.

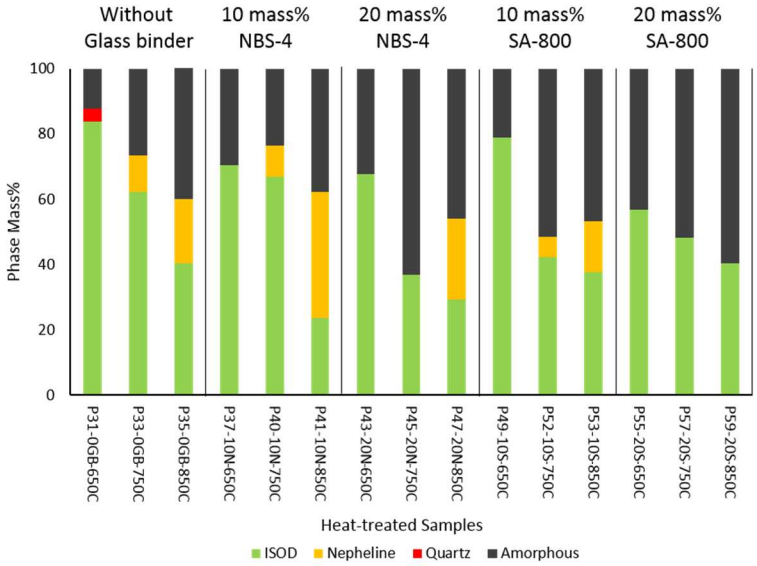

Figure 4. Quantitative XRD analysis based on Rietveld refinement, for aqueous iodosodalite samples without or with 10 or 20 wt% glass binders and sintered at 3 temperatures.

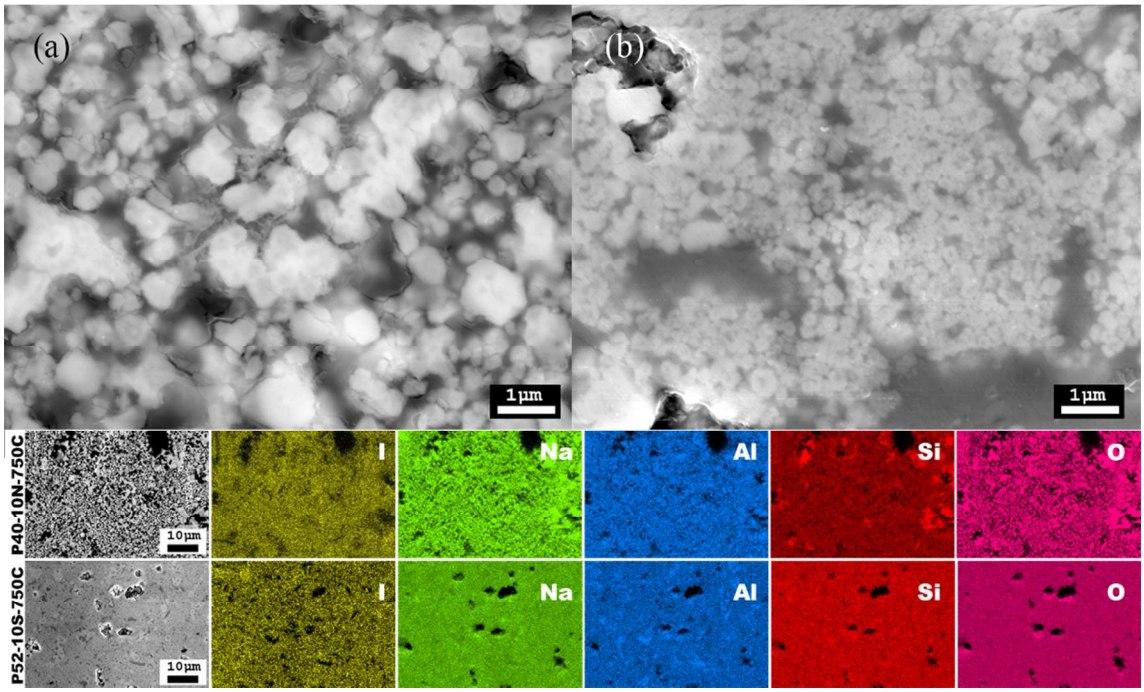

Figure 5. SEM on (a) P40-10N-750C and (b) P52-10S-750C with their elemental maps at the bottom.

The iodine masses in P40-10N-750C and P52-10S-750C quantified using NAA, volumetric, and Rietveld approaches are compared in Figure 6. Among these methods, Rietveld analysis provides the iodine fraction in the crystalline fraction only but not in the amorphous fraction; however, the iodine fraction is expected to be similar to those in other methods as the low solubility of iodine in the borosilicate glass has been reported [2]. Approximately 55-70 % of iodine was retained, although there is some discrepancy in the results among the methods. The addition of NBS-4 resulted in higher iodine fraction compared to SA-800 for pellets fired at the same temperature. The loss of iodine during the synthesis can be due to transition of sodalite to nepheline and decomposition of the β-cages. In addition, weakly-bonded iodine in the amorphous fraction can be volatilized easily. With similar iodine fractions between the two samples with different glass binders, SA-800 might be the better choice as it has lower porosity at 750°C although samples made with NBS-4 are expected to be more chemically durable.

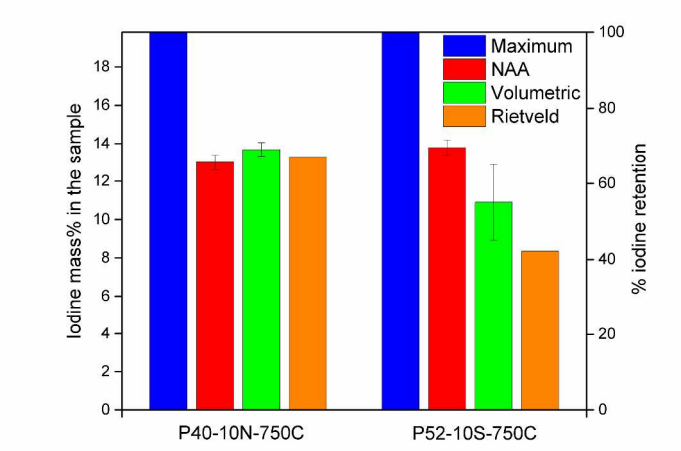

Figure 6. Iodine quantification of aqueous iodosodalite with NBS-4 (left) or SA-800 (right) glass binders, both heat treated at 750°C. The "maximum" values represent as-batched iodine concentrations used during sample syntheses.

The chemical durability test result is shown in Figure 7. The $NL_{i,c}$ values after the ten 1-d exchanges for P40-10N-750C ($S/V = 80$ m^{-1}) was 7.7 g/m^2. Initial releases of B, Na, and Si were observed, and this is possibly due to release of a non-durable Na-Si-O amorphous phase (not detected by XRD). Since Na, Al, and Si are present in the NBS-4 glass as well as in the sodalite phase, but the release of Al was much lower than Na and Si, it is more likely that a separate amorphous phase was present containing Na and Si following the aqueous synthesis. This could partially be due to NBS-4 dissolution, but the B-release and Al-release behavior were quite different, so while this is a possibility, the incongruity suggests otherwise. The normalized loss rate is larger than another iodosodalite study [18]; however, the chemical durability test and sample preparation used here were different. Further investigation will be performed to understand the dissolution mechanism.

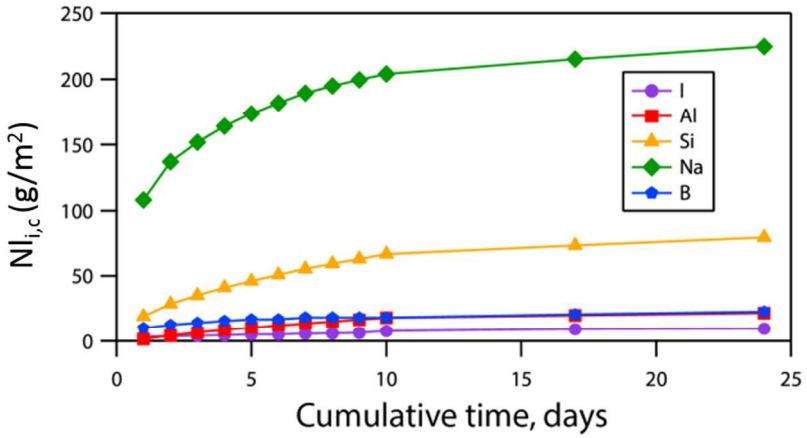

Figure 7. Chemical durability results for iodosodalite with NBS-4 (P40-10N-750C) using ASTM C1308-14

SUMMARY AND CONCLUSIONS

The effects of drying temperature, pH (NaOH concentration), and precursor variation (concentration and identity) on the aqueous synthesis of iodosodalite was investigated. An iodosodalite synthesis procedure was established to yield a product with an iodosodalite phase purity of up to 95% using a kaolinite-based precursor route by drying at 100°C with 15 mL of deionized water. The product had a measured density of 99.4% of the theoretical value. A sample with this high phase purity and density before sintering has never been reported before with aqueous synthesis methods.

For the waste form study, ~55–70 mass% of the original iodine remained in the heat-treated pellets. The loss of iodine is likely due to the decomposition of iodosodalite, transition of sodalite to nepheline, and volatilization of iodine from the amorphous fraction. In general, pellets made with NBS-4 resulted in higher iodosodalite fractions compared to those made with SA-800, but the addition of SA-800 resulted in pellets with lower porosities. The best synthesis conditions for iodosodalite waste forms according to this study are 10 mass% of glass binder and a heat-treatment of 750°C. The chemical durability shows the congruent dissolution of sodalite phase, but there are likely other phases present that contain Na and Si, considering that their dissolution rates are higher than those for I or Al. Further investigation will be performed on iodine dissolution.

Iodosodalite synthesis with aqueous methods may yield higher iodosodalite fractions than hydrothermal methods based on comparison to a previous study [15]. After aqueous or hydrothermal synthesis, not all precursors are converted into iodosodalite, and there is usually an amorphous fraction in the resulting product. In the waste form study, having higher fractions of initial iodosodalite present in the product seems to affect the outcome of the resulting iodine fraction present, because the iodine in the sodalite is less likely to volatilize during heat treatment compared to iodine present in the amorphous fraction due to low iodine solubility in silicate glasses. This results in better iodine incorporation and lower dissolution rate. To optimize the iodine retention in the waste form, more crystalline iodosodalite baseline powder or glass binder with lower sintering temperature are needed.

ACKNOWLEDGMENTS

This research was supported by the U.S. Department of Energy in support of the Nuclear Energy University Program – Advanced Waste Forms program, award # DE-NE0008257. The authors thank Diana Tabada and Donald Wall for help with the NAA, Benjamin D. Williams and Michelle M.V. Snyder for help with chemical durability data collection, and William Ebert for help with chemical durability data interpretation. The authors also thank Amit Bandyopadyay, Owen Neill, Lou Vance, Stephanie Bruffey, and Ashutosh Goel for helpful comments.

REFERENCES

1 B.J. Riley, J.D. Vienna, D.M. Strachan, J.S. McCloy and J.L. Jerden Jr, J. Nucl. Mater. **470**, 307 (2016).
2 B.J. Riley, M.J. Schweiger, D.-S. Kim, W.W. Lukens Jr, B.D. Williams, C. Iovin, C.P. Rodriguez, N.R. Overman, M.E. Bowden, D.R. Dixon, J.V. Crum, J.S. McCloy and A.A. Kruger, J. Nucl. Mater. **452**, 178 (2014).
3 S. Chong, J. Peterson, J. Nam, B. Riley and J. McCloy, J. Am. Ceram. Soc. **100**, 2273 (2017).
4 C. Cao, S. Chong, L. Thirion, J.C. Mauro, J.S. McCloy and A. Goel, J. Mater. Chem. A **5**, 14331 (2017).
5 T. Tomisaka and H.P. Eugster, Mineral. J. **5**, 249 (1968).
6 N.C. Nielsen, H. Bildsøe, H.J. Jakobsen and P. Norby, Zeolites **11**, 622 (1991).
7 A. Stein, G.A. Ozin, P.M. Macdonald, G.D. Stucky and R. Jelinek, J. Amer. Chem. Soc. **114**, 5171 (1992).
8 H. Babad and D.M. Strachan, Method for immobilizing radioactive iodine, USPTO, US4229317 A (1980).
9 I. Bardez, L. Campayo, D. Rigaud, M. Chartier and A. Calvet in Proceedings of *ATALANTE 2008,* (Montpellier, France), pp. O4_19.
10 ASTM, Standard Test Methods for Determining Chemical Durability of Nuclear, Hazardous, and Mixed Waste Glasses and Multiphase Glass Ceramics: The Product Consistency Test (PCT), ASTM Committee C26 on Nuclear Fuel Cycle, ASTM C 1285-02, ASTM International, West Conshohocken, PA (2008).
11 K.L. Konan, C. Peyratout, A. Smith, J.P. Bonnet, S. Rossignol and S. Oyetola, J. Colloid Interface Sci. **339**, 103 (2009).
12 B.J. Riley, J.D. Vienna, S.M. Frank, J.O. Kroll, J.A. Peterson, N.L. Canfield, Z. Zhu, J. Zhang, K. Kruska, D.K. Schreiber and J.V. Crum, J. Nucl. Mater. **489**, 42 (2017).
13 B.J. Riley, W.C. Lepry and J.V. Crum, J. Nucl. Mater. **468**, 140 (2016).
14 ASTM, Standard Test Method for Accelerated Leach Test for Diffusive Releases from Solidified Waste and a Computer Program to Model Diffusive, Fractional Leaching from Cylindrical Waste Forms, ASTM Committee C26 on Nuclear Fuel Cycle, ASTM C 1308-14, ASTM International, West Conshohocken, PA (2014).
15 J. Nam, Aqueous synthesis of iodide sodalite for the immobilization of I-129, Materials Science and Engineering, MS, Washington State University, Pullman, WA (2016).
16 S. Chong, J. Peterson, B. Riley and J. McCloy in Proceedings of *WM2016,* (Waste Management Phoenix, AZ, 2016), pp. 16153.
17 N.C. Hyatt, J.A. Hriljac, A. Choudhry, L. Malpass, G.P. Sheppard and E.R. Maddrell, MRS Proc. **807**, (2003).
18 E. Maddrell, A. Gandy and M. Stennett, J. Nucl. Mater. **449**, 168 (2014).